ET4300
Master Thesis EE

Modelling and Topology Optimisation of Medium Voltage Representative Networks for The Netherlands

Delft University of Technology

Marcel Brouwers, 4728181

TU Delft

Modelling and Topology Optimisation of Medium Voltage Representative Networks for The Netherlands

by

Marcel Brouwers

to obtain the degree of Master of Science
at the Delft University of Technology,

Author:	M. J. H. Brouwers	4728181
Thesis duration:	February 08, 2022 – December 13, 2022	
Supervisor(s):	Dr. P. Vergara Barrios	
Daily supervisor:	Ir. N. K. Panda	
Thesis committee:	Dr. Ir. J. Rueda Torres,	TU Delft
	Dr. P. Vergara Barrios,	TU Delft
	Dr. Ir. K. Bruninx,	TU Delft
	Ir. N. K. Panda,	TU Delft

TU Delft

Abstract

The electrification of modern-day society keeps increasing and the demand for electricity grows along with it. Technologies like EVs and heat pumps are both part of the new types of demand, while PV systems and wind farms are meant to be our main new sources of generation. Contrary to traditional resources connected to the electricity network, most of these resources tend to be placed and operated in a distributed manner, increasing the demand for transport capacity within the LV and MV grid. This demand cannot always be met however, which leads to situations of congestion.

This thesis seeks to reduce this congestion by means of optimising the grid topology in line with the seasonal variations in the supply and demand of electricity. This is done by means of implementing a two-stage reconfiguration algorithm. The benefit of network reconfiguration is that it is a short-term and low-cost solution which can be implemented by the DSO without relying on other external parties.

In the first stage of the reconfiguration algorithm, the positions of the normally open switches within the network are optimised in order to adjust the power flow therein. These optimised positions are subsequently used in the second stage to calculate the network variables. The first stage is implemented as a MILP optimisation in Python, while the second stage consists of a Newton-Raphson calculation in the commercial software PowerFactory. This distinction is made to enhance the accuracy of the final network parameters, while still being able to optimise the switch positions in a deterministic manner.

Rather than day-ahead or real-time reconfiguration, as is often considered in most literature, this thesis focuses on seasonal reconfiguration to accommodate for the manual operation of the switches present within the MV grid in the Netherlands. These manually operated switches severely reduce the frequency by which reconfiguration actions can be performed, but that does not mean that the topology of the grid cannot be enhanced.

The presented reconfiguration algorithm is able to consistently reduce congestion within the analysed network, completely removing it or reducing its severity. It also outperforms two optimisation options in PowerFactory with regards to the objective function value. Those being an iterative exploration of meshes and a genetic algorithm.

Preface

This document contains the thesis about the two-stage reconfiguration algorithm to reduce congestion within the medium voltage grid. This project is carried out for the course ET4300 Master Thesis Electrical Engineering, to obtain the degree of Master of Science at the Delft University of Technology.

It has been a little more than five years since my journey in Delft began. I had next to no prior knowledge within the field of electrical engineering, apart from series and parallel circuits perhaps. Now, I have worked on numerous projects throughout the years, ranging from self-disinfecting facial masks, to rockets. However, this work I consider my crowning achievement. It is the first time that I have truly completed a project all by myself and had direct control over what I wanted to research and how I wanted to do that. I feel like this experience has been a true test of all that I have learned and done over the last few years and the experience has left me feeling proud.

You need to believe in the possibility of big change before you can start to bring it about with small steps.

I am a firm believer in change brought about by personal contribution, not just collective. It has been my dream to make a contribution within the field of Electrical Power Engineering and I will continue to strive for bringing about improvements to how we interact with our electricity system. I hope to have made the first step in that regard here, with the work that you are about to read.

Of course, I have not been left completely to my own devices. I have worked closely with my daily supervisor, Ir. N. Panda, who has been a great help throughout the project. He has been incredibly responsive to my many questions and has truly helped me to bring about a better thesis than I could have done alone. He has gone above and beyond what could have been expected of a daily supervisor, for which I am incredibly grateful. I was also able to rely on the insight and experience of my thesis supervisor, Dr. P. Vergara Barrios. I have discussed numerous topics with him, ranging from the optimisation formulation to the contents of my literature study, and each of these has improved because of it. As such I would like to thank both of them for guiding me during this project.

I would also like to thank Dr. Ir. J. Rueda Torres, who has been a great mentor for me even before I started on this project. His continued support, insight and encouraging attitude have been a great help and a continued source of motivation and inspiration. His suggestions for the thesis have greatly helped to complement the work I had already done, leading to more complete considerations than I would have thought possible.

Finally, there is also the mental stability required to complete a project of this scale. Drive and motivation always waver as time progresses and results remain absent or incomplete. Most readers will probably recognise themselves when I talk about late nights spent trying to make a simulation work as you intended it, with no true solution in sight. However, I had the great fortune of being able to rely on the continued support and encouragement of my family and friends. Working on this project alone has been one of the best learning experiences I could have hoped for, but I never was truly alone because of my parents, my sister and my friends. To each of you, know that you have my everlasting gratitude.

I hope you will enjoy the rest of this thesis.

Marcel Brouwers
December 2022

Contents

Nomenclature

Sets

$\mathscr{F}$	the set of phases (A, B, C)
$\mathscr{N}$	the set of nodes present within the network
$\mathscr{L}$	the set of lines present within the network
$\mathscr{T}$	the set of considered time steps

Indexes

ϕ, ψ	Phase $\phi \in \mathscr{F}$ and $\psi \in \mathscr{F}$
n, m	nodes n $\in \mathscr{N}$ and m $\in \mathscr{N}$
mn	line mn $\in \mathscr{L}$
t	time step t $\in \mathscr{T}$
λ	λ-th block for the piece-wise linearization of $P^2_{mn,\phi,t}$ and $Q^2_{mn,\phi,t}$

Constants

N	total number of nodes within the network
M	a large number (M >>$V^{max,sqr}$)

Variables

$P^L_{mn,\phi,t}$	the active power losses of the branch between nodes m and n
$Q^L_{mn,\phi,t}$	the reactive power losses of the branch between nodes m and n
$V_{m,\phi,t}$	the voltage magnitude at bus m, for phase ϕ, at time t
$V^{sqr}_{m,\phi,t}$	the square term of the voltage magnitude at bus m, for phase ϕ, at time t
$P_{mn,\phi,t}$	the active power of branch mn, for phase ϕ, at time t
$P^{sqr}_{mn,\phi,t}$	the square term of the active power of branch mn, for phase ϕ, at time t
$Q_{mn,\phi,t}$	the reactive power of branch mn, for phase ϕ, at time t
$Q^{sqr}_{mn,\phi,t}$	the square term of the reactive power of branch mn, for phase ϕ, at time t
$P^S_{m,\phi,t}$	the active power supply at bus m, for phase ϕ, at time t
$Q^S_{m,\phi,t}$	the reactive power supply at bus m, for phase ϕ, at time t
$\Delta^P_{mn,\phi,t,\lambda}$	value of block λ used for the piece-wise linearization of $P^2_{mn,\phi,t}$
$\Delta^Q_{mn,\phi,t,\lambda}$	value of block λ used for the piece-wise linearization of $Q^2_{mn,\phi,t}$
$P^+_{mn,\phi,t}$	positive component for the piece-wise linearization of $P^2_{mn,\phi,t}$
$P^-_{mn,\phi,t}$	negative component for the piece-wise linearization of $P^2_{mn,\phi,t}$
$Q^+_{mn,\phi,t}$	positive component for the piece-wise linearization of $Q^2_{mn,\phi,t}$
$Q^-_{mn,\phi,t}$	negative component for the piece-wise linearization of $Q^2_{mn,\phi,t}$
x_{mn}	value of the switch position for branch mn, with $x_{mn} \in 0, 1$
$\eta_{mn,\phi,t}$	slack variable for the calculation of the voltage difference between nodes
$P^{sqr,switch}_{mn,\phi,t}$	square term of the active power for branch mn, taking into account the switch position
$Q^{sqr,switch}_{mn,\phi,t}$	square term of the reactive power for branch mn, taking into account the switch position

Parameters

$R'_{mn,\phi,\psi}$	the transformed line resistance (where $R'_{mn,\phi,\psi} = R_{mn,\phi,\psi}\angle\theta_\psi - \theta_\phi)$
$X'_{mn,\phi,\psi}$	the transformed line reactance (where $X'_{mn,\phi,\psi} = X_{mn,\phi,\psi}\angle\theta_\psi - \theta_\phi)$
$\overline{I}_{mn}$	Maximum current limit for line mn
$P^D_{m,\phi,t}$	Active power demand at node m, for phase ϕ, at time t
$Q^D_{m,\phi,t}$	Reactive power demand at node m, for phase ϕ, at time t
$\widetilde{V}_{m,\psi,t}$	approximation of the voltage magnitude at bus m, for phase ψ, at time t
$\widetilde{P}_{mn,\phi,t}$	approximation of the active power through line mn, for phase ϕ, at time t
$\widetilde{Q}_{mn,\phi,t}$	approximation of the reactive power through line mn, for phase ϕ, at time t
$\rho_{mn,\lambda}$	slope of block λ for the piece-wise linearization of $P^2_{mn,\phi,t}$ and $Q^2_{mn,\phi,t}$
$\overline{\Delta}_{mn,t}$	maximum length of the block for the piece-wise linearization of $P^2_{mn,\phi,t}$ and $Q^2_{mn,\phi,t}$
$V^{min,sqr}$	minimum value of the square of the voltage magnitude
$V^{max,sqr}$	maximum value of the square of the voltage magnitude

1 Introduction

The electrification of modern-day society keeps increasing and the demand for electricity grows along with it. Developments like an increasing number of electric vehicles (EVs) and heat pumps are core examples of contributing factors to this increase. At the same time it has proven imperative that the electricity which is used, is generated in a sustainable manner. The most prominent examples that facilitate this are photovoltaic (PV) installations and wind farms.

This introduces another trend, as most sustainable technologies which are available do not lend themselves to be deployed in a similar manner as traditional large-scale electricity generators. Traditionally, electricity was generated in a centralised manner and the generators were connected to the high-voltage (HV) transmission grid. However, PV installations are often deployed in a decentralised manner, allowing for a large total quantity, but with a small nominal capacity per connection. Additionally, wind farms are restrictive in their placement, meaning that it is often not possible to connect them directly to the HV grid. As a result, most of these technologies are connected to the low-voltage (LV) or medium-voltage (MV) distribution grid, increasing the local penetration of these resources. This also leads to their common designation as Distributed Energy Resources (DERs), which also includes the EVs and heat pumps, as they are placed and operated in a distributed manner rather than a centralised one.

Much like any network though, the distribution system is subject to physical limits. Distribution networks are designed to cope with peak demand and although they have been engineered to withstand a certain degree of growth, the growth over the last few decades is exceeding those expectations [1] and will likely continue to do so. This means that the operating limits are more often reached, or even violated.

1.1. Problem description

One of the situations which can occur as a result of the increased penetration of DERs is called congestion [2]. Congestion occurs when the demand for electrical transport capacity surpasses its availability. For comparison, congestion is a similar effect as a traffic jam [3], but instead of too many cars on the road, there is too much electricity that needs to be transported through the system. Congestion occurs as a result of over-generation or demand, to the point where the operating limits of the lines are closely approached or breached. On a technical level congestion problems can usually be described as voltage variations which exceed the designated limits and/or overloading problems of lines and cables, meaning that the loading is close to or exceeding the thermal limits [4]. If such a scenario occurs it needs to be solved, either in a preliminary planning stage, or in real-time if required.

The organisations responsible for overseeing the distribution systems and solving situations like congestion are called Distribution System Operators (DSO). They are responsible for the network and that it continues to be able to perform its function: efficiently deliver the active power to the consumers with high reliability [4]. Most distribution networks have been designed to be passive networks [5] where most scenarios of peak demand (or generation) could be handled by the network without intervention. But, due to the increase of

DERs and the subsequent challenges that are imposed, this traditional distribution system is transitioning to an active network [6].

Returning to the problem of congestion; there are a couple of actions a DSO can take in order to solve or at least reduce situations of congestion. Traditionally these consisted of long-term solutions, like network reinforcement (for example, replacing lines with ones having a higher current carrying capability and smaller impedance [4]) or network reconfiguration [6]. Short-term solutions could entail redispatch, where the system operator requests an adjustment of the power generation, or power feed-in, in a specific area to change the predicted flow of power. By lowering the power feed-in of one or more power plants within the congested area while at the same time increasing the power feed-in of one or more power plants outside of this area, the total power feed-in remains virtually unchanged, but the congestion is removed [7]. This is provided that the increased generation outside the congested area does not exceed the local transport capacity, because otherwise the problem is simply moved to this new area and the congestion would need to be solved again.

There are some limitations to these actions however. First of which is the timescale. Network reinforcement and network reconfiguration have traditionally been long-term solutions, although there is work being done on using network reconfiguration in day-ahead planning or as a corrective action. Furthermore, congestion usually only occurs around peak moments of either demand or generation, which constitutes a limited number of hours per year. Thus, the large investment needed for grid reinforcement may sometimes exceed the added benefit. The increase in both demand and distributed generation of electrical energy also poses problems for the network reinforcement. There can be a mismatch between the geographical location of the increased demand (like a newly build residential area using no natural gas) and the increased generation (like a new large-scale PV installation), resulting in both parts of the network needing reinforcement [8].

More recently, as the role of the distribution system and subsequently the DSOs became more active, other actions were added to the options available to the DSO. Most prominently are the market methods, which include dynamic tariff and distribution grid capacity market [4].

Despite all of the different options mentioned above, most system operators in the Netherlands are still not able to prevent congestion. A clear illustration of this is given in Figure 1.1a and 1.1b, presenting the current status of the available capacity inside the Dutch electricity grid from an electricity demand and an electricity generation point of view, respectively. In Figure 1.1, yellow means that transportation capacity shortages are expected (but not yet certain), orange represents imminent shortages and the red areas currently experience structural capacity shortages. If there is no additional colour it means that there are currently no capacity shortages. It is evident from Figure 1.1 alone that there is a huge problem of congestion already present inside the Netherlands and unless something is done, this will likely only get worse due to the projected increases in DERs.

In order to analyse different actions which may be able to resolve the problem of congestion, system operators need two things: network data and network models. The data is required in order to design representative models of both the network itself and the assets connected to it, like generators and load profiles. The models, in turn, are required to review possible actions which can be taken to resolve the problem at hand, like congestion. The data needed for the network model used in this thesis is provided by one of the Dutch DSOs as part of a larger project, designated as ROBUST. The benefit of using real data is that the project described herein presents a more accurate representation of the case study analysed than one based on assumptions would be.

In particular, the case study used within this work represents one of the largest cities in the Netherlands. This means a densely populated area, with increases in electrification for many aspects of everyday life as people slowly transition to sustainable alternatives. As such, the earlier mentioned increase in electricity demand (caused by EVs and heat pumps for example) and distributed generation (like PVs) is present in a prominent way. Thus, due to these increases, the operating limits are starting to get reached and violated. This increased stress on the network encourages the use of flexibility, which is where ROBUST is focused on.

ROBUST is the world's first integrated research into a city-wide, future-proof and flexible electricity system. It is working on an integrated flexibility system at city-region level to facilitate more sustainable energy and

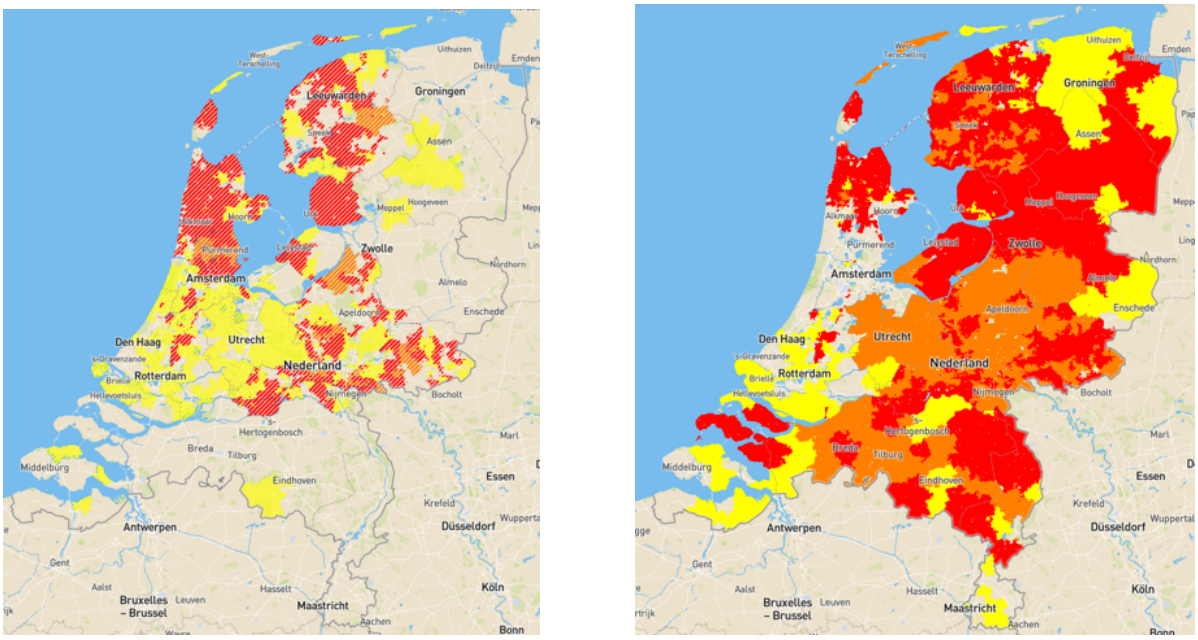

(a) Network capacity for energy demand.

(b) Network capacity for energy generation.

Figure 1.1: Network capacity shortages in the Netherlands, obtained from [9]. Yellow means that shortages are expected (but not yet certain), orange represents imminent shortages and the red areas currently experience structural capacity shortages, if there is no additional colour it means that there is currently no capacity shortages.

electric transport in cities. ROBUST investigates the optimal relationship between grid reinforcement and the use of flexibility, with the aim of reducing congestion problems and providing flexibility to national energy markets [10].

1.2. Research motivation

The focus of this thesis will be on grid reconfiguration. Reconfiguration in the grid refers to the change of the grid structure (or topology) through changing the status of the normally-open switches and normally-closed switches [4]. Changing the status of a switch is also referred to as a switching action. Similarly to the concept of redispatch, network reconfiguration changes the flow of power within the network which can lead to a reduction or removal of the present congestion. Contrary to grid reinforcement, grid reconfiguration does not add any new components to the grid, but rather it seeks to optimise the use of the grid that is already available.

Currently, performing switching actions is only done over long timescales in the Netherlands. Based on discussions with a Dutch DSO, switching actions once every 3 to 4 years is deemed common. The frequency of switching actions is primarily limited due to a need for manual operation of most switching devices present in the grid. This means that there are significant costs and time commitments involved before a switching action can be performed. As a result, most network reconfiguration actions are implemented as long-term solutions in the planning stages of the grid (several years ahead). Such forms of network reconfiguration are also referred to as passive network reconfiguration.

Despite these limitations regarding switching actions, most recent works in literature consider network reconfiguration on a shorter timescale, in the region of day-ahead or even as a corrective action after congestion has already occurred (in other words a timescale of real-time). Such forms of network reconfiguration are also referred to as active network reconfiguration. However, this presents a key problem when considering recent advances in network reconfiguration and their applicability to the electricity networks in the Netherlands.

For active network reconfiguration it is important that the switching actions can be carried out within a short amount of time and over the entire network. The only feasible way in which this can be implemented is by the presence of remotely-operable switches. However, based on discussions with a Dutch DSO, such devices are scarcely present at the moment within the Medium Voltage (MV) network in the Netherlands. There are ef-

forts being made to increase the amount of remote operable switches, as well as advances in digitisation and automation which will eventually enable the Dutch DSOs to perform active reconfiguration from a central control room. However, these efforts are slow due to the sheer amount of switches that need to be replaced. As such, for a short-term solution, assumptions toward system-wide fast remote switching actions are far from realistic.

So, although active reconfiguration for day-ahead and real-time may show promising results in literature, it does not offer a short-term solution for the already present problem of congestion inside the Netherlands, as it cannot be implemented due to the limitations of the assets currently within the grid. Similarly, the passive network reconfiguration which is currently used within the grid has not been able to prevent the current situation. However, there appears to be little consideration for network reconfiguration in-between these timescales.

That is where the main topic of this thesis will focus on; the potential of implementing network reconfiguration on longer timescales to reduce congestion within the grid, especially for future scenarios. In particular, the timescales under consideration are seasonal in nature, where trends can be observed for both yearly generation profiles and load profiles. For example, PV generation peaks in the summer months, whereas electricity demand increases during the winter. This is shown graphically in Figure 1.2 [11]. The location of these assets will likely differ, traditionally implying that both parts of the network would need reinforcing [8]. However, it also implies that the network can likely benefit from a different configuration for both situations.

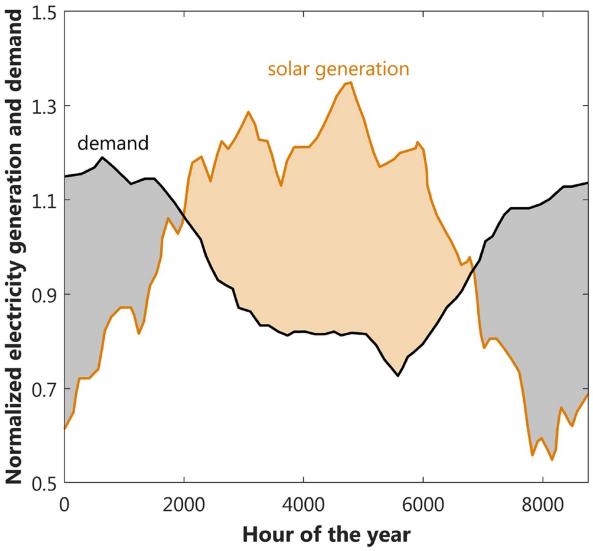

Figure 1.2: "Annual time series of weekly averages that illustrate the seasonal correlation of electricity demand (black line) and solar generation (orange line) for Europe." Found in [11].

Before the research question is covered, it is worth highlighting the work in [12], which presents a review of publications up to 1994. It is important to point out that in [12] a few elements which have been mentioned above are already explored, such as optimal seasonal configurations for the grid. This begs the question of why it is still being researched in this thesis. Part of the reason why is because such actions are still not widely adopted within industry standards. The more important reason however, is because of the changing electricity system as a whole. In [12] the main reason for network reconfiguration is described as: "Distribution systems are designed to be most efficient at times of peak demand: the system configuration is unnecessarily lossy during the off-peak times which are most prevalent." However, the current problem is that the peak demand surpasses the capabilities of the distribution system and the network can no longer cope with the total required transmission capacity. Changes such as higher penetration of renewable energy resources, more distributed generation and increased electricity demand mean that the topic has evolved beyond the original considerations from several decades ago.

1.3. Research questions

This thesis seeks to add to the existing literature and resources by modelling a medium voltage distribution grid representative of networks found in the Netherlands. Additionally, it seeks to add to possible actions which can be taken by the DSO to remove or reduce congestion, by introducing network reconfiguration on a seasonal timescale. The advantage of this approach of a seasonal timescale is that it can be used within the current grid of the Netherlands, rather than assuming the future system will have the required functionality.

In order to achieve this goal there are several parts which need to be researched. The main research question is being formulated as follows:

"How seasonal optimisation of the medium voltage grid topology by the use of a grid reconfiguration algorithm can help to overcome structural congestion?"

Before an answer to the above question can be formulated there are several questions which will need to be answered first, in particular:

- Question 1: What assumptions and network parameters need to be considered in order to design a representative network simulation for a large city in the Netherlands?
- Question 2: How to formulate the mixed-integer linear program meant to implement the network reconfiguration algorithm?
- Question 3: What is the impact of different load profile scenarios on the MV grid?
- Question 4: Is it possible to optimise the topology of the MV grid (in a consistent manner) to cover a wide range of different load profile scenarios by adjusting the normally open switches and thus changing the topology?

1.4. Research methodology

In order to answer the questions posed above, the problem is split into different parts. To start, it is required to model a MV grid in which a situation of congestion can be simulated. This will require translating the network topology into parameters which describe it, like the number of nodes and lines. Additionally, the network will be bounded by several constraints. These can range from maximum current limits for the lines, to the balancing of supply and demand within the considered network. These will need to be translated into their mathematical formulation such that they can be included in the model.

Next, this model needs to describe the current status of the network. In particular, the model needs to determine if congestion has occurred (or is expected to occur) and if so, where it has occurred within the network. Such modelling is done by the use of load flow calculations which will be covered in more detail in the literature review in Chapter 2. The completion of these steps is equivalent to modelling the problem of congestion.

Next, the problem needs to be solved. The method implemented in this work involves the reconfiguration of the network in order to redirect the flow of power, thus alleviating the loading of the lines and resulting in removing (or at least reducing) the encountered congestion. This is done by implementing the reconfiguration as an optimisation problem, which will be bounded by the aforementioned network constraints.

Such an implementation would suffice for solving a single case of congestion. However, this thesis is considering the problem over a seasonal timescale and as such it will be important to not only consider the network in a single instance of time, but over a range of different time horizons.

It is not within the scope of this work to apply network reconfiguration in real-time. Instead, it is considering future scenarios where the occurrence of the phenomenon of congestion is expected to only increase. This should provide DSOs with insight into short-term solutions before long-term actions like grid reinforcement can be applied.

For the seasonal time horizon, both the load and generation profiles within the respective periods of summer and winter (spring and autumn being divided between the two) still need to be modelled. Once these formulations are made it is possible to perform the network optimisation as a multi-period mixed-integer optimal power flow. This in turn should yield an optimised network topology for each season, limiting the required number of switching actions by the DSO to about twice a year.

1.5. Thesis synopsis

The rest of this work describes the process outlined above in greater detail. Chapter 2 will go into further detail regarding some of the background information, conventions and methods used in the rest of this thesis, as well as present an analysis of the state-of-the-art research on the topics discussed.

Next, in Chapter 3, the case study considered within this work is introduced. While the developed methodology can be applied to any MV network, it is deemed useful to provide context within which the modelling considerations are made. The next chapter, Chapter 4, will highlight the developed methodology. This consists of three parts, namely the initial power flow calculation, its linearisation and finally the reconfiguration algorithm itself.

Once the methodology is in place, several scenarios are formulated to test the functionality of the reconfiguration algorithm in Chapter 5. Subsequently, the results of utilising the reconfiguration algorithm on these scenarios are presented in Chapter 6. This chapter will also present a comparison with two other network topology optimisation methods, those being an iterative exploration of meshes and a genetic algorithm, both implemented in PowerFactory.

Finally, a brief summary is provided in Chapter 7, as well as the most important conclusions which can be drawn based on the obtained results. The thesis is completed with several recommendations for future work and possible enhancements of the presented work.

2

Review of theoretical background

To ensure that this thesis can be viewed as a largely self-contained comprehensive work, the following chapter will ensure that the key aspects which are considered are explained in order to facilitate a common point of available information. To be specific, this chapter will give insight into several aspects of the electricity grid, including the operation thereof in Section 2.1. The problems regarding network overloading, the subsequent congestion and possible congestion management techniques will be highlighted in Section 2.2. An analysis of modelling techniques in regards to the electricity network is covered in Section 2.3. This is followed by an analysis of the different constraints, which form the core of these models, in Section 2.4. The Optimal Power Flow (OPF) will be discussed in Section 2.5. And finally there will be a thorough analysis of different advances within network reconfiguration in Section 2.6.

2.1. Distribution systems

The electricity network is divided into different systems, where the transmission system and distribution system are designated by their purpose and/or voltage magnitude level. The transmission system connects the largest power plants to the electricity system and the distribution system distributes the electrical energy between the connected loads [13]. According to voltage level, the system is divided into a high-voltage (HV), medium-voltage (MV) and low-voltage (LV) system. What voltage ranges constitute these levels can differ per country. In the Netherlands, the HV is designated as voltages above $35kV$, the MV ranges between $1kV$ and $35kV$ and the LV is designated as voltages below $1kV$ [14]. The transmission system is usually equivalent to the HV system and the distribution system always includes the LV system. The MV system is somewhere between these two and its exact purpose can differ. It can fulfil both the task of transmission and distribution, but it is primarily associated with the distribution system.

The electricity network structure is formed by the overhead lines, the underground cables, the transformers and the buses between the point of power injection and power consumption [13]. According to [13] the network structure can be designed as either a radial structure, a loop structure or a multi-loop structure. A radial structure is characterised by all nodes being supplied by a single line, which is the least expensive option. In a loop structure every node is fed from two directions, which results in a higher reliability but also higher costs. Finally, in the multi-loop structure the nodes are supplied from more than two directions. These types of networks are very reliable but also the most expensive out of the three.

In the Netherlands most distribution networks have a loop or multi-loop structure but are operated as a radial network, as this keeps the protection of the network simple [13] and it reduces the short-circuit current [15]. This is implemented by means of switching devices within the network which are normally open, but can be closed in order to change the topology of said network. A topology change may be desired when the network experiences a fault. A fault can have different causes and implications, but in general it refers to one or multiple components inside the network structure being out-of-order for a certain time. A line outage is an example of such a fault, which in turn can be caused by congestion. An illustrative example is given in Figure 2.1, where a 6-node network is supplied by an external grid. Between nodes 3 and 4 there is a normally open switch (NOS) and the flow of power is indicated by the green arrows. In Figure 2.1a all six nodes are supplied.

However, a fault occurs between node 1 and node 2, as displayed in Figure 2.1b. Now, due to the line outage, nodes 2 and 3 are no longer supplied with power. To remedy this, NOS is closed and the line between node 1 and node 2 is taken out of service for maintenance, as is shown in Figure 2.1c. Now every node is supplied again.

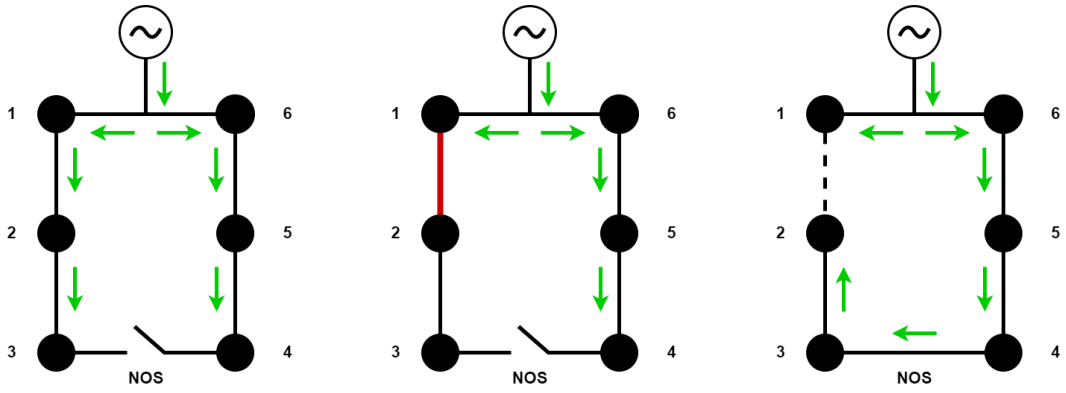

(a) Original network layout. NOS is a normally open switch, but can be closed.

(b) A fault occurs in the line between nodes 1 and 2 (indicated in red), resulting in a line outage.

(c) The line between nodes 1 and 2 is taken out of service (indicated by the dotted line). NOS is closed to ensure the entire network is still supplied.

Figure 2.1: Network reconfiguration due to a line fault.

According to the formal European definition, distribution system operator means: "a natural or legal person who is responsible for operating, ensuring the maintenance of and, if necessary, developing the distribution system in a given area and, where applicable, its interconnections with other systems, and for ensuring the long-term ability of the system to meet reasonable demands for the distribution of electricity" [16].

The distribution networks in the Netherlands are mostly owned by independent network companies, since they were unbundled from the energy companies in 2010 [17]. Due to unbundling rules, DSOs cannot own (or invest) in generation facilities and are instead meant to provide access to the grid in a cost-effective manner, irrespective of the technology or geographical location. In this context, uncertainties due to, for instance, planning consents or financial support pose DSOs with major challenges as to what, where and when to reinforce the electricity network in order to provide connections without the risk of stranded assets [18].

The tasks of a DSO are diverse, but can be summarised as the following: allow for the transportation and trade of electricity on the distribution network, maintain the operational security of the system and ensure maintenance, repairs and expansions of the grid are carried out as necessary. The specific legislative responsibilities for DSOs in the Netherlands are found in Article 16 of the so-called 'Elektriciteitswet 1998' [19], freely translated as 'Electricity law 1998'.

In order to carry out these responsibilities the DSO has multiple methods at its disposal. Most relevant for this thesis are the congestion management methods, multiple of which are outlined in [4]. The methods include both indirect methods, which are mostly market-based, and direct methods. The indirect methods include, but are not limited to: day-ahead dynamic tariff, distribution grid capacity market, intra-day shadow price and flexibility service market. The direct methods include: grid reinforcement, network reconfiguration, reactive power control and active power control. In a worst-case scenario a DSO can also resort to curtailment, where certain loads or generators are temporarily disconnected from the grid.

2.2. Congestion

Congestion has been mentioned multiple times throughout this work as being one of the key problems facing the modern electricity network due to the increase in DERs. A concrete example of such a situation can be found in [20], which is a report commissioned by one of the Dutch DSOs to investigate the possibilities of congestion management techniques for the substation Middelharnis. The report is originally in Dutch and

references to the work in [20] will have been freely translated where applicable.

The report separates the investigation into three parts, namely: predicted future demand of transport capacity, technical congestion management techniques and market-driven techniques. The future scenarios are based on planned enlargement of the local generation capacity. Based on this increase, it becomes apparent that the region will be facing structural congestion. However, technical congestion management techniques are not applicable due to a lack of remote control and information of the switching gear. This lack of remote control of switching gear is also one of the key factors which prevent the application of active network reconfiguration, as discussed in Section 1.2. Furthermore, market-driven congestion management is also not possible due to a lack of applicable parties who could contribute to such a market.

This is not the only example of such a report in recent times ([21] [22] [23]), which is to be expected considering the incredible scale of structured congestion within the Netherlands as highlighted in Figure 1.1. However, it does highlight the common approach for determining structural congestion and the possibility for congestion management techniques.

Examples of both market-driven and technical congestion management can be found in [6]. The market-driven congestion management techniques are separated into price-based and incentive-based techniques. Here, price-based refers to flexible demands responding to the changes of electricity prices by adjusting their consumption profiles. For the incentive-based, one example given is to build a flexibility market in which the DSO can procure flexibility products to handle congestion [6]. The work in [6] goes on to combine a price-based technique of dynamic tariffs with a direct control method of network reconfiguration and an incentive-based technique of re-profiling. By combining the different techniques, the authors attempt to overcome the drawbacks of using any of the methods in a standalone implementation. However, the considered time frame is day-ahead, which makes application in the current grid of the Netherlands rather unrealistic due to the aforementioned lack of remote control of switching gear.

A great example of incentive-based techniques can be found in the Netherlands in the form of GOPACS. GOPACS is an initiative by the Dutch DSOs and TSO to reduce congestion by making use of market-driven flexibility offers by grid-connected parties. When a situation of congestion occurs, it is entered into GOPACS and a market message is issued. Market parties with a connection in the affected area can then place an order on a participating market platform, like ETPA [24]. However, as was discussed in Section 2.4, the power balance in the electricity grid needs to be kept. To do this, the order of decreased electricity consumption inside the congestion area is combined with an opposite order to increase electricity consumption outside the congestion area. GOPACS is responsible for checking if the order does not cause problems elsewhere and if this is not the case, then the order is accepted. If every part is verified and accepted, the grid operators will pay the price difference between the two orders. In this way the two orders are matched on the market platform and the congestion situation can be solved [24].

2.3. Network modelling

In order to analyse a situation of congestion, it is necessary to be able to model the electricity network first. However, the modelling of the electricity network is used for a multitude of reasons, ranging from active monitoring of the state of operation of the grid to discerning certain characteristics like the power flowing through it. Most of the publications analysed in this work, research aspects of the grid related to its topology and capacity. The main topic under consideration is network reconfiguration, but this is detailed later in the chapter in Section 2.6. Another reoccurring topic related to network planning is that of hosting capacity in relation to the placement of DERs. While this is not the same as the network reconfiguration, it shares many of its objectives, where the network layout is modelled and analysed for possible occurrences of congestion [5].

The diversity in modelling objectives also leads to a diversity in modelling techniques. In [18] a number of modelling techniques for distributed generation planning are discussed. These methods include the following.

- Analytical analysis
- Exhaustive analysis

- Linear programming
- Optimal power flow
- Metaheuristics
- Probabilistic analysis

Both the network reconfiguration and hosting capacity utilise the optimal power flow (OPF), which will be discussed in detail in Section 2.5. But, before that, there are a few more points to discuss regarding the network modelling, in particular the recent advances therein. When taking the modelling of the network as a topic itself, a recent publication which concerns itself with the modelling of the distribution network can be found in [25], which holds particular interest for this thesis due to its considerations in regards to the modelling of the feeders. It is important to note that [25] is based on the Australian electricity network, meaning that 22 kV is already designated as HV, while this would be MV in the Netherlands.

The work in [25] provides a step-wise analysis of the different network components which will be modelled, like: cables and overhead lines, substations, transformers, capacitors and the coordinates of these different components. As well as the different parameters relevant to the modelling. For cables and overhead lines for example, this includes parameters like the type and length, but also the positive and zero sequence resistances, reactances and capacitances. The authors of [25] go on to present the topology and general characteristics of four modelled feeders, including the behaviour of the feeders using data from a preceding project.

Another project from the same university is presented in [1], which also makes use of the data presented in [25] for the feeder modelling. The report presents the modelling considerations and results of a highly-granular, detailed EV hosting capacity assessment done on urban and rural networks in Australia. The work includes the demand-profile modelling of the EVs, the PV generation and the resulting case-studies in the subsequent chapters. The work in [1] considers six different case-studies. They do not differ in terms of modelling approach, but they represent the six different feeders which are considered.

Both [1] and [25] represent a similar modelling approach for the grid model as is used for the original grid in this thesis. However, instead of a simulation in OpenDSS, as is done in [1], the model has been made in PowerFactory. A full analysis of this model is made in Chapter 3. For now, it is important to note that one of the aspects which can be modelled with the use of similar network models is the occurrence of congestion within the network. This is a key feature necessary to validate the results of the network reconfiguration algorithm.

2.4. Grid constraints

At the core of the network models and the operation of the grid itself are the grid constraints. The constraints can be legislative in nature or practical for the sake of maintaining the operation of the system. In either case, the constraints all originate from the responsibilities of the DSO, which is ensuring the continued operation of the grid. The DSOs also have the responsibility to grant grid access to the users, within predetermined quality limits with respect to voltage and frequency stability in order to prevent damage to the assets behind the connections [26].

The legislative constraints for the distribution system operators are mostly captured in the 'Electricity Law 1998' [19] and the Dutch grid codes, which can be found in [14]. However, a couple of aspects are interesting to specifically highlight here.

One of the most important aspects of the electricity system is that generation and consumption of electricity need to be in constant balance. This balance is required because it is not possible to store large quantities of electricity inside the grid. As such, all electricity which is generated needs to be (almost) instantly consumed. This constraint of power balance is also included in article 1.1 p of the 'Electricity law 1998' [19].

Another important constraint usually maintained during the operation of the electricity grid is the so-called N-1 constraint. The N-1 constraint is a standard maintained by most system operators, which entails that the entire system should continue operation in case a single component fault occurs without loss of load or

violating any operating constraints [27]. This standard is usually maintained during planned maintenance work by the system operator.

While this standard is commonplace for most DSOs, it is not a legislative requirement. The DSOs choose to maintain this standard in their system. As a result, there are usually some places inside the network which are only N secure (meaning that any component failure may result in violation of operating constraints). These parts of the grid are primarily encountered in areas where there is distributed generation. However, in such cases there is always the drive to go to a N-1 secure network.

It is also possible to identify several constraints based on existing literature in which the grid is modelled ([4], [5], [15], [28], [29], [30], [31], [32]), such as:

- **Power flow constraints**
  Problems like congestion are formed by overloading of the lines and cables which need to facilitate the transport of power. Most lines therefore have maximum loading constraints associated with the power flowing through them.
- **Voltage constraints**
  The voltage within the system will fluctuate due to imbalances. As such it forms an indicator of the system state. The voltage should thus remain within certain boundaries to guarantee the functionality of the grid. This is mostly implemented through maximum voltage deviations.
- **Current constraints corresponding to thermal limits**
  When current is going through lines they will heat up as a result of energy losses. The materials forming the different components of the electricity system (like the lines and transformers) have a certain maximum thermal limit which they can withstand before they are being permanently damaged. Thus, it is important to keep the current below values where such a situation can occur.
- **Network radiality constraints**
  As was mentioned in Section 2.1, most distribution networks have a loop or multi-loop structure, but are operated as a radial network. As such, when a certain topology for the network is considered, it is important that it is formed as a radial network rather than a loop or multi-loop structure.

The above constraints are usually supplemented by case-specific constraints based on different aspects of the grid operation and stability, but these are not relevant to the general considerations outlined here.

2.5. Optimal power flow analysis

An optimal power flow (OPF) analysis is a load flow computation, in which the calculation of the node voltages and the optimisation of the controllable variables are carried out simultaneously. The load flow computation solves the node voltages in a given network under specified load conditions and generation [13]. The OPF can be used for a number of applications, including but not limited to: state estimation and energy management, charging of plug-in electric vehicles, unit commitment, voltage stability and voltage regulation in power distribution systems [33]. Concrete examples of the use of OPF can be found in [28] and [30]. The work in [28] relates to Section 2.2 as it uses OPF to mitigate congestion in the distribution network. Meanwhile, [30], relates to Section 2.4, as it proposes a mathematical model to manage all technical operating constraints affecting distributed generation penetration within a distribution network by the use of OPF.

More recent work regarding different OPF applications can be found in [34], which discusses a number of optimal power flow applications including expansion planning, regular operation, markets, network resiliency, and unit commitment. Each of the discussed applications holds some relevance as to how to handle uncertainty: whether by stochastic programming, robust optimisation, or alternative definitions of risk [34]. This also returns in [35], which discusses deterministic OPF, risk-based OPF, and OPF under uncertainty. Here, risk-based OPF utilises risk-based security criteria which depend on the assumed contingency probabilities. This form of OPF can be divided again depending on the implementation of risk, ranging from: an additional term in the objective function, one overall risk constraint, a combination of both, or one risk constraint per individual contingency [35]. The OPF under uncertainty stems mostly from the increase in penetration of

renewable energy sources (RES) within the grid. Additionally, with the transition toward smarter grids, deferrable loads and storage devices also contribute towards the higher uncertainty.

All of the above examples utilise OPF in some way. While they may all be different, they do share the same fundamental formulation. A general abstract formulation for the OPF is provided in [13] and copied here for convenience.

$$\begin{aligned} \text{Minimise} \quad & f(\mathbf{x},\mathbf{u}) \\ \text{Subject to} \quad & \mathbf{h}(\mathbf{x},\mathbf{u}) = \mathbf{0} \\ & \mathbf{g}^{min} \leq \mathbf{g}(\mathbf{x},\mathbf{u}) \leq \mathbf{g}^{max} \\ & \mathbf{u}^{min} \leq \mathbf{u} \leq \mathbf{u}^{max} \end{aligned}$$

Where $\mathbf{x}$ is the vector with the state variables, such as the unknown voltages. $\mathbf{u}$ is the vector with the controllable variables, such as the injected power. f($\mathbf{x}$,$\mathbf{u}$) is the objective function, which could be minimising the losses for example. $\mathbf{h}(\mathbf{x},\mathbf{u})$ is the vector with the equality constraints, such as power balance. And finally, $\mathbf{g}(\mathbf{x},\mathbf{u})$ is the vector with the inequality constraints, such as maximum and minimum voltage limits.

The optimal power flow can be formulated in different ways. These primarily correspond with the typical optimisation classifications: linear, quadratic and nonlinear. The OPF without simplifying assumptions is formulated as a nonlinear program [13], which in literature is often referred to as ACOPF [36]. This formulation can be hard to solve directly and is therefore more commonly solved using an iterative method. Commonly, the Newton-Raphson method as described in [13] is used, for example in the widely adopted simulation software PowerFactory [37].

An example of recent work in ACOPF can be found in [38], where an iterative approach is suggested to improve the quality of solutions for ACOPF problems. The main motivation being that existing solvers for ACOPF problems are generally successful in finding local solutions, which satisfy first and second order optimality conditions, but they cannot guarantee a global optimum. The iterative process relies on duality theory, utilising the output of each iteration to warm start existing solvers for the subsequent iteration. To be precise, the solution of the NLP solver is used to formulate a partial Lagrangian, which in turn is minimised. The solution of this minimisation is used as the new initial value for the NLP solver. This process is repeated until the solutions stop changing or up to a predefined number of iterations [38].

To reduce the computation time, a linear approximation of the OPF can be made, this is also referred to as DCOPF [13]. The DCOPF is principally different from the ACOPF. This is due to the DCOPF linearising the nonlinear load flow equations, which will affect the final result. The following approximations are made for the DCOPF [13]:

- The node voltage magnitudes are 1 per unit (pu).
- The resistances of the lines are neglected.
- The differences between the voltage angles are small.

In most cases both the linear and nonlinear version can be formulated and the main trade-off will be in regards to the accuracy of ACOPF, compared to the computation time and convergence of DCOPF [39]. In that regard, [39] provides a welcome complement to the work in [13] by formulating a complete DCOPF in a stepwise manner. An example of recent work in DCOPF can be found in [40], where a new linear model for line losses is introduced. Similar to the motivation for DCOPF over ACOPF, the advantage of the method is that it can be used for large networks and does not require AC feasible prior points as warm starts. Being an outer approximation method, it can be used for multi-period, stochastic optimisation problems and also on mixed-integer programs [40].

Another formulation for the OPF is by means of semidefinite programming (SDP). This approach was first applied to OPF problems in [41], where the OPF is first formulated as a quadratic problem and then transformed into a SDP. The SDP formulation is subsequently solved using an Interior Point Method (IPM), which

can guarantee a global optimal solution. The advantage of SDP combined with IPM is that it is convex and does not require deriving and computing the Jacobian matrices and the Hessian matrices for each particular problem separately [41]. Additionally, it can be solved using well-developed linear solvers. A disadvantage of the SDP formulation presented in [41] is that the CPU and memory usage is severely larger than for a NLP formulation, especially for larger systems. Additionally, the SDP relaxation of the ACOPF is able to provide an optimal solution for radial networks, provided that there is no lower bound on generation. If this bound is present however, the SDP relaxation can have three possible approximation outcomes: (1) SDP relaxation may be exact, (2) SDP relaxation may be inexact, or (3) SDP relaxation may be feasible while the optimal power flow (OPF) instance may be infeasible [42].

More recent usage of the SDP for OPF can be found in [33] and [43]. The work in [33] seeks to extend the types of networks for which SDP relaxation on the OPF can be used, which in most cases is limited to radial networks. The authors of [33] investigate sufficient conditions for which the SDP relaxation is exact for specific cyclic networks. It is important to note that the conditions under which this work is applicable are somewhat strict, requiring the objective function to be specified as a linear function of active powers or an increasing function of reactive powers. The work in [43] on the other hand, tries to broaden the applicable objective functions for SDP relaxation. Due to the rising demand for electricity, as was also discussed in Chapter 1, various aspects, such as minimising fuel costs, losses, environmental pollution, and so on, are essential to be taken into consideration for satisfactory power system operation and planning [43]. The work in [43] offers a way to cope with this multitude of objectives by investigating multi-objective OPF with the use of SDP. The presented method is able to outperform heuristic methods generally used for the solution of multi-objective OPF [43].

Recent works also highlight OPF as a tool for both technical and market-driven congestion management techniques. Both of which are considered when trying to resolve congestion, as became apparent from Section 2.2. An example of technical congestion management is network reconfiguration, which is covered in the next section (Section 2.6).

An example of market-driven congestion management through the use of OPF can be found in [44]. In [44], OPF is used as a tool to solve the congestion management problem in relation to the centralised market and the bilateral and multi-lateral transactions. The OPF is implemented with the use of a genetic algorithm called Enhanced Genetic Algorithm. A traditional genetic algorithm is capable of locating a near-optimal solution, but requires a large number of iterations to converge. An enhanced genetic algorithm makes use of problem-specific operators, derived from the nature of the problem, to enhance the performance [44]. However, it is important to note that deterministic calculations based on future scenarios are not possible with genetic algorithms due to their probabilistic nature.

2.6. Grid reconfiguration

Reconfiguration in the grid refers to a change of the grid structure or topology by changing the status of the normally-open switches and normally-closed switches [4]. The basic action of grid reconfiguration, as presented in Figure 2.1, is already discussed in Section 2.1. However, this discussion is an example of network reconfiguration as a corrective action, when a fault has already occurred. The goal of network reconfiguration in the context of this work is as a preventive action. The reconfiguration is meant to prevent a situation of congestion from occurring by minimising the branch overloads while also keeping the number of control actions taken by the DSO to accomplish this to a minimum. The first part of this goal, minimising branch overloads, should result in a reduction in the occurrence of congestion. The second part has to do with the operation of the grid. The control actions, or in this case the switching actions, can accelerate the degradation of expensive switching gear, such as circuit breakers, and it may also lead to system instability [31]. As such, it is important to minimise these actions when network reconfiguration is implemented.

The applicability of network reconfiguration in improving the operation of the grid has been proven in numerous works of literature. It can be implemented as both a preventive action before a contingency occurs in the system, or as a corrective action. The preventive action identifies the optimal base-case topology to serve the demand, while the corrective action (implemented after the contingency has occurred) can reconfigure the lines to actively change the power flow, which in turn should relieve post-contingency network congestion

[32]. Both implementations can lead to reduced losses (and subsequent cost savings) and reduced branch overloading [29] [31] [45] [46].

2.6.1. Historic analysis

The first proposal of using grid reconfiguration in the distribution system was made as early as 1975 in [47], for the purpose of minimising line losses. Utilising corrective switching as a means of reducing network overloads was already proposed in the 1980s [29].

Despite the field of study already existing for several decades, network reconfiguration, especially on shorter time-scales, remains a tool which only sees infrequent use. Part of the early reason can be found in [48], which presents a review of the literature up to 1999. One of the main difficulties identified for implementing network reconfiguration is in regards to the discrete values which represent the current state of the switches (either open or closed) and the computing power available for implementing the algorithms. A similar conclusion in regards to the computing power is drawn in [49] for genetic algorithms.

However, due to the ever-increasing computing power, these problems are disappearing; although exceptions do remain, such as AC-based network reconfiguration. In fact, the first formulation of AC-based optimal transmission switching (which is implemented as a mixed-integer nonlinear program formulation) was introduced as late as 2012 [34] in the work of [50], 37 years after the first publication regarding grid reconfiguration.

For a very detailed outline on the publications surrounding network reconfiguration, interested readers can also refer to [51], in which a review is presented for publications related to network reconfiguration of almost every year between 1975 up to 2020.

2.6.2. Grid reconfiguration formulation types

The problem of distribution network reconfiguration is a highly complex, combinatorial, non-differentiable, non-convex, mixed-integer nonlinear program (MINLP) optimisation problem, due to the binary status of the switches and nonlinear three-phase power flow equations [29] [41] [52]. Network reconfiguration can be viewed to be an extension of an OPF, adding additional variables and constraints to account for the status of the switches, but this also represents a considerably greater computational burden [12]. Add to this the radiality constraint as discussed in Section 2.4 and the problem can be considered complicated [15].

Multiple formulation types have been developed over the years in order to encompass the most relevant aspects within the considered model. To keep this as a largely self-contained comprehensive work, the most common examples of possible formulation types are briefly outlined below to highlight their applicability, advantages and disadvantages, which hold for any implementation utilising such a formulation.

MINLP

The deterministic formulation of the network reconfiguration is a MINLP. One of the main benefits of the MINLP formulation is that it does not take any simplifying assumptions and as such it can be argued that the MINLP represents the problem the most accurately, but this comes at the expense of higher complexity and a longer computation time. However, the application in this work does not need fast computation times as it is considering future scenarios and seasonal time-scales. Thus, this disadvantage has little impact on the considerations made for this thesis.

What does form a disadvantage in regards to the MINLP formulation for application in this thesis is the availability of solvers which can handle MINLP problem formulations with large problem sizes. The problem under consideration is a MV electricity distribution grid, which usually consists of over a hundred substations and even more lines and cables interconnecting them. Most readily available software which can handle MINLP to begin with can only do so for small problem sizes, which makes application in this thesis difficult. This does not mean that MINLP solvers do not exist. An example is the KNITRO solver, however this solver is only capable of solving convex MINLP and is a heuristic for non-convex problems [53].

MILP

The MINLP problem can be linearised to a mixed-integer linear program (MILP) by formulating the problem using DC approximations [39]. This is identical to the linearisation discussed for the OPF in Section 2.5. The

advantage of the MILP formulation is that it reduces the computational complexity and the solution process is deterministic. Examples of such an implementation can be found in [39] and [54].

NLP or LP

Alternatively, the integer part of the MINLP formulation is removed and instead incorporated into the solvers (or the solving process) of a NLP. A linearisation can be applied in combination with this approach to achieve a LP. However, a disadvantage of this method is that the global optimum may not be found [4]. An example of a NLP formulation can be found in [55], where the problem is originally formulated as a MINLP, but the solver which is used necessitates it being implemented as a NLP.

Meta-heuristic approaches

The formulations above are all deterministic approaches. Many sources also consider a meta-heuristic approach for the network reconfiguration, for example the so-called genetic algorithms (GA) [28] [44] [56]. An advantage of meta-heuristic approaches, such as GA, is that they provide multiple potential solutions, rather than just a single optimum [44]. Additionally, the radiality constraint for the network topology is imposed implicitly [28] and does not need to be explicitly implemented as a constraint. However, one of the main drawbacks of meta-heuristic approaches is that they do not guarantee to find a global optimum and they tend to be more computationally intensive than for example a MILP formulation.

A detailed description of a genetic algorithm applied to network reconfiguration can be found in [46]. A comparison between a MILP formulation and a genetic algorithm is made in [29], where the authors conclude that the MILP is better suited for online application due to its faster and guaranteed convergence. The GA is argued to be better for offline applications as it is more versatile in its application.

2.6.3. Recent advances in grid reconfiguration

Finally, to highlight some of the more recent works regarding grid reconfiguration specifically. To provide a better overview, the references have been ordered according to a general topic, but there will be overlap between them.

Uncertainty modelling

As good a place as any to start is the increase in uncertainty modelling and the role of network reconfiguration therein. Due to the increased penetration of RES and the increase in energy demand, the energy system is experiencing a rise in uncertainty considerations for both energy demand and generation. Matching this rise, is a rise of research into this topic.

A good example of uncertainty modelling concerning network reconfiguration is presented in [57], which analyses the effect on the active power losses and voltage stability inside a distribution network when both distribution network reconfiguration and optimal distributed generation allocation are incorporated in the system, making use of probabilistic load flow (PLF). The optimisation is solved using a meta-heuristic technique, called: adaptive modified whale optimisation algorithm A-MWOA. Additionally, the work in [57] presents a method to check the radiality constraints by using Depth First Search Identified Matrix (DSIM). Both the A-MWOA and the DSIM are described in a step-wise manner with pseudo-code being provided for the implementation. The PLF is implemented using two different point estimate methods, namely: probabilistic two-point estimate method and probabilistic three-point estimate method, the main difference being that a two-point estimate takes less time while a three-point estimate is more accurate.

The used algorithm is able to find an optimal radial network configuration, where more reactive power capability is provided. However, similarly to many publications, the considered time-frame (being real-time in this case), prevents industry adaptation (at least in the Netherlands) in the short term due to a lack of remotely controllable switches.

Another example of uncertainty modelling is given in [31], where stochastic optimal power flow (SOPF) with the inclusion of network reconfiguration in the dispatch model is analysed. The motivation for utilising SOPF instead of OPF is that the deterministic approach of OPF largely ignores the uncertainty associated with intermittent renewable power. The SOPF is implemented in four different variations, namely: relaxed SOPF,

normal SOPF, enhanced SOPF and enhanced SOPF with network reconfiguration. Here, the relaxed SOPF is used as a baseline for comparison of the congestion-induced costs. The normal SOPF only includes base-case network constraints while the enhanced SOPF also includes contingency-case constraints. Finally, the enhanced SOPF with network reconfiguration also includes post-contingency network reconfiguration [31].

The work in [31] goes on to show that network reconfiguration can relieve congestion and reduce congestion-induced undesired renewable curtailment. However, similar to many other publications, [31] considers the network reconfiguration as a corrective action. This presents an unlikely implementation for the current MV grid in the Netherlands due to the manual nature of the switching operations, rather than automated remote operations. Not only that, but the authors themselves also point out that the SOPF with network reconfiguration is much more computationally intensive than a normal OPF, resulting in longer simulation times and a subsequent inability to be used as a corrective action, at least for now.

A broader concern for the uncertainty considerations is given in [58], which also regards more traditional sources of uncertainty, such as weather conditions, or the more recent COVID-19 pandemic which greatly altered energy demand and generation. To be specific, the work in [58] covers a base-case scenario of a distribution network, which is subsequently compared to a scenario with load variation and a scenario with a line outage. In order to solve the reconfiguration optimisation, the authors propose the usage of the meta-heuristic Manta Ray Foraging Optimization (MRFO), which is also the main novelty of the publication. MRFO has a search mechanism where it moves between different update procedures of found solutions, which aims to enhance the chance of avoiding local optimal solutions and instead find near-optimal solutions [58].

Despite the increases in uncertainty, there is also an increase in available data to help cope with this uncertainty. SCADA has traditionally been the main measuring equipment of the grid, nowadays being supplemented with the rising deployment of smart-meters [52]. However, the relatively new technology of Phasor Measurement Units (PMU) offers great improvements compared to the SCADA system. A comparison between the two can be found in [59]. Relevant to this thesis is that the PMU also enables research as presented in [52].

The work [52] proposes a data-driven method based on the measurements of μPMUs [60] to determine the hourly optimal configuration of a distribution grid in a real-time manner. To be specific, the authors propose a two-phase method. First, the node voltage and injected current phasor measurements of the μPMUs are processed via a linear state estimation to determine the net load at each node. Subsequently, this data was analysed using a bi-level information granulation [52]. Second, the output of the first phase provides the probability distribution (or uncertainty bounds) and numerous information granules for running a stochastic robust optimisation (SRO) to determine the optimal hourly network reconfiguration in real-time, which is modelled as a Mixed Integer Second Order Conic Programming (MISOCP) problem [52]. One of the interesting advantages presented in [52] is the robustness of the method to generation and load uncertainties, which is due to the uncertainty bounds being based on the measurements of μPMUs in real time without using forecast models.

Machine Learning

The method described in [52] utilises machine learning in parts of its process. Indeed, the authors of [52] state that one of the best ways to take advantage of the μPMUs data is through machine learning. Although the topic of machine learning itself is outside the scope of this thesis, the advances made with the application thereof are still interesting to explore.

The uncertainty considerations within network reconfiguration with the application of machine learning returns in [61] for example, which considers a multi-objective stochastic network reconfiguration model, which balances absorption rate of high penetration wind power generation and voltage stability. To be specific, the work in [61] develops a modified multi-objective Bayesian optimisation algorithm (MMOBOA) to obtain a Pareto front. This will represent the trade-off between absorption rate and voltage stability. Next, a technique for order preference by similarity to an ideal solution (TOPSIS) is used to determine the reconfiguration, by comparing the solution to a pre-defined ideal solution.

The MMOBOA iteratively searches for non-dominated solutions, which are kept in an archive. Then, MMOBOA applies a Bayesian network to estimate the joint probabilistic distribution of these non-dominated solutions, where a new population is generated by hierarchically sampling the obtained Bayesian network [61]. The MMOBOA is designated as an evolutionary algorithm in [61] and as such its results are compared with other evolutionary algorithms. The MMOBOA demonstrates a solution with lower curtailment of wind power and lower voltage deviation compared to the considered algorithms. However, no results are presented regarding the computation time, nor about other types than the evolutionary algorithms, making it hard to infer the applicability of the presented work.

The consideration of voltage stability is also analysed within [62], which goes over the development of a deep learning-based method (DLBM) for distribution network reconfiguration (DNR) with the goal of short-term voltage stability (STVS) enhancement. The main cause of short-term voltage instability, according to [62], is the tendency of dynamic loads to restore consumed power in the time frame of a few seconds. With the increase of DERs and the growth of low-inertia compressor motor loads, the STVS issues become more prominent [62].

In [62] a STVS evaluation network is implemented, based on deep convolution neural networks (CNNs), in order to map the distribution network topology and system parameters onto the STVS performance, which is trained using historical data. Next, the STVS evaluation network estimates the root-mean-squared voltage-dip severity index (RVSI) of all considered topologies and shortlists the topologies that meet the STVS requirement [62].

The results presented in [62] are positive with regards to efficiency and reliability. Additionally, according to the authors, the scalability of the presented work for large-scale systems can be extended by combining it with heuristic search algorithms. However, much like the other works presented in this section, the application is oriented on small time-scales, preventing short-term adaptation.

The work in [63] presents another example of machine learning applied to network reconfiguration. In particular, the work presents a Reinforcement Learning (RL) based approach to train agents that proposes topology control actions to a system operator. Emphasis is placed on the potential application of RL-based agents to act in conjunction with human network operators in the form of decision support tools, able to identify and suggest control actions that human operators and traditional solution techniques are unaware of or unaccustomed to [63].

The policy of the agent is modelled using a feed-forward neural-network with 2 hidden layers. The input layer has the size of the state space (which includes generator, load and line parameters). The size of the output layer consists of the action space (represented by the different possible implementations of the network topology) [63]. The reward at each time step reflects the remaining available transport capacity: the loading of all lines are combined and the reward increases (decreases) if the loading of the network decreases (increases) [63]. The approach in [63] shows good convergence and a capability for generalisation. It is expressed that the RL approach presented is well-suited as a baseline for future studies on larger and more realistic power networks, as the approach itself is rather simple and only considers a small network with a single scenario.

Model effectiveness and efficiency

One of the simplifications made in [63] is neglecting the radial operation of most distribution networks, as discussed in Section 2.1. The topic of radial operation itself also remains a point of improvement, as is discussed in [64]. In particular, the main concern raised in [64] is that existing methods of formulating the radiality constraints can cause under-utilisation of distribution system flexibilities.

A different radiality constraint is proposed and implemented as a two-step method. First, network radiality is ensured by having a spanning tree as the distribution system's topology super-graph. Second, a more flexible reconfiguration in enabled by allowing the distribution system to select a sub-graph of the spanning tree to be the actual network topology [64]. Another way of looking at this implementation is that the final network topology is allowed to be a combination of smaller sub-networks which operate independently, rather than one connected network.

The proposed method enables more flexibility when considering network reconfiguration. Given examples include: more adaptive merge or separation of sub-grids and more flexible allocation of power sources into sub-grids [64]. A disadvantage of the work in [64] is the assumption of forming sub-networks within the distribution grid as a consequence of the spanning tree super-graph and the spanning forest sub-graph, which may not be desirable or even allowed. Additionally, the focus is on network reconfiguration as a corrective action, whereas this thesis has a focus on preventive actions.

One of the main concerns raised in Section 2.6 in regards to network reconfiguration is the model efficiency (computation time for larger systems, convergence rate, etc.), which also returns in the work presented in [31]. An example of recent advances towards higher efficiency is presented in [51], which presents a mathematical model for loss minimisation in distribution network reconfiguration, considering the system voltage profile. First, a classical formulation of the problem as a MINLP is made. However, the nonlinear nature of the problem prevents the use of fast linear solvers. Thus, the authors of [51] also present the problem modelled as a convex mixed-integer conic program (MICP), which allows the use of linear solvers which are (usually) more efficient than nonlinear solvers. The authors of [51] go on to describe several different case studies in which network reconfiguration is applied and they also present a section dedicated to comparing the obtained results to previous works. However, one of the major drawbacks of any convex formulation is that verifying convexity can be hard and one of the common approaches of only allowing for modelling operations that preserve convexity [65] may not always be feasible.

Similarly, the model efficiency (in particular the computation time) can be improved upon for the meta-heuristic algorithms. Recent work in this regard can be found in [66], which presents a multi-step reconfiguration procedure, utilising the recent Harris hawks optimisation (HHO) algorithm accompanied by pre-processing of the search space and initial feasible population generation, as well as post-processing regarding solution refinement. These phases are aimed at improving the search for near-optimal configurations, within a reasonable time.

HHO is a recent population-based nature-inspired meta-heuristic algorithm proposed in [67], which mimics the hunting behaviour of Harris-type hawks [66]. Interesting to note is that meta-heuristic algorithms were initially used for defining real-valued solutions in continuous optimisation problems. However, the network reconfiguration requires integer values to correspond with the switch positions [66]. To this end, the work in [66] utilises a rounding procedure before evaluating the corresponding performance.

The results presented in [66] are especially positive regarding larger networks, providing the highest performance in terms of minimised power losses and enhanced voltage profile, with the highest success rate and the lowest running time compared to the other considered meta-heuristic algorithms (the other two being particle swarm optimisation and the Cuckoo search algorithm). The main drawback of the work presented in [66] is that it considers a single-phase model, rather than a three-phase one. This limits the direct applicability of the results to the more typical three-phase distribution systems as they cannot be verified.

To continue along the trend of improving the computation time, the work in [68] analyses the computational complexity of dynamic reconfiguration in near real-time and the underlying optimal scheduling problem. Since the full dynamic reconfiguration problem has been considered computationally intractable, the approaches found in literature treat the problem approximately, not fully addressing its complexity, according to [68]. Contrary to this, the authors of [68] present a future prospect utilising quantum computing to handle this full complexity and enable the computation of the optimal solution.

A number of different formulations are explored and compared on problem complexity, number of operations and computation time. The formulations include: unrestricted optimal reconfiguration, optimal static configuration, time-bounded linear dynamic reconfiguration, time-unbounded cyclic dynamic reconfiguration and open cyclic dynamic reconfiguration. The work in [68] continues to show how the complexity of the optimal reconfiguration problem scales with the number of candidate switching operations, rendering the problem infeasible in practical terms with just three operations.

To resolve this practical infeasibility, the authors of [68] propose new approaches based on quantum computing as realistic options to solve the problem in the future. What enables quantum computing to potentially

acquire an effective solution is based on the unique phenomena of quantum superposition and quantum entanglement which enables the computation parallelisation with an exponential scaling with the quantum hardware size (or the number of quantum bits) as opposed to the linear scaling with the number of cores of classical computing [68]. However, it should be noted that this is still speculation. As the authors of [68] themselves state: quantum computing is still in its infancy, suffering from noise and limited in the problem size they are able to handle.

Improving distribution grid operation

Apart from improving the efficiency of the network reconfiguration itself, the application thereof to improve the operation of the distribution grid by using it as an active tool for system operators is also a topic of continued research [45].

A recent example of such research is presented in [32]. The work in [32] studies network reconfiguration as a preventive and corrective action for transmission flexibility in day-ahead stochastic security-constrained unit-commitment (SSCUC), while considering a multi-scenario RES output. The preventive action is designated as preventive network reconfiguration (PNR), which identifies the optimal base-case topology of the network. The corrective action is referred to as corrective network reconfiguration (CNR) and is implemented after the contingency has occurred. The authors of [32] consider four different variations of SSCUC, namely: SSCUC, SSCUC with PNR, SSCUC with CNR and SSCUC with both PNR and CNR.

Based on the obtained results, the authors of [32] conclude that CNR actions should be carried out closer to generation buses. This, because it enables the commitment of cheaper generation units, or the discharge of energy system storage (ESS) devices, during low RES penetration periods. PNR actions on the other hand should be performed on key lines closer to the low-voltage side or loads of the network. The results of the PNR, which itself resembles the desired implementation in this thesis the closest, are also deemed more favourable due to its frequent occurrence in the studied scenarios.

One of the interesting findings in [32] is that only a few reconfiguration strategies are key to addressing system congestion, which would alleviate the concern raised before in Section 2.6 regarding the degradation of switching components. However, the day-ahead nature of the implementation which is presented prevents an adaptation in the Dutch MV network due to a lack of remote-controlled switches.

Complementary to only considering network reconfiguration is a combination of network reconfiguration with the ever-increasing number of EVs. An example of such work can be found in [69], where the authors outline the potential benefits of utilising autonomous EVs (AEVs) for coping with distributed energy generation. However, employing AEVs in this way in a standalone manner seems unlikely due to certain restrictions: the inherent radial topology of distribution networks requires that the power stored in AEVs can only be supplied to certain downstream nodes. Even if this restriction was revoked and reverse flow is allowed, the total flow passing through the feeders will increase due to V2G (vehicle to grid) services [69]. Network reconfiguration offers a way of coping with these restrictions due to its capability of altering the power flow by changing the network topology while maintaining radiality.

The travel behaviour of the AEVs is modelled as a combination of a multinomial logit model to describe the choice of different charging locations and a combined distribution and assignment (CDA) model to calculate the equilibrial travel time and facility selection [69]. This is combined with an AEV charging behaviour and a battery degradation model to complete the AEV modelling, where the traffic pattern is explicitly connected with the spatial-temporal distribution of the electricity demand [69]. This is combined with a dynamic distribution network reconfiguration (DDNR). As the focus is on the potential impacts of coordinating AEVs charging/discharging with DDNR, the intermittent renewable generation is incorporated as a net load from the modelling perspective [69].

The results presented in [69] highlight that DDNR technologies complement V2G well in terms of minimising the total system cost, despite the V2G services imposing extra battery degradation costs. As a side benefit, the amount of switching actions are shown to actually decrease slightly following the coordination with AEVs [69]. Similarly to [32] however, the application of the work presented in [69] is prevented by its reliance on remotely controlled switches being present within the network.

Simultaneously, while EVs can provide system flexibility by shifting the peak demand and operating as flexible loads/generators to reduce system congestion (when aggregated), they can also be a source of additional uncertainty. Both of these aspects of EVs are considered in [70], which investigates the optimal grid reconfiguration strategy considering the random behaviour of electric vehicle fleets and wind energy uncertainty. This, with the aim of increasing system flexibility and reducing expected operating costs. In addition to the uncertainty of wind generation, the proposed stochastic framework models the uncertainty associated with the departure and arrival times of the EV fleets, state of charge (SOC) of batteries and number of EVs in a fleet [70].

To ensure that the solution for large-scale systems remains tractable, the Benders' decomposition (BD) [71] is proposed by the authors of [70] to decompose the original large-scale problem into one tractable master problem and several sub-problems. The sub-problems are designated as normal condition and stress condition. The normal condition checks the hourly grid security and its reconfiguration. The stress condition evaluates the optimality in each scenario by checking the convergence to a pre-defined level of satisfactory accuracy.

The results presented in [70] show great advantages when including the grid reconfiguration, such as a reduction in operating costs, expected energy not delivered (EENS) and expected wind energy curtailment (EWEC). However, only a MILP model with DC power flow is considered within the work, lowering the overall accuracy of the power flow calculation compared to a non-linear formulation.

3

Introducing the case study

Before discussing the different modelling and simulation aspects, it may be useful to place those within context. Thus, the case study is introduced first, to which the rest of the methodology in Chapter 4 is applied. It is important to stress that the methodology can be used for any MV network and the presented case study is just an example. Knowing this, the network under consideration will be discussed in Section 3.1. Additionally, the different components present within this network (and relevant for its analysis) are discussed in Section 3.2.

3.1. Network analysis

As mentioned in Chapter 1, the case study analysed within this work is one of the largest cities in the Netherlands. To give a more detailed description: the network is a 143-node grid, connected by a total of 153 lines (or cables since it they are underground). A graph plot of the network is presented in Figure 3.1. The grid is designated as a medium voltage network, with a nominal voltage of 10.5 kV.

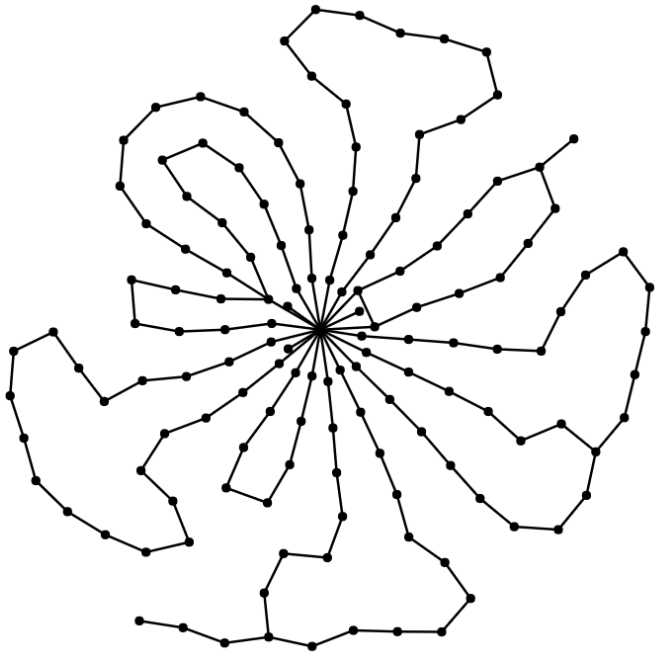

Figure 3.1: Graph plot of the base-case meshed network.

As was mentioned in Chapter 2, in the Netherlands most distribution networks have a loop or multi-loop structure but are operated as a radial network. This case study is no exception. To this end, 11 of these 153

lines are open in the base case. A visualisation of the radial network (as operated in the base case) is depicted in Figure 3.2.

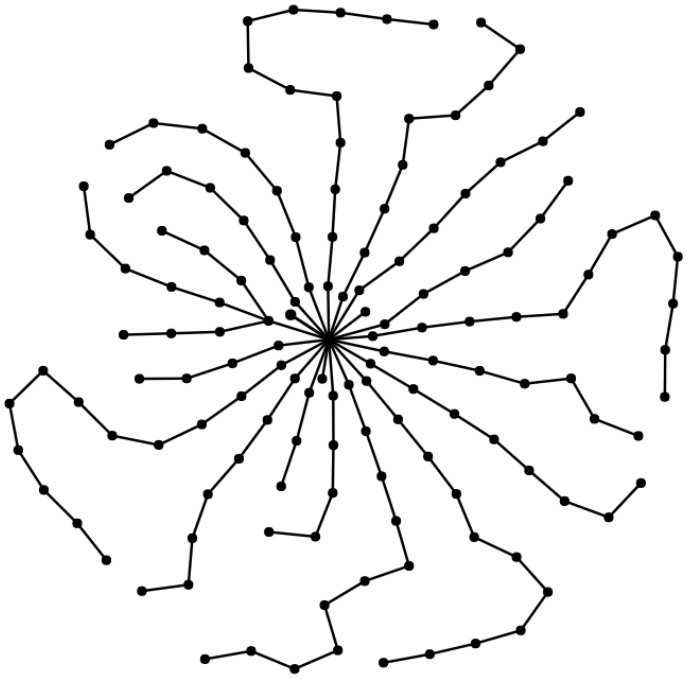

Figure 3.2: Graph plot of the base-case radial network.

As mentioned in Chapter 1, this project had access to real data from one of the Dutch DSOs. In order to represent this data, the respective network is implemented in a PowerFactory model. PowerFactory is a leading power system analysis software environment used for analysing different kinds of systems, ranging from industrial to full distribution or transmission systems. Additionally, with the feature of added scripting and interfacing, PowerFactory can be used for automated and integrated modelling and analysis [72]. This last feature is especially important as it allows PowerFactory simulations to be run through the high-level programming language Python. This feature will be used throughout this project to retrieve data, compare simulation results and analyse the network in general.

3.2. Component analysis

There are several components within the network relevant for the analysis thereof. For this work the loads, generators, lines, cables, switching systems and substations are of particular interest. All of these components are discussed in detail below, starting with the loads

Loads

The loads within the network are modelled as constant P Q loads. This entails that the nominal rated power will not change, as long as the supplied voltage is equal to, or greater than, the minimum supply voltage. If the supplied voltage drops below the minimum rated value, the load behaves as a constant impedance load to limit the formation of large currents which could trigger overcurrent relays [73].

Another characteristic of the loads is the used technology. In PowerFactory, the technology type is designated as *3PH-'D'*. The 3PH refers to the fact that the loads are 3-phase load types. The 'D' term has to do with the way the different phases are connected. In this case, all loads are balanced loads, where the load is shared equally amongst the phases [74], this is also referred to as a delta connection. For a visualisation of how a balanced load is connected, refer to Figure 3.3.

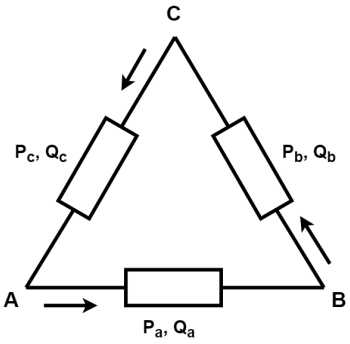

Figure 3.3: Three-phase delta-connected balanced load. In PowerFactory referred to as 3PH-'D' load model [74].

There is also a distinction between general load elements and MV load elements within PowerFactory. The distinction is that MV load elements include transformer type data and LV network parameters, which does not apply to general load elements [75]. This means that MV loads can act both as loads, but also as generators, depending on the specified data. General loads on the other hand will only ever act as loads. The difference is perhaps best expressed using a visualisation, which is presented in Figure 3.4. In Figure 3.4a, the MV load is depicted, which consists of both the transformer and the load forming one component attached to the terminal. In Figure 3.4b, the general load is depicted, which is just a load-type component connected to the terminal. Finally, Figure 3.4c depicts how a MV load can be implemented using a general load, which requires a separate transformer and generator.

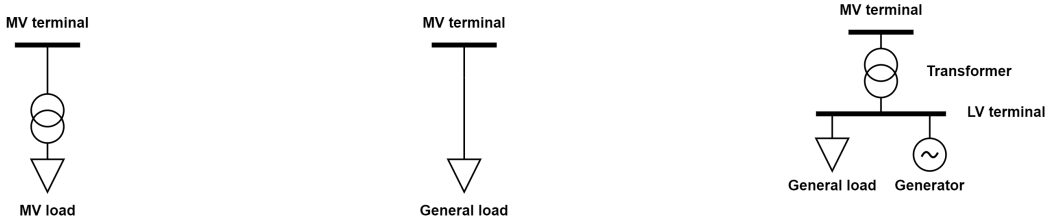

(a) MV load type in PowerFactory.

(b) General load type in PowerFactory.

(c) Equivalent MV load implemented using a transformer, general load and generator.

Figure 3.4: Visualisation of the difference between a MV load and a general load. Adapted from the work in [75].

Generators

There are no traditional large-scale centralised generators connected to the considered MV grid. Instead, there are a number of 3-phase PV generators present. The generators are modelled as static generators, meaning that their frequency is controlled by the network to which they are connected. The presence of these generators means that some of the load within the network could potentially be supplied locally. However, it should also be noted that the generation tends to be relatively low compared to the overall demand of the system. This is illustrated in Figure 3.5a and Figure 3.5b, displaying the yearly active power generation and active power demand, respectively, with hourly precision. When analysing the average amplitude of both, it becomes apparent that the demand can be more than 30 times higher, even during peak generation. Thus, most of the electricity demand will still need to be supplied by the external grid.

In Figure 3.5 it can also be observed that a similar trend as from Figure 1.2 (displaying the yearly demand and PV generation in Europe) is found within the demand and generation for the considered network. Thus, the earlier stated intention of analysing a summer and winter switching profile remains valid for the considered network.

Substations

The substations are the main point of consideration for this thesis in terms of scope, as the network will be analysed on this level. It is also important to clear up some terminology. The substations inside the MV grid,

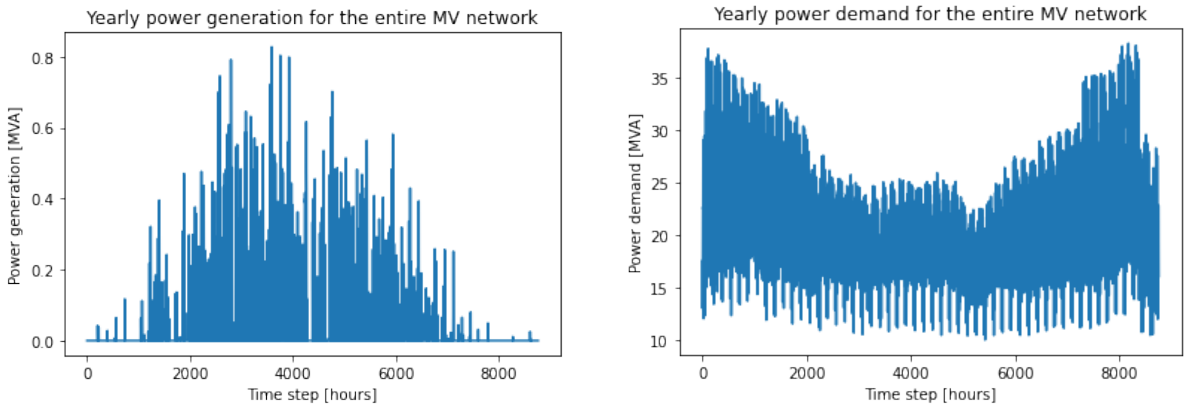

(a) Yearly PV generation within the considered MV network.

(b) Yearly power demand within the considered MV network.

Figure 3.5: Yearly profiles of demand and generation of the MV network with hourly precision.

in terms of graph theory, are the same as nodes for this thesis. Within each of these nodes, there are so-called terminals to which the different components (like loads or lines) are connected. An example of such a terminal inside PowerFactory is provided in Figure 3.6. The distinction is ultimately only important when considering the format in which the data is available, as all components are connected through a terminal and indexed relative to this terminal. The terminals within a substation will be aggregated such that the entire system is considered at substation level.

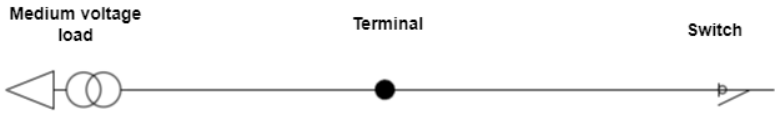

Figure 3.6: An example of a terminal inside PowerFactory. Connected to the terminal are a medium voltage load on one side and an open switch on the other.

Cables

There are four different kinds of cable types present within the MV grid, those being: XLPE, GPLK, KUDI and ones referred to as Line 10kV. The latter type consists of connection pieces between the different assets and the terminals, as such referring to them as cables is not fully accurate within the typical context of cables within electrical engineering. They do not have active operating limits and are not considered when analysing congestion within the network. The other types are differentiated by their type of insulation. GPLK cables are insulated using lead and paper impregnated with a combination of oil, resin and wax [76]. The XLPE cables are insulated using cross-linked polyethylene and KUDI refers to distribution system cables insulated with plastic [76].

There are several operating constraints which need to be taken into account for each of the cables. Most prominent amongst them when considering situations of congestion is the line loading. For the GPLK cables the lines may be loaded up 70% of the rated current during normal operation and 100% during a disturbance or maintenance. The XLPE cables may be loaded up to 100% during normal operation and 120% during a disturbance or maintenance. Finally, the KUDI cables are operated with the same loading constraints as the XLPE cables.

Switches

Finally there are the switches. There are three different kinds of switches present inside the network under consideration, those being: circuit breakers, load-break-disconnectors and disconnectors.

4

Developed methodology

In order to answer the posed research question, it is necessary to implement the required functionality within an algorithm, hereafter referred to as the reconfiguration algorithm. This algorithm will be used to optimise the network configuration by altering the status of the switches present within the network, such as to reduce network congestion present therein. In this chapter, the process of developing the reconfiguration algorithm will be discussed, which is depicted graphically in Figure 4.1.

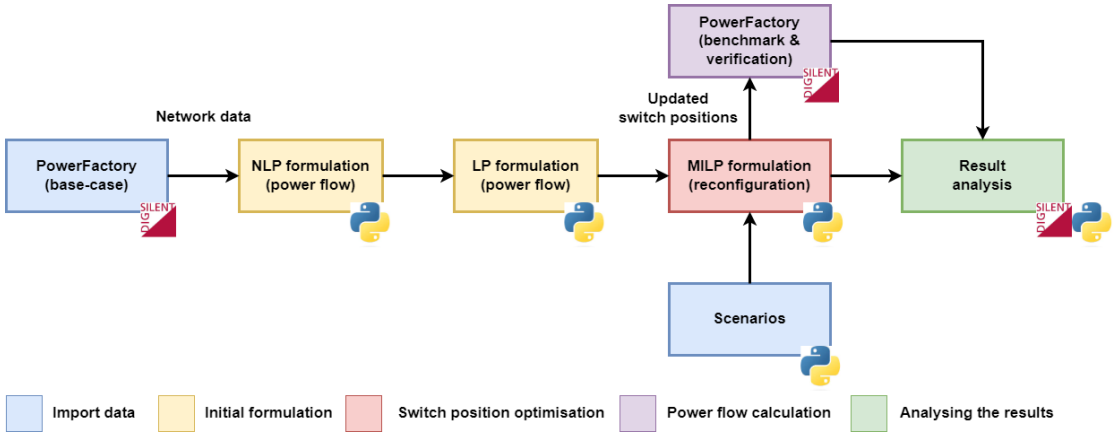

Figure 4.1: Development of the reconfiguration algorithm. The logos are used to highlight in which environment the step is performed: either using Python, or DIgSILENT PowerFactory.

In Chapter 3 it is mentioned that the original model of the network under consideration is implemented in PowerFactory. Additionally, it is mentioned that it is possible to interface PowerFactory with Python, which will be the programming language used to develop the reconfiguration algorithm. As such, it is possible to access all the functionalities of PowerFactory through the software environment developed in Python. The PowerFactory model will initially be used to retrieve the base-case network data, which is the first block in Figure 4.1.

Next, in the second block and as a first step towards implementing the reconfiguration algorithm for network congestion reduction, it is important to know whether or not congestion is present (or predicted) in the network. To this end, a NLP power flow algorithm is formulated in Section 4.1 to compute the different network variables of interest and provide insight into the steady-state behaviour of the system [13]. This power flow formulation will additionally serve as the basis for the subsequent reconfiguration algorithm.

Ideally, with the nonlinear formulation finished the integer variables representing the switch positions within the network would be added, transforming it to a MINLP. However, as covered in Section 2.6.2, it is currently not possible for this project to use a solver capable of solving the MINLP in a deterministic manner. As such, a different approach has been conceived. The complete reconfiguration algorithm will be formulated as a two-

step approach. First, a MILP formulation is used to optimise the switch positions within the network. Next, the variables within the network are calculated using the power flow calculation from PowerFactory. This approach is graphically displayed in figure 4.2. The advantage of this approach is that it will enable the deterministic optimisation of the switch positions throughout the network, while still taking the other network parameters and variables into account with as much accuracy as possible. At the same time, there will be no loss of accuracy for the final network variables, as these are calculated after the switch positions have been updated. Please note that the reconfiguration algorithm will refer to the optimisation of the switch positions, whereas the power flow in Powerfactory will refer to the second step of Figure 4.2, however the combination will be used to obtain the final results.

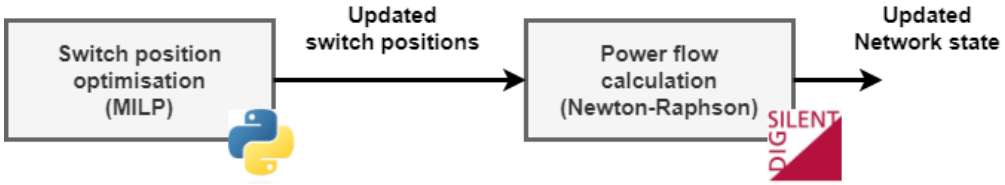

Figure 4.2: Two-step approach to the reconfiguration algorithm. First, the switch positions are optimised using Python. Next, the network variables are calculated using PowerFactory.

In order to formulate the reconfiguration algorithm, the NLP power flow formulation is linearised in the third block of Figure 4.1, which is the topic covered in Section 4.2. And with the linear power flow, it is possible to add the switch position variables to the formulation, leading to the MILP switch position optimisation as discussed in Section 4.3, forming the red block within Figure 4.1. Once this point has been reached it is also possible to add additional scenarios to the input of the algorithm, but more on this in Chapter 5.

Once a new network topology has been acquired through the use of the MILP reconfiguration algorithm, the results will be verified using the PowerFactory model, or the purple block in Figure 4.1. Notice how the red and purple blocks in Figure 4.1 together form the two-step approach as shown in Figure 4.2. The motivation for implementing a separate power flow formulation and reconfiguration algorithm besides the functionality offered by PowerFactory is mostly dependent on accessibility. While PowerFactory is a very detailed and accurate simulation environment, it requires a license to work, which is not readily available outside academic environments. Additionally, formulating the reconfiguration algorithm from scratch allows for more customisation of constraints and objectives than what is offered by PowerFactory, which will be highlighted in Section 4.3.5.

4.1. Nonlinear power flow

4.1.1. Power flow algorithm overview

The power flow algorithm is presented graphically in Figure 4.3. The algorithm can roughly be divided into four pieces: data import, pre-processing, power flow calculation and comparison. The data import consists of loading the different network parameters from PowerFactory to reconstruct the network in Python. The pre-processing consists of cleaning up the data and placing it in usable formats adequate for the formulation as presented in Section 4.1.3, as well as ensuring certain operating constraints are followed; in particular the radial operation of the network. These topics are covered in Section 4.1.5 and Section 4.1.6, respectively. The power flow calculation is carried out twice; once by the formulation as described in Section 4.1.3 and once by making use of PowerFactory. Finally, the results of both of these simulations are compared in terms of accuracy in Section 4.1.7.

It is important to note that the power flow algorithm will be considering multiple time steps. This will not be an iterative process however, where the algorithm is carried out for each individual time step. Instead, the algorithm will optimise the solution while considering the entirety of the provided time frame at once. The reason for this is that the final reconfiguration algorithm does not seek to optimise the power flow for every time step. Instead, since the considered period is half a year, the algorithm seeks to optimise the switch positions (and subsequently the power flow) for this half-year period. The switches will not change position

within this period, but only once at the start.

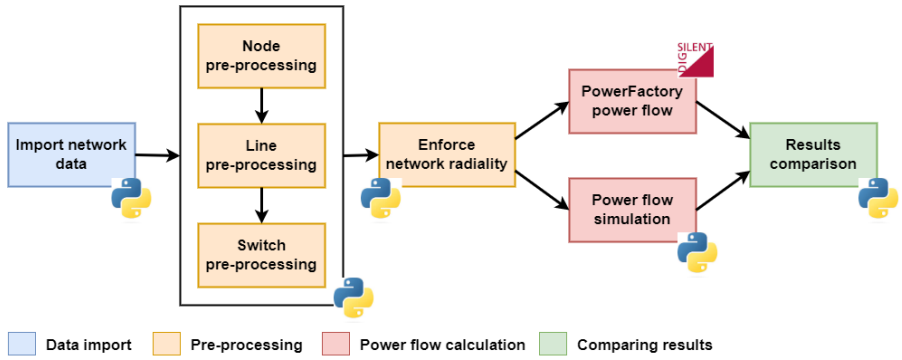

Figure 4.3: Representation of the power flow algorithm implemented for this thesis, each block representing a different step inside the coded implementation. The logos represent in which environment the steps are carried out: either Python or DIgSILENT PowerFactory.

4.1.2. Important assumptions

Before the details of the rest of the power flow algorithm are covered, it is important to go over some key assumptions which are made regarding the power flow algorithm and the simulation as a whole.

First of all, the nominal voltage level within the MV grid is rated at 10.5 kV. However, the transformer from the HV to the MV grid already imposes a drop on this value. Modelling of the transformer is deemed to be outside the scope of this work and as such the transformer drop is assumed to be known. This value is retrieved by utilising the PowerFactory model of the MV grid and extracting the value on the low-voltage side of the transformer. This value will be used as the voltage level of the reference node. An example is given in Figure 4.4, which displays a PowerFactory simulation with the value of the voltage at both terminals of the transformer. The HV side equals the rated value of 50 kV. However, it can be observed that the low voltage side has a value of 10.477 kV, rather than the rated 10.5 kV.

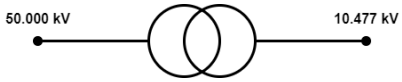

Figure 4.4: Depiction of the voltage drop over the transformer connecting the HV grid to the MV grid in PowerFactory. The rated voltage for the MV grid is 10.5 kV, however the transformer imposes a drop to 10.477 kV.

Secondly, the current formulation of the power flow does not accommodate for parallel lines between two nodes. There are several instances of such a situation within the analysed grid and as such, it needs to be accounted for. This is done by making use of two different PowerFactory models. The first one is the base-case PowerFactory model as described within Chapter 3. The second model is completely the same, only without the parallel lines. The first model is used for benchmarking the results to ascertain the accuracy of the power flow algorithm. The second is used for loading in the network data, as will be described in Section 4.1.4. A visualisation is presented in Figure 4.5, where the difference between the two models is depicted based on an example node which in reality has parallel lines connected to it.

Finally, it is important to note that certain parameters which primarily affect the reactive power will not be taken into account, like the line-to-ground and line-to-line capacitances for example. This choice is made because modelling these aspects are considered to be too in-depth to be implemented accurately within the time frame set for completing this thesis. This means that the value for the reactive power is expected to be rather erroneous and as such this parameter will not be considered for any decision-making and will not be further covered within this work.

4.1.3. Power flow formulation

The power flow formulation is covered next in order to offer context into the other aspects of the full algorithm, as it is designed to accommodate the formulation. The power flow formulation used within this thesis

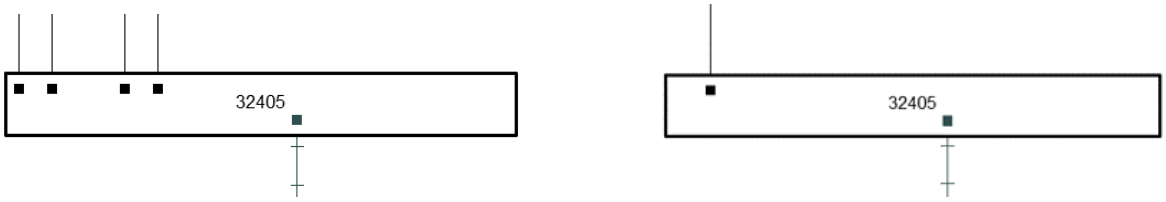

(a) Model as seen by the PowerFactory simulation.

(b) Model as seen by the Pyomo model.

Figure 4.5: Depiction of the two different models used for the power flow algorithm. One as seen by the PowerFactory simulation used as a benchmark and one as seen by the Pyomo simulation forming the basis of the network reconfiguration algorithm.

is based on the work in [77], which formulates the three-phase optimal power flow, used to define the state of the electrical grid in distribution systems. The full derivation will not be presented here, but merely the final formulation forming the non-linear program. Also note that not all constraints from [77] return, as not all of them are relevant for this thesis.

First is the objective function, which is presented in Equation 4.1. The objective function is formulated as the minimisation of the active power losses in all branches [15] [51] [54] [62].

$$min\left\{\sum_{mn\in\mathscr{L},\psi\in\mathscr{F},t\in\mathscr{T}} P^{L}_{mn,\psi,t}\right\} \tag{4.1}$$

Next there are the different constraints, which can roughly be categorised into four different sets of equations. First are the active and reactive power losses, as they are also used for the objective function. They are presented in Equation 4.2 and Equation 4.3, representing the active and reactive power losses, respectively.

$$\begin{aligned} P^{L}_{mn,\phi,t} = & \sum_{\psi\in\mathscr{S}} \frac{1}{|V_{m,\psi,t}||V_{m,\phi,t}|}(R'_{mn,\phi,\psi}P_{mn,\phi,t}P_{mn,\psi,t} \\ & + R'_{mn,\phi,\psi}Q_{mn,\phi,t}Q_{mn,\psi,t} + X'_{mn,\phi,\psi}P_{mn,\phi,t}Q_{mn,\psi,t} \\ & - X'_{mn,\phi,\psi}Q_{mn,\phi,t}P_{mn,\psi,t}) \quad \forall mn\in\mathscr{L},\forall\phi\in\mathscr{F},\forall t\in\mathscr{T} \end{aligned} \tag{4.2}$$

$$\begin{aligned} Q^{L}_{mn,\phi,t} = & \sum_{\psi\in\mathscr{S}} \frac{1}{|V_{m,\psi,t}||V_{m,\phi,t}|}(-R'_{mn,\phi,\psi}P_{mn,\phi,t}Q_{mn,\psi,t} \\ & + R'_{mn,\phi,\psi}Q_{mn,\phi,t}P_{mn,\psi,t} + X'_{mn,\phi,\psi}P_{mn,\phi,t}P_{mn,\psi,t} \\ & + X'_{mn,\phi,\psi}Q_{mn,\phi,t}Q_{mn,\psi,t}) \quad \forall mn\in\mathscr{L},\forall\phi\in\mathscr{F},\forall t\in\mathscr{T} \end{aligned} \tag{4.3}$$

Next are the active and reactive power balance constraints, formulated as in Equation 4.4 and Equation 4.5 for the active and reactive power balance, respectively.

$$\sum_{km\in\mathscr{L}} P_{km,\phi,t} - \sum_{mn\in\mathscr{L}}(P_{mn,\phi,t} + P^{L}_{mn,\phi,t}) + P^{S}_{m,\phi,t} = P^{D}_{m,\phi,t} \quad \forall m\in\mathscr{N},\forall\phi\in\mathscr{F},\forall t\in\mathscr{T} \tag{4.4}$$

$$\sum_{km\in\mathscr{L}} Q_{km,\phi,t} - \sum_{mn\in\mathscr{L}}(Q_{mn,\phi,t} + Q^{L}_{mn,\phi,t}) + Q^{S}_{m,\phi,t} = Q^{D}_{m,\phi,t} \quad \forall m\in\mathscr{N},\forall\phi\in\mathscr{F},\forall t\in\mathscr{T} \tag{4.5}$$

Then there is the voltage magnitude drop for each of the branches, formulated as in Equation 4.6.

$$\begin{aligned} |V_{m,\phi,t}|^2 - |V_{n,\phi,t}|^2 = & \ 2\sum_{\psi\in\mathscr{S}}(R'_{mn,\phi,\psi}P_{mn,\psi,t} + X'_{mn,\phi,\psi}Q_{mn,\psi,t}) \\ & + \frac{1}{|V_{m,\phi,t}|^2}\left(\sum_{\psi\in\mathscr{S}} R'_{mn,\phi,\psi}P_{mn,\psi,t} + X'_{mn,\phi,\psi}Q_{mn,\psi,t}\right)^2 \\ & + \frac{1}{|V_{m,\phi,t}|^2}\left(\sum_{\psi\in\mathscr{S}} R'_{mn,\phi,\psi}Q_{mn,\psi,t} - X'_{mn,\phi,\psi}P_{mn,\psi,t}\right)^2 \quad \forall mn\in\mathscr{L},\forall\phi\in\mathscr{F},\forall t\in\mathscr{T} \end{aligned} \tag{4.6}$$

And finally, there are the maximum current limits as formulated in Equation 4.7.

$$\frac{P^2_{mn,\phi,t} + Q^2_{mn,\phi,t}}{|V_{m,\phi,t}|^2} \leq \bar{I}^2_{mn} \forall mn \in \mathscr{L}, \forall \phi \in \mathscr{F}, \forall t \in \mathscr{T} \tag{4.7}$$

All of these formulations are implemented in Python using the optimisation package called Pyomo. Pyomo is a Python-based, open-source optimisation modelling language [78], which makes it ideal for implementing the optimisation formulation of the power flow and later the reconfiguration.

4.1.4. Network data

For the first step of the power flow algorithm, it is necessary to have access to the same data as is present inside PowerFactory. Due to the ability to interface PowerFactory with Python, it is possible to directly import any network parameters which are also available in PowerFactory. This includes data for nodes, lines, switches, loads and generators. Below follows an overview of the relevant data which is imported for each of the different types of network assets. It can already be noted that for every component the name will be stored such that a component-specific analysis can be performed after a simulation is carried out, should this prove necessary.

Nodes, loads and generators

The interesting information related to the nodes is primarily related to what components are connected to them. The local demand and generation will ultimately determine the necessary flow of power towards any node in particular. As a result, the local loads and generators of each node are imported and indexed based on the node name. It is assumed that any local generation is allowed to feed local loads independently, this will become important when considering the radiality constraints in Section 4.1.6. As such, the net consumption/generation is determined by summing the local values of the loads and generators while accounting for sign differences between the two. Finally, it is important to identify the reference node (also referred to as slack bus). The reference node is the node connecting the medium voltage and high voltage grid together. As such, this node will either import or export any remaining electrical energy demand or generation after the local generators have supplied what they can of the local load. The values of the local parameters like voltage magnitude and active power demand are constant for this node.

Lines

The lines have several parameters of interest, most prominently the impedance values. There are several ways in which the impedance of a line can be expressed. In PowerFactory this is done by the positive and zero sequence impedance values: $Z_1 = R_1 + jX_1$ and $Z_0 = R_0 + jX_0$ respectively. The maximum rated current is also an important parameter as it will directly translate to the constraint given in Equation 4.7. Finally, for the formulation of the network itself, it is important to know the nodes to which each line is connected. These values can later be used to identify each line by using it as an index value.

Switches

Finally there are the switches. There are three different kinds of switches present inside the network under consideration, those being: circuit breakers, load-break-disconnectors and disconnectors. The circuit breakers are for safety purposes and will not be considered in the network reconfiguration. Additionally, most of the normal disconnectors tend to be relatively old and difficult to operate, requiring two people rather than one. They also have the added constraint that there can be no current or voltage on the switch when they are operated. This would impose severe operating constraints on any switching action which may be taken. As such, only the load-break-disconnector type switches will be considered for the network reconfiguration. For the other types it is only important to take into account their initial position, which will be done during the pre-processing.

4.1.5. Data pre-processing

The pre-processing primarily consists of cleaning up the data from PowerFactory and placing it in a format usable for the power flow formulation. For the nodes, this means that the different loads and generators will be aggregated from the terminal level to the substation level, the local demand and generation will be summed and the reference node is assigned.

As discussed in Section 4.1.2, the power flow formulation cannot account for parallel lines. These lines are thus not present within the network data. However, similar values for the current are expected to move through the one cable that is remaining in such cases. To ensure that the cable will not be continuously overloaded, its maximum current limit is multiplied by the number of parallel lines previously present. Take the example of Figure 4.5, where previously there were four parallel lines, meaning that the maximum current rating for the line which remains is multiplied by four. This approach is only valid if the previous parallel lines are all more or less the same in terms of their characteristics.

Additionally there is the matter of the impedance formulation of the lines. The data from PowerFactory defines the impedance values based on the positive and zero sequence components. However, the power flow formulation as discussed in Section 4.1.3, requires the impedance values to be in self and mutual phase impedance notation (Z_{aa}, Z_{ab}, Z_{ac}, etc.). A full derivation for transforming the phase impedance values to sequence components is presented in [79]. The relevant parts of which have been adapted for this work and can be found in Appendix A. This formulation allows for a direct transformation of the positive and zero sequence components to the self and mutual phase impedance values.

Then there are the switches. There are a number of switches designated as load-switch-disconnectors. However, only the ones which are connected to lines between the different nodes are of interest to changing the topology. As such, the remainder of the switches will not be considered.

Finally, for most lines it holds that they are connected by two switches, one on each end, as depicted in Figure 4.6. However, as was discussed in Section 2.6, it is beneficial to limit the number of switching actions. Since opening one of the switches or two of the switches does not make a difference for the power flow (assuming that the impedance of the line itself is relatively low compared to other values in the system), only one of the switches is considered for each line.

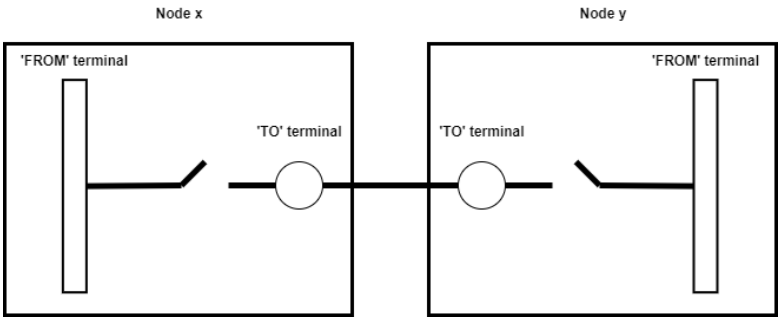

Figure 4.6: General switch configuration within the MV grid. Note that both switches would normally be closed if the line was used.

4.1.6. Network radiality

As a final step before the power flow formulation in Pyomo can be used, it is necessary to ensure the network is radial. This keeps the protection of the network simple [13] and it reduces the short-circuit current [15].

The definition of radiality used within this work is adapted from [15], which presents two conditions which need to be met before one can state that a network is radial.

1. For a network consisting of N nodes, the final network must have N-1 lines (also referred to as edges) connecting these nodes.
2. The final network needs to be connected. Or, to relate this once more to graph theory, the final network should have an edge connectivity equal to 1.

The first of these conditions can be checked before the power flow is carried out (provided that the network topology is static) as both the lines and nodes have been processed by this point. The nodes will remain

the same, but the number of lines in use needs to be made equal to the number of nodes minus one. This primarily involves removing certain lines within the network data set of which the switch is open (after pre-processing, meaning that every line only has 1 switch). The second condition is met by a combination of the first condition and Equation 4.4. Equation 4.4 guarantees that every node which cannot supply its own demand and instead needs to be supplied by the network will be connected. The first condition in turn guarantees that there will be N-1 lines connecting these nodes. If both of these are true, then the network should have an edge connectivity equal to 1. This can also be checked beforehand in case the network topology is considered static.

It is important to point out two assumptions which are taken when these conditions are set. First of all, it is assumed that the distributed generation is allowed to feed some of the loads independently [15]. Second, there are certain nodes inside the network that have neither generation nor load during certain times of the day. If for some reason, these nodes are considered only during moments when they have no load nor generation, then they are referred to as transfer nodes. Depending on the application, the conditions would have to be altered in case transfer nodes are present within the network. However, since all nodes are part of the final radial topology, a simple solution is to assume a small load value (0.001 p.u. for example) for each of the nodes, which will ensure that the previous conditions can always be met [15].

4.1.7. Comparison against PowerFactory simulation

Apart from the power flow formulation presented in Section 4.1.3, there will also be an additional power flow carried out using PowerFactory. The power flow functionality of PowerFactory can be called using a Python interface, allowing for the functionality of getting the same format of results for both power flows. These results will be used as a benchmark. As the data being used is real historic data and since PowerFactory is a professional simulation software also used within industry and other academic endeavours, the results from PowerFactory are assumed to reflect the reality of the power flow within the network. This forms the primary motivation for PowerFactory being used as the benchmark to which the formulation in Python is compared.

When both power flows are complete, it is time to compare the results of both simulations and assess the accuracy of the Pyomo model. For the power flow formulation in Pyomo it holds that it is solved using the nonlinear optimiser Ipopt [80]. For the results presented in this section, it holds that the considered time frame was the third week of the year, or the 336th hour until the 504th hour (meaning that the winter season is considered). The generation and demand within the network during this period are displayed in Figure 4.7a and Figure 4.7b respectively. Once again notice how the scales of both plots are different, highlighting the need for power import from the external HV network. Similar results can be obtained from other weeks by utilising the same techniques and adjusting the considered time frame during the initialisation.

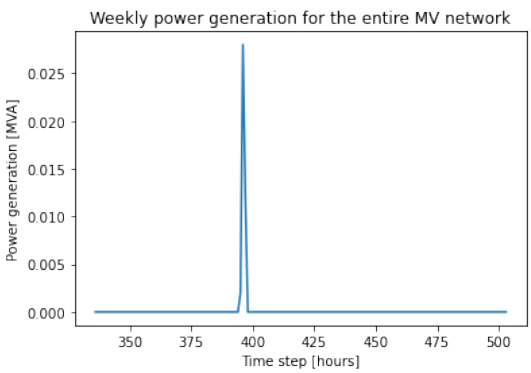

(a) Power generation within the network for the third week of the year.

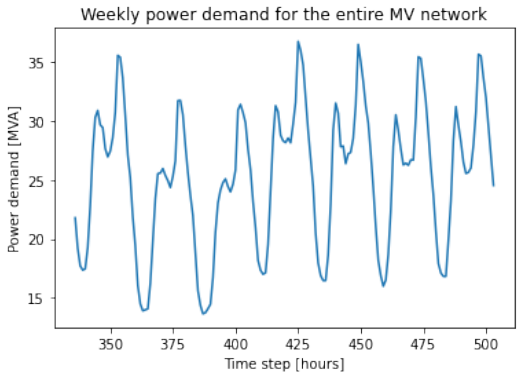

(b) Power demand within the network for the third week of the year.

Figure 4.7: Generation and demand within the network during the third week of the year (ranging between hour 336 and 504).

To highlight the accuracy of the simulation implemented in Python, the relative error of three parameters is analysed. Those parameters being the voltage magnitude, current and active power. The active power is displayed, since the optimisation is based on the minimisation of the active power losses. Thus, an accu-

rate active power would imply that the optimisation is being performed based on an accurate parameter, which would lead to an accurate solution. The current is displayed, as congestion is usually defined based on the maximum current loading of the lines (which were discussed previously in Section 3.2). Thus, an accurate current parameter means that the congestion can be accurately analysed. Finally, the voltage magnitude tends to be a welcome complement for completion's sake when the current and power are already being analysed. Additionally, the voltage magnitude is closely related to power losses, which once again relates to the objective function.

For the relative error calculation, the PowerFactory model (in the figures referred to as PF) was used as a base case to which the python simulation result (in the figures referred to as SIM) was compared. For all figures it holds that both the error heat map and occurrence distribution are plotted. The heat map offers insight into the occurrence of errors throughout the network, displaying the relation between the size of the error, each individual line and the time dependency. It is also relevant to point out that the lines on the y-axis are ordered in an ascending manner compared to the voltage magnitude at the start of each line. This means that the lines closer to the slack bus are displayed towards the bottom of the heat maps. The same holds for the buses when the voltage magnitude by itself is considered. The occurrence distribution is a complement to the heat map, which becomes especially useful in case a single large error occurs. Finally, before the results are discussed, the average and maximum error values are displayed for each of the parameters within Table 4.1.

Table 4.1: Average and maximum error values for the voltage magnitude, current and active power. Comparing the Pyomo implementation flow to PowerFactory.

Parameter	Average error value [%]	Maximum error value [%]
voltage magnitude	0.229	1.589
Current	0.615	18.855
Active power	0.110	1.525

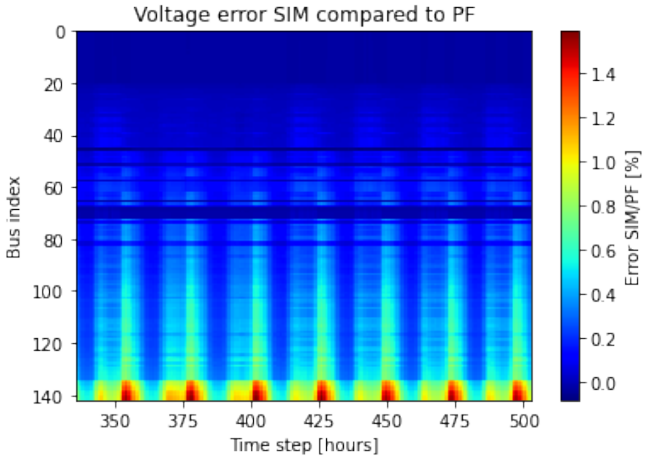

(a) Heat map of the voltage magnitude error within the network. SIM referring to the Pyomo simulation and PF to the PowerFactory simulation

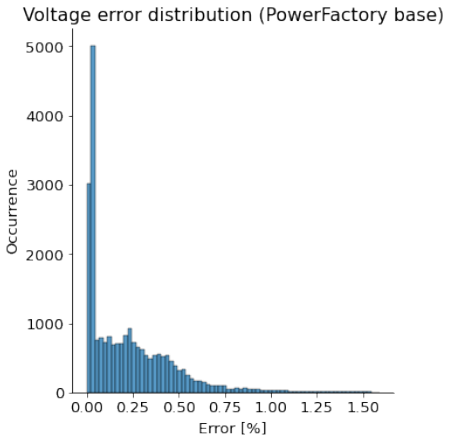

(b) Occurrence distribution of the errors within the considered data. The total amount of data points considered consists of 23856 points.

Figure 4.8: Visualisation of the voltage magnitude error within the network for the considered time frame.

The voltage magnitude error is displayed in Figure 4.8, the current error is displayed in Figure 4.9 and the active power error is displayed in Figure 4.10. Taking into account the generation and demand profile from Figure 4.7, it can be observed that the peak in generation within the network does not seem to influence the error within any of the considered heat maps. This is positive, as the error is likely to be highest during peak demand and peak generation and the generation at least is not causing high errors. However, any significant impact of the peak in generation may also be lacking due to its relative small amplitude compared to the power demand within the system. Still, since the generation originates from a relatively small amount of nodes within the network it would have been likely to observe an error for these nodes (or the connected

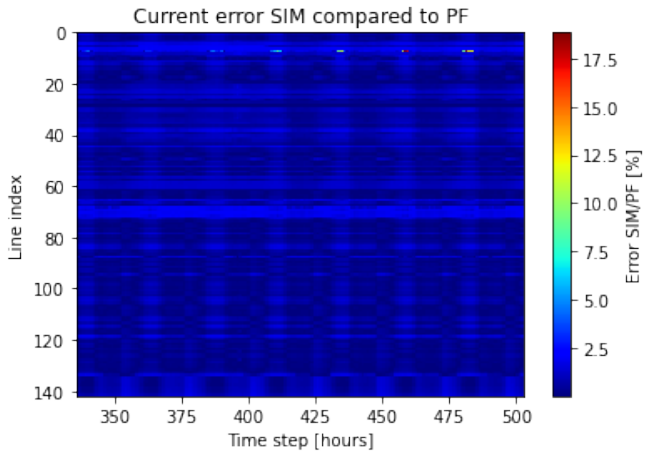

(a) Heat map of the voltage magnitude error within the network. SIM referring to the Pyomo simulation and PF to the PowerFactory simulation

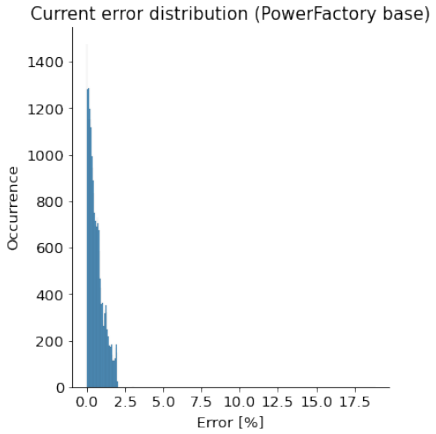

(b) Occurrence distribution of the errors within the considered data. The total amount of data points considered consists of 23856 points.

Figure 4.9: Visualisation of the current error within the network for the considered time frame.

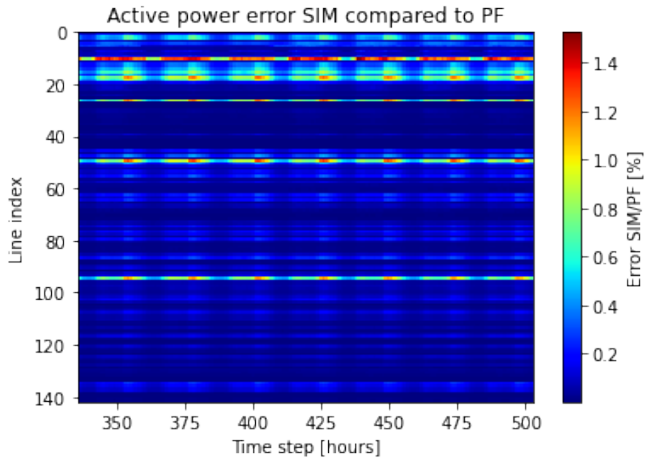

(a) Heat map of the voltage magnitude error within the network. SIM referring to the Pyomo simulation and PF to the PowerFactory simulation

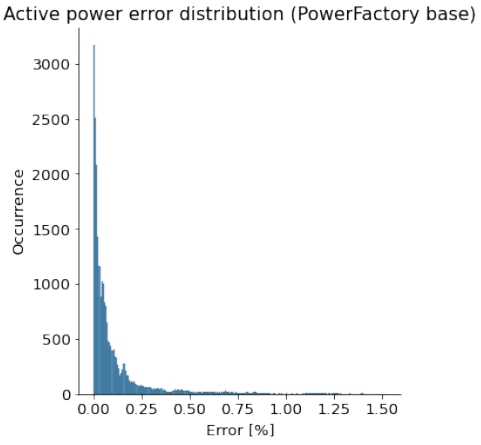

(b) Occurrence distribution of the errors within the considered data. The total amount of data points considered consists of 23856 points.

Figure 4.10: Visualisation of the active power error within the network for the considered time frame.

lines) in case an error was caused by the local generation.

In Figure 4.8a the voltage magnitude error tends to be relatively low, averaging at 0.229% with a maximum error of 1.589%. The largest errors can be observed for moments of peak demand, closest to the slack bus (taking into account the demand profile from Figure 4.7b). When looking at the distribution of the error size in Figure 4.8b, it can be observed that almost half of the errors (42%) are smaller than 0.1%. Overall, the voltage magnitude error can be deemed satisfactory for the considered time frame.

When first observing the current error in Figure 4.9a it may not offer the same insight as the heat map from the voltage magnitude. The explanation for this can be found by looking at the occurrence distribution in Figure 4.9b. Within this figure it can be observed that the maximum error of 18.855% is a rare exception compared to the other data points. The average error of 0.615% is a lot more promising, as is the visible part of the occurrence distribution, which roughly ends around 2.5%. Indeed, when going into detail, only 21 data points have an error larger than 2.5%. However, the occurrence of such a large error should not be disregarded immediately. As such, when considering the base case scenario (for which perfect knowledge is available), the current error will be verified in case a situation of congestion is analysed. This, to make sure that any conclusion based on the occurrence of congestion and the possible reduction thereof as a result of the recon-

figuration algorithm, will have a reasonably low error. The large error is likely caused during the conversion from the PowerFactory import data to the input data for the power flow calculation. Since the occurrence is rather rare and since potentially resolving the error completely will likely consume a large amount of time it will be disregarded in the scenarios where perfect knowledge of the data and solution are unavailable.

The active power error displayed in Figure 4.10a has the least consistent pattern in regards to which lines have the highest errors. Several lines towards the end of feeders (low index numbers on the y-axis) tend to have the higher error values. However, there are also some lines closer to the slack bus that can have the higher values, as can be observed for line 98 for example. Both the start and the end of feeders can thus suffer from relatively larger errors, making their occurrence inconsistent. If a higher error is observed it tends to display a similar dependency on the peak active power demand, as was also observed for the voltage magnitude. It is important to relativize these observations though. By looking at the occurrence distribution in Figure 4.10b it becomes apparent that most data points have an error lower than 0.2%. This is also reflected in the average value of 0.110%.

Overall, the errors observed for the different parameters have a low value, with the average values for each of the parameters being lower than 1%. In the case of exceptions present within the current specifically, the larger errors occur very sparsely, which is supported by the error distribution plots. To conclude, the power flow model implemented within python is validated to a satisfactory level and accurately represents the PowerFacotry benchmark.

4.2. Linearised power flow

Now that the nonlinear formulation is finished, it can be linearised, leading up to the MILP formulation. This will be covered in the following sections, starting with a brief analysis of different linearisation methods in Section 4.2.1. Next, the adjustments to the NLP power flow formulation will be made in Section 4.2.2. Finally, a comparison between the linear and nonlinear formulation will be presented in Section 4.2.3 to establish the accuracy of the linearisation.

4.2.1. Comparing linearisation methods

linearisation of the nonlinear power flow equations can be done using several methods. Three such methods are analysed within [81]. To be specific the first-order Taylor series approximation (FOT), fixed-point linearisation (FP) and forward-backward sweep linearisation (FBS) are discussed. In [81], the authors conclude that the FOT provides the best solution, but the FBS is significantly faster. However, the computation time is less relevant for the application within this thesis as the reconfiguration is only implemented in half-year periods. Thus, the FOT would be more favourable as it offers better accuracy. To complement the work in [81], a dedicated comparison between the FOT and FP method is discussed in [82], where the authors also conclude that the FOT in general provides a better approximation. The FOT is perhaps the most traditional approximation method, implemented as in Equation 4.8. This equation is also known as Euler's Method [83].

$$f(\mathbf{x}) \approx f(\mathbf{p}) + \bigtriangledown f(\mathbf{p})(\mathbf{x}-\mathbf{p}) \tag{4.8}$$

In Equation 4.8 a known value for the function f at point(s) $\mathbf{p}$ is taken. Added to this is the gradient respective to $\mathbf{p}$, multiplied by the difference between $\mathbf{x}$ and $\mathbf{p}$. Here, $\mathbf{x}$ is the point(s) of which the function value is to be determined and $\mathbf{p}$ is a value near $\mathbf{x}$ of which the function value can be 'easily' determined. The challenge is to choose $\mathbf{p}$ and determine $\bigtriangledown f(\mathbf{p})$, which are both non-trivial.

Another linearisation method is presented in [77] where a combination of parameter approximations and piece-wise linearisation is used, hereafter referred to as PWL. The key difference between the FOT as applied in the works above and the PWL is that the PWL is only used to obtain the switch positions. The final state of the grid is analysed based on the NLP power flow. Thus, this represents a two-stage approach. Now, it can be argued that the FOT can also be used to this end. However, when comparing the FOT to the PWL, some aspects are worth discussing. First of all, the first-order Taylor series approximation requires the choice of a point near the point of interest for which the constraint can already be filled in. Determining such a point however is not trivial and can introduce rather large errors if chosen too far away from the point of interest. It is also important to take into account that this choice would have to be made for every parameter, for

every line, for every time step. This presents a lot of opportunities for the introduction of errors, as well as increasing the computational burden of the final implementation. Additionally, the first-order Taylor series approximation would introduce more constraints than the PWL. Finally, the formulation presented in [77] has already been validated in regards to its accuracy compared to the NLP power flow, which gives a higher certainty than the other methods regarding its successful implementation. In the end, the choice was made to utilise the PWL, rather than the FOT.

4.2.2. Linear power flow formulation

The power flow formulation as presented in Section 4.1.3 will be linearised using the PWL as outlined in [77]. Only the nonlinear parts will need to be adapted, which is discussed in this section. The first constraints which need to be altered are the power losses constraints. Both constraints are linearised in the same manner, by providing an initial estimate of the voltage magnitudes ($V_{m,\psi,t} = \widetilde{V}_{m,\psi,t}$) and the active and reactive power flows through the lines for each phase ($P_{mn,\phi,t} = \widetilde{P}_{mn,\phi,t}$, $Q_{mn,\phi,t} = \widetilde{Q}_{mn,\phi,t}$). Additionally, the impedance is assumed constant at the nominal frequency value. This results in the reformulated constraints for the active and reactive power losses as presented in Equation 4.9 and Equation 4.10, respectively. The estimates are based on the load flow calculations performed in PowerFactory.

$$\begin{aligned} P^{L}_{mn,\phi,t} = & \sum_{\psi\in\mathscr{S}} \frac{1}{|\widetilde{V}_{m,\psi,t}||\widetilde{V}_{m,\phi,t}|}(R'_{mn,\phi,\psi}\widetilde{P}_{mn,\phi,t}P_{mn,\psi,t} \\ & + R'_{mn,\phi,\psi}\widetilde{Q}_{mn,\phi,t}Q_{mn,\psi,t} + X'_{mn,\phi,\psi}\widetilde{P}_{mn,\phi,t}Q_{mn,\psi,t} \\ & - X'_{mn,\phi,\psi}\widetilde{Q}_{mn,\phi,t}P_{mn,\psi,t}) \quad \forall mn\in\mathscr{L},\forall\phi\in\mathscr{F},\forall t\in\mathscr{T} \end{aligned} \tag{4.9}$$

$$\begin{aligned} Q^{L}_{mn,\phi,t} = & \sum_{\psi\in\mathscr{S}} \frac{1}{|\widetilde{V}_{m,\psi,t}||\widetilde{V}_{m,\phi,t}|}(-R'_{mn,\phi,\psi}\widetilde{P}_{mn,\phi,t}Q_{mn,\psi,t} \\ & + R'_{mn,\phi,\psi}\widetilde{Q}_{mn,\phi,t}P_{mn,\psi,t} + X'_{mn,\phi,\psi}\widetilde{P}_{mn,\phi,t}P_{mn,\psi,t} \\ & + X'_{mn,\phi,\psi}\widetilde{Q}_{mn,\phi,t}Q_{mn,\psi,t}) \quad \forall mn\in\mathscr{L},\forall\phi\in\mathscr{F},\forall t\in\mathscr{T} \end{aligned} \tag{4.10}$$

Next is the voltage magnitude drop constraint, where the quadratic terms will need to be linearised. First, the square of the voltage on the left-hand side of Equation 4.6 is replaced by a new variable: $|V_{m,\phi,t}|^2 = V^{sqr}_{m,\phi,t}$. Second, the voltage on the right-hand side is replaced by an estimate: $V_{m,\psi,t} = \widetilde{V}_{m,\psi,t}$. And third, the square terms of the active and reactive power will need to be altered. To this end, Equation 4.6 is rewritten and, similarly to the voltage, the square terms are replaced by new variables resulting in Equation 4.11.

$$\begin{aligned} V^{sqr}_{m,\phi,t} - V^{sqr}_{n,\phi,t} = & \; 2\sum_{\psi\in\mathscr{S}}\left(R'_{mn,\phi,\psi}P_{mn,\psi,t} + X'_{mn,\phi,\psi,t}Q_{mn,\psi,t}\right) \\ & - \left(R'^{2}_{mn,\phi,\phi} + X'^{2}_{mn,\phi,\phi}\right)\frac{P^{sqr}_{mn,\phi,t} + Q^{sqr}_{mn,\phi,t}}{\widetilde{V}_{m,\phi,t}} \quad \forall mn\in\mathscr{L},\forall\phi\in\mathscr{F},\forall t\in\mathscr{T} \end{aligned} \tag{4.11}$$

These new variables representing the squares of the active and reactive power are also used for the current limit constraint, now formulated as in Equation 4.12.

$$0 \le P^{sqr}_{mn,\phi,t} + Q^{sqr}_{mn,\phi,t} \le V^{sqr}_{m,\phi,t}\bar{I}^{2}_{mn} \quad \forall mn\in\mathscr{L},\forall\phi\in\mathscr{F},\forall t\in\mathscr{T} \tag{4.12}$$

As a last step to the linearisation the terms $P^{sqr}_{mn,\phi,t}$ and $Q^{sqr}_{mn,\phi,t}$ will need to be approximated, which is achieved using a piece-wise linear representation. The piece-wise linearisation is achieved by dividing the function under consideration into different blocks and approximating the slope. The more blocks that are used, the higher the accuracy; similar to a Riemann sum for integrals. The piece-wise linearisation is implemented using Equations 4.13 to 4.22.

$$P^{sqr}_{mn,\phi,t} + Q^{sqr}_{mn,\phi,t} \approx \sum_{\lambda=1}^{\Lambda} \rho_{mn,\lambda} \left(\Delta^{P}_{mn,\phi,t,\lambda} + \Delta^{Q}_{mn,\phi,t,\lambda} \right) \quad \forall mn \in \mathscr{L}, \forall \phi \in \mathscr{F}, \forall t \in \mathscr{T} \tag{4.13}$$

$$P^{+}_{mn,\phi,t} + P^{-}_{mn,\phi,t} = \sum_{\lambda=1}^{\Lambda} \Delta^{P}_{mn,\phi,t,\lambda} \quad \forall mn \in \mathscr{L}, \forall \phi \in \mathscr{F}, \forall t \in \mathscr{T} \tag{4.14}$$

$$Q^{+}_{mn,\phi,t} + Q^{-}_{mn,\phi,t} = \sum_{\lambda=1}^{\Lambda} \Delta^{Q}_{mn,\phi,t,\lambda} \quad \forall mn \in \mathscr{L}, \forall \phi \in \mathscr{F}, \forall t \in \mathscr{T} \tag{4.15}$$

$$P_{mn,\phi,t} = P^{+}_{mn,\phi,t} - P^{-}_{mn,\phi,t} \quad \forall mn \in \mathscr{L}, \forall \phi \in \mathscr{F}, \forall t \in \mathscr{T} \tag{4.16}$$

$$Q_{mn,\phi,t} = Q^{+}_{mn,\phi,t} - Q^{-}_{mn,\phi,t} \quad \forall mn \in \mathscr{L}, \forall \phi \in \mathscr{F}, \forall t \in \mathscr{T} \tag{4.17}$$

$$P^{+}_{mn,\phi,t}, P^{-}_{mn,\phi,t} \geq 0 \quad \forall mn \in \mathscr{L}, \forall \phi \in \mathscr{F}, \forall t \in \mathscr{T} \tag{4.18}$$

$$Q^{+}_{mn,\phi,t}, Q^{-}_{mn,\phi,t} \geq 0 \quad \forall mn \in \mathscr{L}, \forall \phi \in \mathscr{F}, \forall t \in \mathscr{T} \tag{4.19}$$

$$0 \leq \Delta^{P}_{mn,\phi,t,\lambda} \leq \overline{\Delta}_{mn,t} \quad \forall mn \in \mathscr{L}, \forall \phi \in \mathscr{F}, \forall t \in \mathscr{T}, \lambda = 1...\Lambda \tag{4.20}$$

$$0 \leq \Delta^{Q}_{mn,\phi,t,\lambda} \leq \overline{\Delta}_{mn,t} \quad \forall mn \in \mathscr{L}, \forall \phi \in \mathscr{F}, \forall t \in \mathscr{T}, \lambda = 1...\Lambda \tag{4.21}$$

$$\rho_{mn,\lambda} = (2\lambda - 1)\overline{\Delta}_{mn,t} \quad \forall mn \in \mathscr{L}, \forall t \in \mathscr{T}, \lambda = 1...\Lambda \tag{4.22}$$

4.2.3. Comparing the linear to nonlinear power flow

Finally, it is important to validate the accuracy of the linearisation. For the sake of consistency, the third week of the year will be used once again to highlight the results. In this case the voltage magnitude, current and active power will be compared between the NLP formulation and the LP formulation, with the NLP formulation being the reference.

Table 4.2: Average and maximum error values for the voltage magnitude, current and active power. Comparing the linear power flow to the nonlinear power flow.

Parameter	Average error value [%]	Maximum error value [%]
voltage magnitude	0.002	0.017
Current	0.077	0.505
Active power	0.025	0.096

The average and maximum value of the error for each parameter is presented in Table 4.2. Something which can immediately be noticed is the low value for both the maximum error and the average error for each of the parameters. This observation is further reinforced by the heat map for each of the parameters; presented in Figure 4.11 for the voltage magnitude error, Figure 4.12 for the current error and Figure 4.13 for the active power error. From each of the figures it can be observed that the error between the linear formulation and the nonlinear formulation is small for all instances considered. One of the only interesting features appears to be that the current error in Figure 4.12 has taken a similar colour distribution as the voltage magnitude error from the nonlinear power flow of Figure 4.8a. Taking into account these results it is safe to conclude that the linear power flow formulation provides an accurate approximation of the nonlinear formulation for the purposes of this thesis.

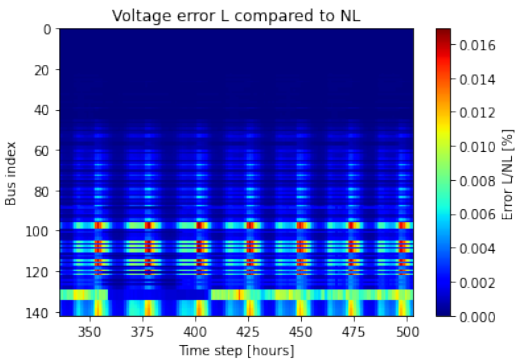

Figure 4.11: Heat map of the voltage magnitude error of the linear power flow (L) compared to the nonlinear power flow (NL).

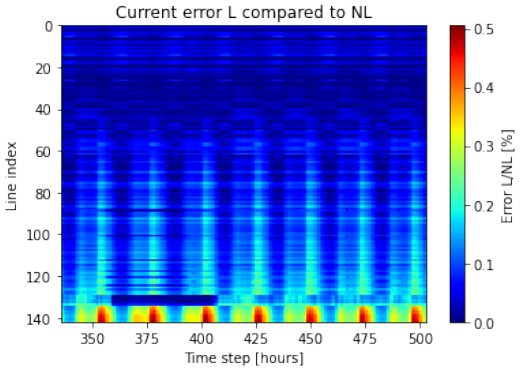

Figure 4.12: Heat map of the current error of the linear power flow (L) compared to the nonlinear power flow (NL).

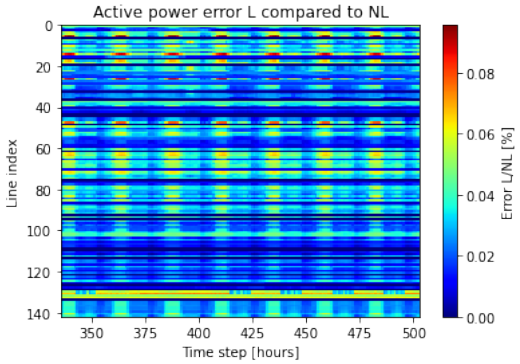

Figure 4.13: Heat map of the active power error of the linear power flow (L) compared to the nonlinear power flow (NL).

4.3. Reconfiguration algorithm

4.3.1. Network reconfiguration algorithm overview

Now, with both the power flow and its linearisation being taken care of, it is time to add the integer switch positions and formulate the reconfiguration algorithm as a MILP. However, before the adjustments to the formulation as a result of the introduction of the integer variables are presented, it may be interesting to revisit the algorithm overview for the power flow from Figure 4.3 and highlight the changes for the reconfiguration algorithm. The new diagram is depicted in Figure 4.14, where the first two steps (data import and pre-processing) are still the same. However, the old network radiality block has been removed as the radial network is no longer an input to the algorithm, but its output. Instead, it is important to select a number of the available switches for both practical application purposes, as well as computation time reduction, as will be discussed in Section 4.3.3. Next, the old power flow algorithm has been replaced by the reconfiguration algorithm, the formulation of which is discussed in Section 4.3.2. The initial estimated values for both the active and reactive power, which were introduced previously in Section 4.2.2, are also added to the algorithm. Finally, once a new configuration for the network has been obtained, its effect on the power flow is verified by using the power flow calculation with the updated switch positions. The results of the initial network reconfiguration are discussed in Section 4.3.4, highlighting the functionality of the reconfiguration algorithm.

4.3.2. Network reconfiguration formulation

Below follows the full mathematical formulation of the reconfiguration algorithm, in which the switch positions will be implemented using the variable x_{mn}, where mn is the line to which the switch is connected. It is important to note that in case the switch is open $x = 0$ and in case the switch is closed $x = 1$. First of all is the objective function in Equation 4.23, which is the same as for the power flow formulation. The power losses in Equation 4.24 and Equation 4.25 are the same as for the linear formulation, only now with the added variable x_{mn}. And a similar statement holds for the power balance constraints implemented in Equation 4.26

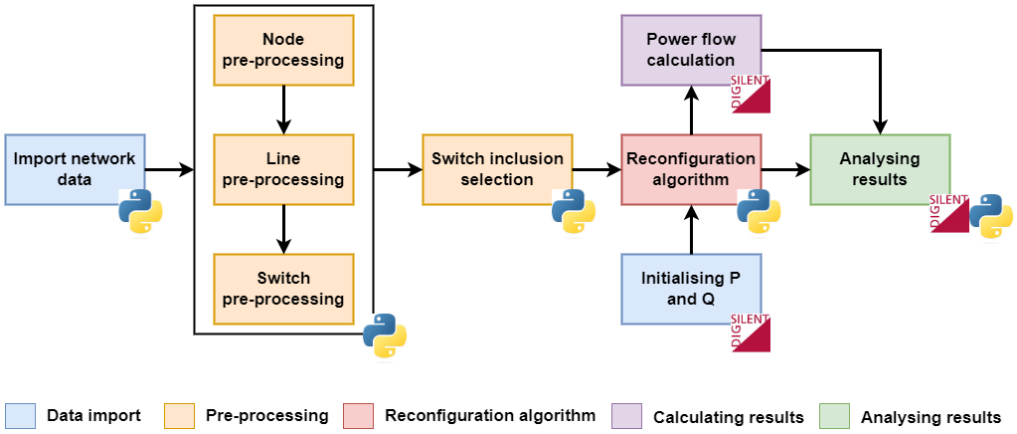

Figure 4.14: Representation of the reconfiguration algorithm implemented for this thesis, each block representing a different step inside the coded implementation. The logos represent in which environment the steps are carried out: either Python or DIgSILENT PowerFactory.

and Equation 4.27.

$$min\left\{\sum_{mn\in\mathscr{L},\psi\in\mathscr{F},t\in\mathscr{T}} P^{L}_{mn,\psi,t}\right\} \tag{4.23}$$

$$\begin{aligned} P^{L}_{mn,\phi,t} = \; & x_{mn}\sum_{\psi\in\mathscr{S}}\frac{1}{|\widetilde{V}_{m,\psi,t}||\widetilde{V}_{m,\phi,t}|}(R'_{mn,\phi,\psi}\widetilde{P}_{mn,\phi,t}P_{mn,\psi,t} \\ & + R'_{mn,\phi,\psi}\widetilde{Q}_{mn,\phi,t}Q_{mn,\psi,t} + X'_{mn,\phi,\psi}\widetilde{P}_{mn,\phi,t}Q_{mn,\psi,t} \\ & - X'_{mn,\phi,\psi}\widetilde{Q}_{mn,\phi,t}P_{mn,\psi,t}) \quad \forall mn\in\mathscr{L},\forall\phi\in\mathscr{F},\forall t\in\mathscr{T} \end{aligned} \tag{4.24}$$

$$\begin{aligned} Q^{L}_{mn,\phi,t} = \; & x_{mn}\sum_{\psi\in\mathscr{S}}\frac{1}{|\widetilde{V}_{m,\psi,t}||\widetilde{V}_{m,\phi,t}|}(-R'_{mn,\phi,\psi}\widetilde{P}_{mn,\phi,t}Q_{mn,\psi,t} \\ & + R'_{mn,\phi,\psi}\widetilde{Q}_{mn,\phi,t}P_{mn,\psi,t} + X'_{mn,\phi,\psi}\widetilde{P}_{mn,\phi,t}P_{mn,\psi,t} \\ & + X'_{mn,\phi,\psi}\widetilde{Q}_{mn,\phi,t}Q_{mn,\psi,t}) \quad \forall mn\in\mathscr{L},\forall\phi\in\mathscr{F},\forall t\in\mathscr{T} \end{aligned} \tag{4.25}$$

$$\sum_{km\in\mathscr{L}} x_{km}P_{km,\phi,t} - \sum_{mn\in\mathscr{L}} x_{mn}\left(P_{mn,\phi,t} + P^{L}_{mn,\phi,t}\right) + P^{S}_{m,\phi,t} = P^{D}_{m,\phi,t} \quad \forall m\in\mathscr{N},\forall\phi\in\mathscr{F},\forall t\in\mathscr{T} \tag{4.26}$$

$$\sum_{km\in\mathscr{L}} x_{km}Q_{km,\phi,t} - \sum_{mn\in\mathscr{L}} x_{mn}\left(Q_{mn,\phi,t} + Q^{L}_{mn,\phi,t}\right) + Q^{S}_{m,\phi,t} = Q^{D}_{m,\phi,t} \quad \forall m\in\mathscr{N},\forall\phi\in\mathscr{F},\forall t\in\mathscr{T} \tag{4.27}$$

The voltage magnitude drop constraint implemented in Equation 4.28 has been altered compared to the one discussed in Section 4.2.2 to accommodate for the fact that the input of the optimisation will no longer be a radial network. Instead, the input will be the complete meshed network and certain lines will be opened during the optimisation process to form a radial network. To elaborate on the consequences for the voltage constraint; in the old constraint, if the line between two nodes is opened then the value of the power flowing between these nodes will be zero, meaning that the right-hand side of the voltage magnitude drop constraint will be zero. As a consequence, the voltage magnitude drop between the nodes will also be zero according to the old constraint. However, there will likely still be a voltage difference between the two nodes even if they are not connected, because the end of each feeder is not connected to a common copper plate with common voltage. To accommodate for this, an additional variable is introduced in Equation 4.28 and defined as in Equation 4.29, referred to as the voltage slack variable: η. In the case that a line between two nodes is opened ($x = 0$), the value of η will be limited to an arbitrarily large number, allowing the voltage drop between the two nodes to take on the required value without the constraint limiting this to be equal to zero. If the line is

closed ($x = 1$), η will be equal to zero. To ensure that the voltage magnitude within the network is still limited to the operating constraints of the DSO, a voltage limit constraint is introduced in Equation 4.30. Similarly, the current constraint is still in effect as implemented in Equation 4.31.

$$\begin{aligned} V^{sqr}_{m,\phi,t} - V^{sqr}_{n,\phi,t} + \eta_{mn,\phi,t} = \; & 2 \sum_{\psi \in \mathscr{S}} \left(R'_{mn,\phi,\psi} P_{mn,\psi,t} + X'_{mn,\phi,\psi,t} Q_{mn,\psi,t} \right) \\ & - \left(R'^{2}_{mn,\phi,\phi} + X'^{2}_{mn,\phi,\phi} \right) \frac{P^{sqr}_{mn,\phi,t} + Q^{sqr}_{mn,\phi,t}}{\widetilde{V}_{m,\phi,t}} \quad \forall mn \in \mathscr{L}, \forall \phi \in \mathscr{F}, \forall t \in \mathscr{T} \end{aligned} \tag{4.28}$$

$$|\eta_{mn,\phi,t}| \leq M(1 - x_{mn}) \quad \forall mn \in \mathscr{L}, \forall \phi \in \mathscr{F}, \forall t \in \mathscr{T} \tag{4.29}$$

$$V^{min,sqr} \leq V^{sqr}_{m,\phi,t} \leq V^{max,sqr} \quad \forall m \in \mathscr{N}, \forall \phi \in \mathscr{F}, \forall t \in \mathscr{T} \tag{4.30}$$

$$0 \leq P^{sqr}_{mn,\phi,t} + Q^{sqr}_{mn,\phi,t} \leq V^{sqr}_{m,\phi,t} \bar{I}^{2}_{mn} \quad \forall mn \in \mathscr{L}, \forall \phi \in \mathscr{F}, \forall t \in \mathscr{T} \tag{4.31}$$

The radiality of the optimised network still needs to be guaranteed by the reconfiguration algorithm, which necessitates the introduction of new constraints. First of these is the value of the switches, which is limited to the integer values 0 and 1, implemented as in Equation 4.32. Additionally, the final implementation of the topology for the MV network is still required to be radial to conform to the operating standards of the DSO. To enforce this, a radiality constraint is implemented in Equation 4.33, which is the mathematical implementation of the first constraint for radiality: *For a network consisting of N nodes, the final network must have N-1 lines (also referred to as edges) connecting these nodes.*

$$x_{mn} \in \{0, 1\} \quad \forall mn \in \mathscr{L} \tag{4.32}$$

$$\sum_{mn \in \mathscr{L}} x_{mn} = \mathbf{N} - 1 \quad \forall mn \in \mathscr{L} \tag{4.33}$$

The final addition to the reconfiguration algorithm is in regards to the values for P^{sqr} and Q^{sqr}. These variables also need to be adjusted depending on the switch position. However, rather than adding the switch position variable x_{mn} to every individual constraint of the piece-wise linearisation, two additional constraints are introduced in Equation 4.34 and Equation 4.35. The variables $P^{sqr,switch}$ and $Q^{sqr,switch}$, represent the normal value of P^{sqr} and Q^{sqr}, unless the switch for that specific line is open, in which case the value will be zero. Because of this implementation, only Equation 4.36 needs to be adjusted compared to the linear formulation. Equations 4.37 to 4.45 are the same as for the linear formulation.

$$P^{sqr,switch}_{mn,\phi,t} = x_{mn} P^{sqr}_{mn,\phi,t} \quad \forall mn \in \mathscr{L}, \forall \phi \in \mathscr{F}, \forall t \in \mathscr{T} \tag{4.34}$$

$$Q^{sqr,switch}_{mn,\phi,t} = x_{mn} Q^{sqr}_{mn,\phi,t} \quad \forall mn \in \mathscr{L}, \forall \phi \in \mathscr{F}, \forall t \in \mathscr{T} \tag{4.35}$$

$$P^{sqr,switch}_{mn,\phi,t} + Q^{sqr,switch}_{mn,\phi,t} \approx \sum_{\lambda=1}^{\Lambda} \rho_{mn,\lambda} \left(\Delta^{P}_{mn,\phi,t,\lambda} + \Delta^{Q}_{mn,\phi,t,\lambda} \right) \quad \forall mn \in \mathscr{L}, \forall \phi \in \mathscr{F}, \forall t \in \mathscr{T} \tag{4.36}$$

$$P^{+}_{mn,\phi,t} + P^{-}_{mn,\phi,t} = \sum_{\lambda=1}^{\Lambda} \Delta^{P}_{mn,\phi,t,\lambda} \quad \forall mn \in \mathscr{L}, \forall \phi \in \mathscr{F}, \forall t \in \mathscr{T} \tag{4.37}$$

$$Q^{+}_{mn,\phi,t} + Q^{-}_{mn,\phi,t} = \sum_{\lambda=1}^{\Lambda} \Delta^{Q}_{mn,\phi,t,\lambda} \quad \forall mn \in \mathscr{L}, \forall \phi \in \mathscr{F}, \forall t \in \mathscr{T} \tag{4.38}$$

$$P_{mn,\phi,t} = P^{+}_{mn,\phi,t} - P^{-}_{mn,\phi,t} \quad \forall mn \in \mathscr{L}, \forall \phi \in \mathscr{F}, \forall t \in \mathscr{T} \tag{4.39}$$

$$Q_{mn,\phi,t} = Q^{+}_{mn,\phi,t} - Q^{-}_{mn,\phi,t} \quad \forall mn \in \mathscr{L}, \forall \phi \in \mathscr{F}, \forall t \in \mathscr{T} \tag{4.40}$$

$$P^{+}_{mn,\phi,t}, P^{-}_{mn,\phi,t} \geq 0 \quad \forall mn \in \mathscr{L}, \forall \phi \in \mathscr{F}, \forall t \in \mathscr{T} \tag{4.41}$$

$$Q^{+}_{mn,\phi,t}, Q^{-}_{mn,\phi,t} \geq 0 \quad \forall mn \in \mathscr{L}, \forall \phi \in \mathscr{F}, \forall t \in \mathscr{T} \tag{4.42}$$

$$0 \leq \Delta^{P}_{mn,\phi,t,\lambda} \leq \overline{\Delta}_{mn,t} \quad \forall mn \in \mathscr{L}, \forall \phi \in \mathscr{F}, \forall t \in \mathscr{T}, \lambda = 1...\Lambda \tag{4.43}$$

$$0 \leq \Delta^{Q}_{mn,\phi,t,\lambda} \leq \overline{\Delta}_{mn,t} \quad \forall mn \in \mathscr{L}, \forall \phi \in \mathscr{F}, \forall t \in \mathscr{T}, \lambda = 1...\Lambda \tag{4.44}$$

$$\rho_{mn,\lambda} = (2\lambda - 1)\overline{\Delta}_{mn,t} \quad \forall mn \in \mathscr{L}, \forall t \in \mathscr{T}, \lambda = 1...\Lambda \tag{4.45}$$

4.3.3. Switch selection

If simply considering all switches which can be considered for the MILP the total number of possible configurations would be $\frac{150!}{11!(150-11)!} = 1.4885 * 10^{16}$. Considering all 150 switches for half a year is computationally too intensive to be carried out by the available hardware. Additionally, the DSO will likely not consider all switches to be available for network reconfiguration to begin with. Normally, the DSO will have certain switches which they do not consider, because they are hard to reach or already rather old for example. Thus, a selection will be made of which switches to consider inside the reconfiguration algorithm.

The method for the switch selection is as follows. First, a random half-day of the year is selected. The network data for this day is used as input for the network reconfiguration algorithm, which is subsequently run. All switches are considered by the algorithm during this run. The result will be a list of the switches altered by the algorithm, which will be reasonable candidates to be considered within the final implementation of the reconfiguration algorithm. This process is also graphically displayed in Figure 4.15.

It should be noted that this process is computationally already very intensive, with a single iteration already lasting more than a day (using an HP ZBook Studio G5 laptop). Since this thesis is only a proof of concept and since this selection process would likely not be adapted for practical implementations, the choice was made to only perform this process five times. However, the same process can be repeated for as many iterations as desirable.

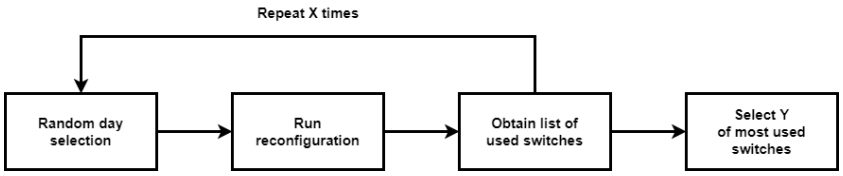

Figure 4.15: Switch selection process.

The result of this process has been a list of 25 different switches which will be considered for the final implementation. Considered, in this case, means that these switches will be used as integer variables within the MILP. The position of the other switches will be held constant. Ten of the considered switches are the original switches which were open in the base topology and the other fifteen were obtained with the method described above. The locations of these switches within the network are illustrated in red and blue below in Figure 4.16.

The one switch from the original eleven switches which will not be considered, and will thus remain open, is the switch highlighted in purple. The reason for excluding this switch is that it can only be closed if one of the two lines originating from the centre, which are attached to the same nodes as the originally open line, is opened instead. At least one of these three lines needs to be open for the network to fulfil the radiality constraint. Since the other two lines are not considered, the originally open line must remain open in every considered realisation, making its inclusion obsolete.

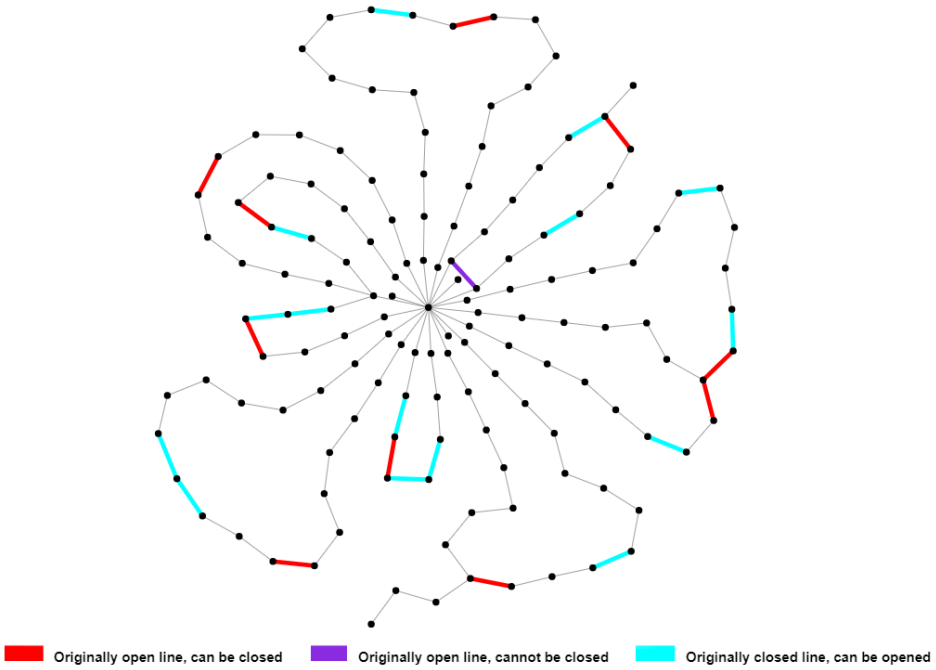

Figure 4.16: Locations of the switches considered for the final implementation of the reconfiguration algorithm. The red lines represent the switches which were opened in the original network configuration. The blue lines are added based on the switch selection process.

4.3.4. Base-case topology optimisation

As an initial test of the functionality of the reconfiguration algorithm, the base-case network data (including demand and generation as presented in Chapter 3) will be used as input for the reconfiguration algorithm, which is subsequently solved using the Gurobi optimiser [84]. The reason for replacing the Ipopt solver used in the power flow formulation is that the Gurobi solver is specialised in linear and mixed-integer programs, whereas the Ipopt solver is aimed at nonlinear programs. This holds for all subsequent mentions of both algorithms as well, where an individual power flow is solved using Ipopt and the reconfiguration algorithm is solved using Gurobi. Apart from that, the third week of the year is once again considered for the simulation. Using the base topology from Figure 4.16, where the purple line and red lines are open, the total power losses within the network add up to 10.19 MW.

Using the reconfiguration algorithm a new selection of switches is obtained. The used switches are highlighted in green in Figure 4.17. The red lines within the same figure still highlight the originally open lines, however they are no longer opened. Thus, with the reconfiguration algorithm, a total of five new switches are selected to be opened. The other six are still the same as in the base topology. Four out of the five new switches are located relatively close to the old location, only having moved one line. However, one noticeable exception to this is the red line in the top right corner of Figure 4.17, where the new opened line has moved three positions.

The new network topology is used within the power flow calculation to validate its improvement compared to the base topology. The resulting active power losses within the network using the new topology presented in Figure 4.17 add up to a total of 9.93 MW over the considered time frame, which is a reduction of 0.26 MW compared to the 10.19 MW of the base topology. This reduction may seem somewhat small at first, however it is worth placing it in context. By merely changing the position of ten switches within the network (5 are closed, 5 are opened) the active power losses can be reduced by 2.55%. This is within a network that is not even experiencing congestion yet, which is meant to be the main point of improvement by the algorithm.

It is worth pointing out here that even as the topology has changed due to the optimisation, it cannot be concluded that the new topology is more efficient in every way than the base topology. It is only an improvement in terms of the active power losses. This becomes evident from the objective function, which currently only considers the active power losses, similar to [38] [58] [66] for example. Contrary, there are many more consid-

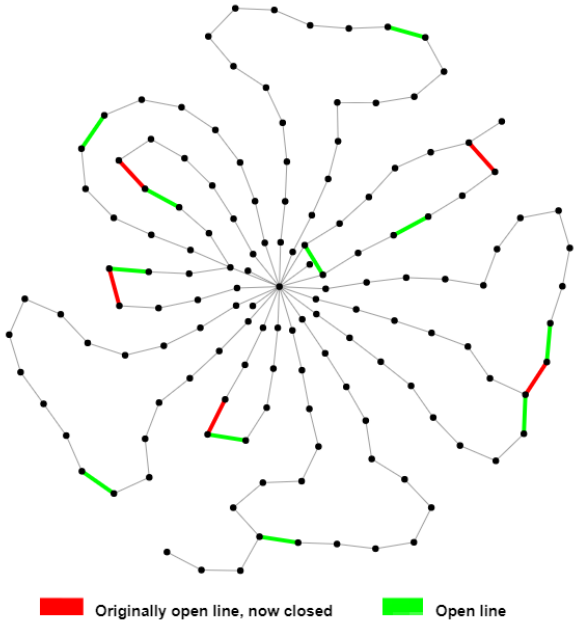

Figure 4.17: The new network topology obtained using the reconfiguration algorithm for the third week of 2021. Within the figure, green lines indicate open lines and red lines indicate the previously open lines of the original network topology.

erations which can be taken into account when looking at the network topology, such as cost minimisation, priority loads and areas with ageing equipment where the number of switching actions needs to be limited. However, the data necessary to include such considerations is not available for this thesis. As such, the objective function will be confined to minimising the active power losses.

The functionality in regards to reducing congestion is tested in the next chapters. Further conclusions regarding improvements compared to the base topology will be made knowing that these improvements can have either less or more impact depending on further considerations taken with regards to the objective function.

Taking all of the above into consideration, it can be concluded that the presented reconfiguration algorithm in Equation 4.23 up to Equation 4.45 provides satisfactory functionality to determine a more efficient network topology with regards to active power losses.

4.3.5. Comparison to PowerFactory

The software environment of PowerFactory also offers a similar functionality with regards to optimising the network topology, referred to as tie open point optimisation (TOPO). To further explore the capabilities of the presented reconfiguration algorithm, a comparison will be made with two of the available methods for TOPO. The methods in question are a deterministic variant, where an iterative exploration of the meshes is carried out, and a meta-heuristic variant, where a genetic algorithm is used. Both methods will utilise the same objective function similar to the reconfiguration algorithm; minimising the losses within the network. Specifically selecting active power losses is unfortunately not possible.

Apart from the objective function, the TOPO will have similar constraints as the reconfiguration algorithm. The network is represented as a balanced three-phase network, in this case utilising the positive sequence. Additionally, only the load-break-disconnnectors will be considered for altering the topology. Finally, with regards to the constraints, the TOPO will use the same voltage constraints and thermal limits (translating to maximum current values for the lines) as the reconfiguration algorithm. Once again, the third week of the year will be considered for the optimisation.

Next the comparison, first of which will be the iterative mesh exploration. A successful reconfiguration is car-

ried out by PowerFactory while considering all switches within the network. Note that this deviates from the switch selection pre-processing done for the reconfiguration algorithm presented in this thesis, since such functionality is not available in PowerFactory. The optimised configuration by PowerFactory is displayed in Figure 4.18.

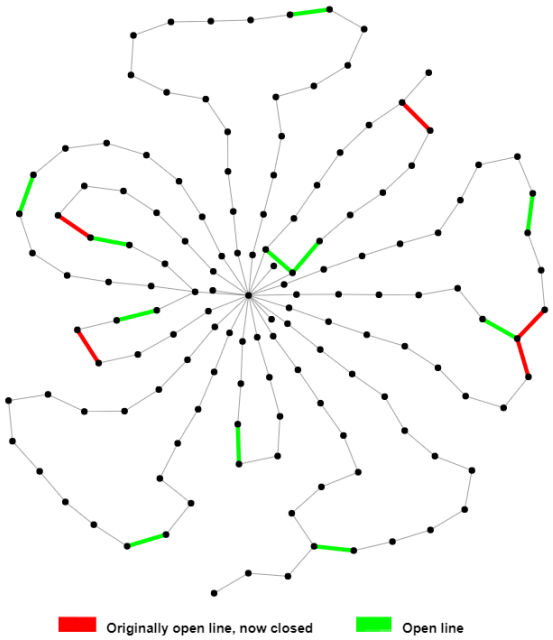

Figure 4.18: The new network topology obtained using the iterative mesh exploration method of PowerFactory for the third week of 2021. Within the figure, green lines indicate open lines and red lines indicate the previously open lines of the original network topology.

For most selected switches the difference between the reconfiguration algorithm and PowerFactory is not too severe, either being the same or having moved one line further away from the original switch position. However, there are some noticeable differences between the results of both methods. Most noticeably perhaps being the top-right loop, where the switch was previously opened at the top of the loop in the base case, opened halfway along the right side in the optimised topology from the reconfiguration algorithm, and has now been moved even closer to the centre by PowerFactory. Another noticeable difference is found in the right-most loops, where the top switch has been opened three lines higher and the bottom switch has moved to the left.

The resulting active power losses of the new network configuration have been calculated as well, resulting in a total of 10.11 MW for the entire network, over the considered time frame. Compared to the original 10.19 MW, this is a reduction of 0.79%. This is less of an improvement than the one offered by the reconfiguration algorithm. Additionally, PowerFactory was able to consider all available switches within the network, whereas the reconfiguration algorithm could only select the ones allocated after the switch selection process. This goes to highlight the functionality of the reconfiguration algorithm for providing an improved topology while offering more flexibility in terms of constraints for the optimisation.

The second comparison will be between the reconfiguration algorithm and a genetic algorithm used by PowerFactory. Note that the base population settings provided by PowerFactory were used, as fine-tuning the genetic algorithm is outside the scope of this thesis. The parameters in question can be found in Appendix C. The TOPO in PowerFactory is run and a new configuration is obtained, which is displayed in Figure 4.19.

The solution provided by the genetic algorithm shares most similarities with the solution using the iterative mesh exploration. The most noticeable difference is once again in the right-most loops, where the lower switch has now been closed and a switch much closer to the centre has been opened instead. Using the topology in Figure 4.19 results in the active power losses adding up to 10.57 MW over the considered time

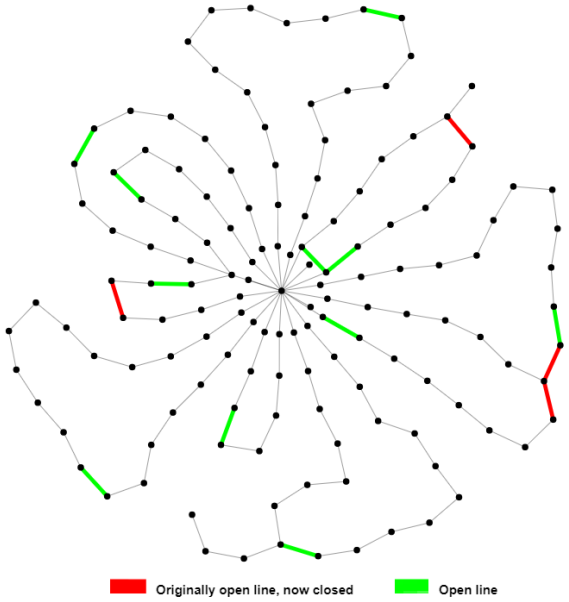

Figure 4.19: The new network topology obtained using the genetic algorithm of PowerFactory for the third week of 2021. Within the figure, green lines indicate open lines and red lines indicate the previously open lines of the original network topology.

frame, which is actually a deterioration of the objective function value compared to the base case. There are two arguments which can be made as to why. First of all, the genetic algorithm is a meta-heuristic approach which cannot guarantee a global optimal solution. Second, the population settings have not been altered from the standard settings offered by PowerFactory. Optimising these parameters would likely improve the obtained result.

Regardless, even when considering optimising the population settings for the genetic algorithm, this would be an additional step which is not required for the reconfiguration algorithm, nor for the iterative mesh exploration for that matter. Adding to this that the genetic algorithm is not able to guarantee a global optimum and the use of the genetic algorithm for the considered case study becomes the least attractive option.

Overall, the reconfiguration algorithm provides the best solution in terms of the objective function, while offering more versatility for constraining the optimisation than both considered algorithms offered by PowerFactory. This second part can be especially important when other operational constraints of the DSO need to be considered which are not encompassed by standard voltage and thermal limits or switch type selection.

5

Scenario formulation

In order to validate the capabilities of the network reconfiguration algorithm, to reduce congestion within the network, several scenarios are formulated to simulate future developments within the considered MV grid. To keep the formulation within scope of the thesis, some assumptions will be made based on different sources, which will be highlighted as the different aspects are discussed.

To be specific, a total of three future scenarios will be formulated for the years 2030, 2040 and 2050. These scenarios are made up of three parts. First, there is the increase of the base energy demand within the network. Second, there is the increase in electricity generation by distributed PV installations. And third, there is the increase in energy demand due to the increased use of electric vehicles within the urban environment. The latter two will also be applied to the base year of 2021. Each of these parts is discussed in more detail in Section 5.1. This is followed by an analysis in Section 5.2 of the effects caused by these scenarios within the base-case topology.

Additionally, a stochastic scenario will be formulated, which is used to enhance the insights offered by the deterministic scenarios by no longer assuming perfect knowledge. The stochastic scenario will only be formulated for the year 2030, as this already tends to be a long-term time span with regards to planning considerations for most system operators. Thus, this should already be able to illustrate the added benefits offered by the inclusion of stochastic models. The details of the stochastic modelling will be discussed in Section 5.3.

5.1. Scenario components

The first part of the scenarios, the base load increase, will be an increase of 1.43% per year compared to the base load presented in Section 3.2. This percentage is based on the historic electricity demand increases from 2015 to 2022 in [85], as well as the future demand increases predicted in [86]. A combination of sources is chosen to ensure that the offset caused by the recent COVID-19 pandemic is mitigated as much as possible. The total base-load increase for each of the scenarios compared to the initial starting year of 2021 can be found in Table 5.1.

Table 5.1: Load increase for each scenario compared to the base case in 2021.

Scenario	Load increase compared to 2021 [%]
2030	13.6
2040	31.0
2050	50.9

Next, there is the increase of distributed PV generation. The PV generation is included within the scenarios for several reasons. Most prominent among them being that the PV installations are the only distinguishable source of generation within the MV grid. Other technologies may be present within the LV grid, but this cannot be stated with certainty as the generation data is all aggregated to the generation of the MV loads. There are also the considerations of increased accessibility to PV installations due to their lower costs combined

with the motivation to increase renewable generation.

The scenarios for the PV generation are based on installed capacity predictions by the DSO which also supplied the initial network data. This capacity is subsequently multiplied with a normalised version of the generation profile presented previously in Section 3.2, assuming that the irradiation pattern will not change much in subsequent years. This results in additional generation profiles for several of the nodes within the network which can be added to the base network generation profile. The total added generation per year is graphically displayed in Figure 5.1. Note that not every node will have an increase in installed capacity, but the ones that do will have a profile as in Figure 5.1. It is also important to note that the initial year of 2021 is also displayed as additional generation. This is intentional, as it is assumed that the added generation originates from the aggregated LV grid. Since the technologies used within the LV grid cannot be distinguished, the PV generation is added explicitly based on the scenarios from the DSO.

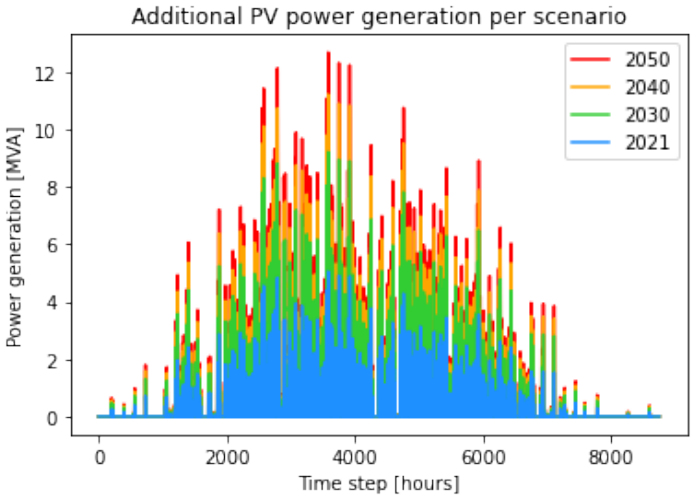

Figure 5.1: Future PV generation scenarios for the years 2021, 2030, 2040 and 2050

Finally, there is the increase in distributed energy demand due to increased deployment and use of EV's. This data is based on other work done within the ROBUST project and its predecessors, for example in [87], and is adapted for this thesis to highlight the same considerations regarding distributed energy demand due to EV's. It is assumed that the current network data does not include EV's within the considered energy demand. As such, the EV scenario data will be added to the existing load profiles, similar to the PV scenarios. A graphical representation of the total added load from the EV scenarios per year is presented in Figure 5.2. It is important to emphasise that the load profile from Figure 5.2 is the aggregated profile; the increased energy demand per node will vary and not every node will have an increase to begin with. This is in contrast to the PV scenarios where the shape of the profile for each individual node is the same, but the resulting generation is dependent on the installed capacity.

5.2. Scenarios in the base network topology

Finally, before the results of the network reconfiguration can be analysed, it is important to place the different scenarios within context. In Figure 5.4, the results of the power flow calculation for each scenario using the base-case topology are displayed. In this case, if a line is green, it means that there is no congestion within the line. If a line is orange, it means that there is formally no congestion yet, but the automated detection within the control room would flag the line as being congested, after which a manual verification is carried out. This is an additional measure to prevent network issues in case of a fault. For example, the loading limit for GPLK cables is set at 70% during normal operation, however it is flagged as being congested at 60% loading. For this reason, a distinction is made between formally congested lines (which surpass the loading limit given in Chapter 3) and lines which will be flagged as being congested, but are formally still within the limits. And finally, if a line is red, it means that the line is congested at one point (or multiple points) during the consid-

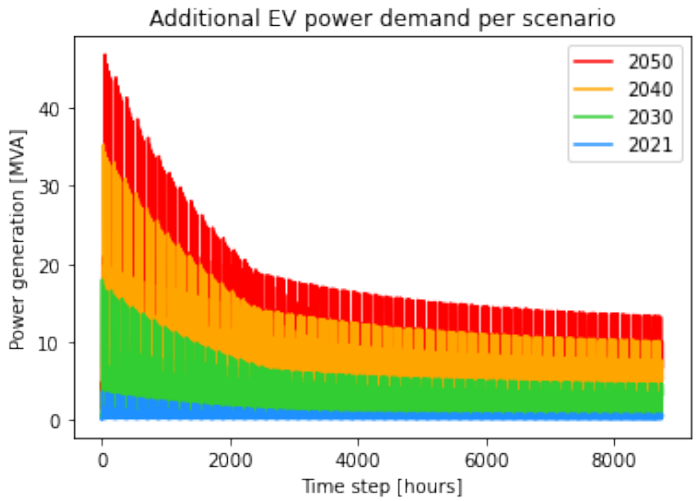

Figure 5.2: Future EV load scenarios for the years 2021, 2030, 2040 and 2050

ered time frame. Congestion is being defined as the amount of current overloading on a line surpassing the given limits of 70% for GPLK cables and 100% for XLPE and KUDI cables. The calculations are once again done for the third week of the year, representing the winter configuration. The net electricity demand for this period for each scenario is displayed in Figure 5.3. A combination of the scenario formulation and the results presented in Chapter 6 is also given in Appendix B for the 26th week of the year (starting at hour 4200), representing the summer configuration.

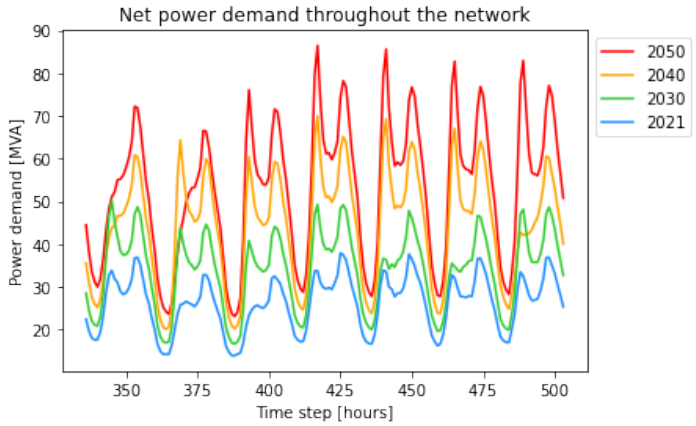

Figure 5.3: Net power demand within the considered network for the 3rd week of the year.

With the addition of the PV generation and EV load to the 2021 scenario, it is possible to observe the occurrence of congestion within the network, as can be seen in Figure 5.4a. This is also an important motivation for the formulation of the scenarios to begin with, as the purpose of the reconfiguration algorithm is to reduce congestion. Thus, congestion needs to be present before any conclusions about the algorithm's functionality can be drawn. Several more cases of congestion can be observed in Figure 5.4b for the 2030 scenario with the increases in base load, PV generation and EV load. These occurrences only increase for the following scenarios in Figure 5.4c and Figure 5.4d. It is also interesting to note that the congestion is occurring in different lines of the network first. The right-hand side of the network is already experiencing congestion in 2030, whereas the bottom left is still secure even in 2050.

Note that the networks displayed in Figure 5.4 do not contain any quantitative data as this will be presented and discussed within Chapter 6 with respect to the reconfiguration algorithm. However, it is worth pointing out that the current limits for the colouring are based on discussions with one of the Dutch DSOs, but during

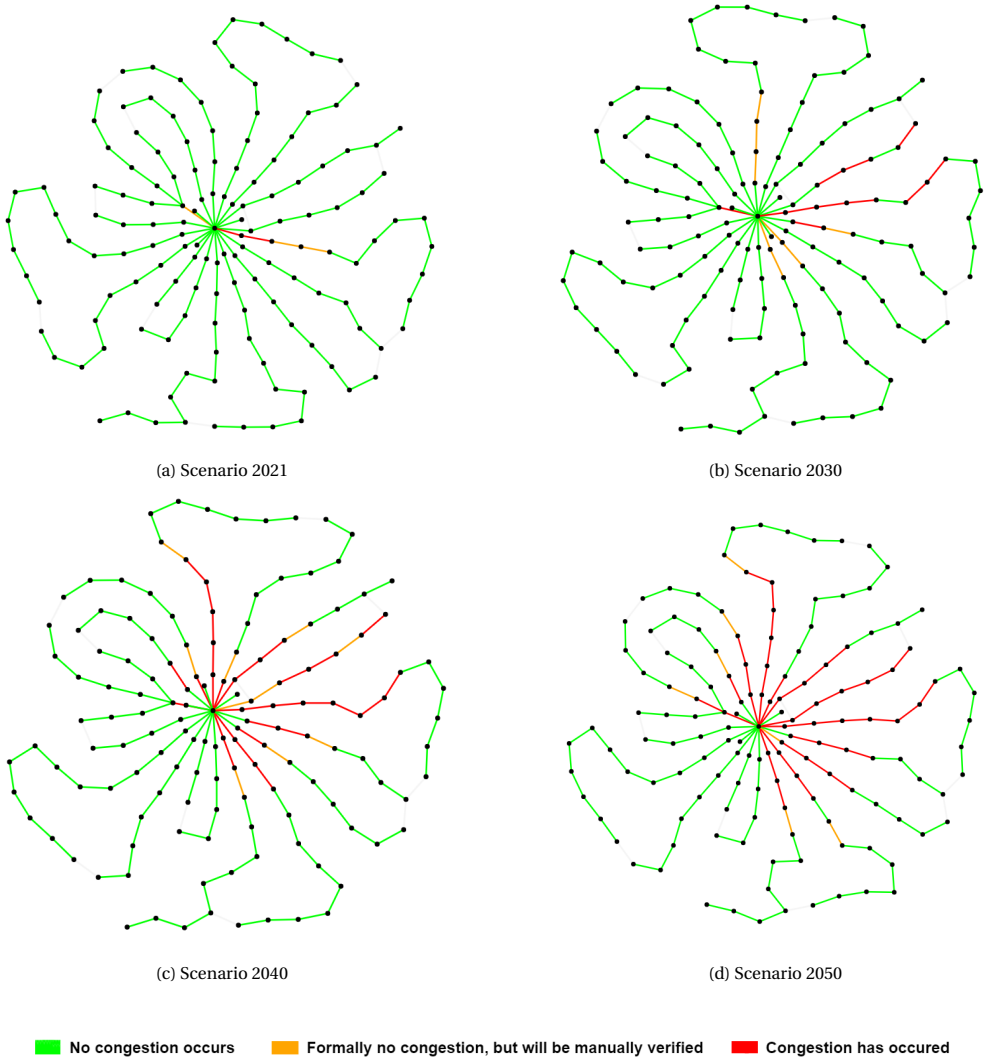

(a) Scenario 2021

(b) Scenario 2030

(c) Scenario 2040

(d) Scenario 2050

Figure 5.4: Overview of the effect of the different scenarios with regards to the occurrence of congestion within the base network topology. Within the images a green colour indicates a line without congestion. An orange colour indicates that the line is formally not experiencing congestion yet, but its status will be manually checked. A red colour indicates that a line has experienced one or more moments of congestion during the considered time frame.

that same discussion it was also mentioned that these limits may change depending on ongoing research. In particular, it is investigated whether components can be operated under higher loading. Thus, it is important to take into account any potential updates within the operating limits in case of future reference. For now, it is important that the scenarios highlight the increasing strain on the electricity system if it is left within its current state and provide an opportunity for the implementation of measures to reduce said strain.

5.3. Introducing stochasticity

The final addition to the modelling considerations will be the introduction of a stochastic scenario. The primary motivation for this addition is the large factor of uncertainty which is involved when considering scenarios of one or multiple decades into the future. The scenarios formulated previously will likely differ from the true developments in electricity demand and supply, although to which extent is by the same logic hard to predict. The stochastic scenario is meant to provide some measure of insight regarding the possible consequences of the assumptions made for the deterministic scenarios and into what happens to the provided solution in case the true developments differ from these assumptions.

In order to formulate the stochastic scenario, a couple of components are necessary. First, the stochastic scenario will consist of several variations of the initial deterministic scenario. The scenario for the year 2030 will be used as a base for the stochastic scenario. The number of variations is to a degree arbitrary, although this does depend on what form the stochastic model will take. For now, to keep the computation time reasonable, ten variations will be taken.

Second, it is important to discuss how these variations are made. The variations will be constructed by formulating different power demand profiles, which will happen according to Equation 5.1.

$$P^D(s) = (1 + n(s) \times P_{dev})\, P^D \tag{5.1}$$

In Equation 5.1, P^D is the deterministic demand profile. P_{dev} is the maximum deviation from the deterministic value, which is taken to be 5% (or 0.05). The symbol $n(s)$ is a random sample taken from a normal distribution: $n(s) \in \mathcal{N}(\mu, \sigma^2)$ [88], where μ is taken to be 0 and σ is taken as 0.8. Here, s is one of the ten variations of the deterministic model. Finally, $P^D(s)$ is the stochastic variation s of the deterministic power demand scenario. The realisations of the random samples for each variation s used within this work are shown in Table 5.2.

Table 5.2: Random samples of a normal distribution used for creating the variations for the stochastic scenario.

s	1	2	3	4	5	6	7	8	9	10
$n(s)$	−0.055	−1.096	0.263	1.316	0.360	0.591	−0.882	−1.357	−0.813	0.747

Next, it is important to know how likely each of these variations is to occur. For this, two possibilities have been considered. First, as the realisations of $n(s)$ are taken from a normal distribution, this same distribution could be used to formulate probabilities for the different stochastic scenarios. To be specific, formulating the probabilities such that the values of $n(s)$ which are closer to the mean would have a higher probability of occurring. However, this has two major drawbacks. First, the point of the different stochastic scenarios is to highlight that the deterministic scenarios may differ from the future realisation; perhaps by a large margin. Thus, assuming that the probability of larger variations is lower, would be a poor reflection of this difference. Second, since the samples taken from the normal distribution are randomised, it would be hard to determine what the probability of each realisation would be while still considering a complete search space of mutually exclusive realisations. This led to the decision to formulate the probability of each stochastic variation as an uniform probability, taken as one over the total number of variations (1/10 in this case). Other possibilities would have been considered if the scenario formulation was one of the focus points of this thesis, however this is not the case, as was already covered at the start of this chapter.

With the formulation of the stochastic scenario out of the way, it is time to highlight how it affects the deterministic reconfiguration algorithm discussed in Chapter 4. The first important change is made to the variables of the formulation, which each receive an additional index s, for the different variations of the stochastic scenario. The only exception to this is the switch position x_{mn} as it will be optimised for the combination of stochastic scenario variations. Next, the parameters for the active and reactive power, P^D and Q^D, also get the additional index for the stochastic scenario. Finally, the objective function is updated with the probability of each variation of the stochastic scenario p_s, as is shown in Equation 5.2.

$$min \left\{ \sum_{mn \in \mathcal{L}, \psi \in \mathcal{F}, t \in \mathcal{T}, s \in \mathcal{S}} p_s \, P^L_{mn,\psi,t,s} \right\} \tag{5.2}$$

It is important to stress that these changes to the formulation of the reconfiguration algorithm will only be used for the stochastic scenario analysed in the next chapter. The deterministic formulation as presented in Chapter 4 will be used for the previously discussed deterministic scenarios.

6

Discussion of results

With the model and scenario formulation completed, it is time to look at the capabilities of the reconfiguration algorithm to reduce congestion within the analysed network. Each of the scenarios outlined in Chapter 5, where the winter period is considered, will be discussed separately. To be specific, Section 6.1 will cover the new base scenario in 2021, which now includes the initial PV and EV data (which deviates from the base scenario used in Chapter 4). Following this will be Section 6.2, Section 6.3 and Section 6.4, covering the scenario for 2030, 2040 and 2050, respectively. A separate analysis of these scenarios for the summer period is presented in Appendix B. The analysis of the solutions offered by the reconfiguration algorithm is followed by a comparison to the solution provided by PowerFactory for the 2030 scenario in Section 6.5. Finally, the stochastic scenario will be covered separately in Section 6.6.

For each of the scenarios there are a couple of parameters of interest. First is the active power losses, as this is the term being optimised within the optimisation process. If this term is reduced, it means the optimisation is performing adequately. Another point of interest is the number of lines experiencing congestion. Just to repeat, congestion is being defined as the amount of current overloading on a line surpassing the given limits of 70% for GPLK cables and 100% for XLPE and KUDI cables. Ideally, this number would be improved upon as it would indicate that the reconfiguration algorithm has completely resolved the congestion within one of the lines. However, the likelihood of this happening for the later scenarios is rather small, as the overloading of the lines gets quite severe. Thus, a parameter which will offer more insight for the later scenarios will be the total amount of occurrences of congestion within the considered time frame. For each scenario, a week will be simulated, meaning that there are a total of 23856 data points (one for each hour for each line). One of these data points is counted as being congested when the respective maximum line loading is breached (70% for GPLK, 100% for XLPE and KUDI).

If congestion does occur within the network, it is also important to consider its size. As a consequence, the average size of line overloading (the percentage by which the line current surpasses the given limit) will be reported and the same holds for the maximum encountered value. Finally, the different lines have two line loading limits: the first during normal operation and the second during a disturbance or maintenance (refer to Chapter 3). The number of occurrences of congestion surpassing this second limit will also be reported. The motivation being that congestion can be classified as a disturbance, in which case the lines are allowed to be loaded up to the second limit for up to five working days, according to the standards set by the DSO.

6.1. Scenario 2021

For the first scenario there are two lines which experience congestion during the considered time frame. Thus, the reconfiguration algorithm can be used to obtain a new topology for the network. Having said that, the new configuration of the MV grid topology obtained by the reconfiguration algorithm is displayed in Figure 6.1, where the blue lines are opened and the pink lines were previously open within the base topology but are now closed. Within the figure it is possible to observe that five new switches have been selected to be opened compared to the original topology. Additionally, the new line loading is displayed in Figure 6.2. The

great thing which can be observed within this figure is that the red lines have disappeared compared to the original topology from Figure 5.4a, meaning that the congestion has been resolved.

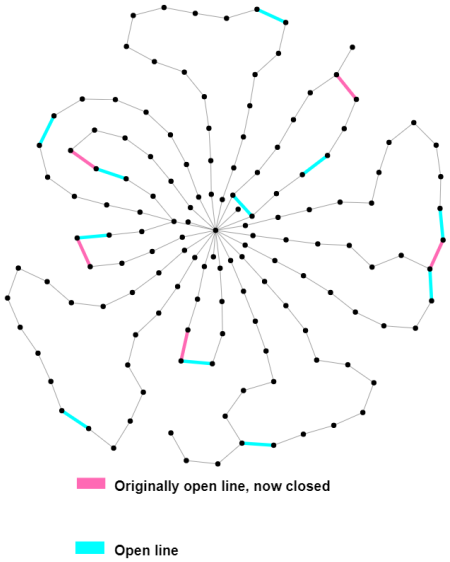

Figure 6.1: The new network topology obtained from using the reconfiguration algorithm for the third week of scenario 2021.

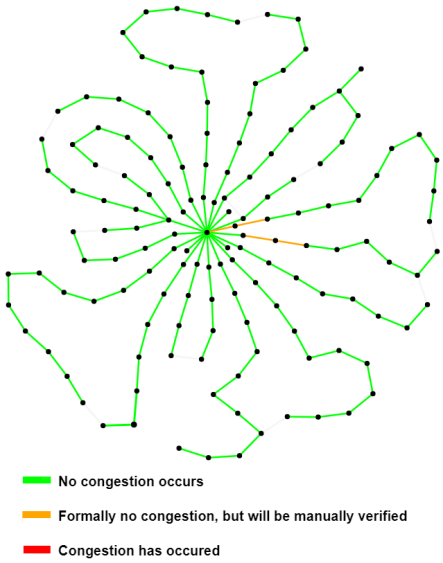

Figure 6.2: The occurrences of congestion within the new network topology for the third week of scenario 2021.

For more details regarding the parameters of interest, one can refer to Table 6.1. From the table, it becomes clear that the active power losses have not actually dropped, remaining at 10.64 MW. More importantly however, is the reduction from 2 to 0 lines experiencing congestion within the considered time frame. This means that the reconfiguration algorithm has successfully removed the congestion from the network for the 2021 scenario. While it should also be noted that congestion did only occur 11 times during the considered time frame with a maximum overloading of 4.95%, it is still a satisfactory result to see that the reconfiguration algorithm is able to remove congestion from the network.

Table 6.1: Summary of results for scenario 2021.

	Base topology	Optimised topology
Active power losses [MW]	10.64	10.64
Number of lines experiencing congestion	2	0
Instances of congestion	11	0
Average overloading size [%]	1.61	0.00
Maximum overloading size [%]	4.95	0.00
Instances of congestion above maintenance/disturbance limit	0	0

6.2. Scenario 2030

In the 2030 scenario the occurrences of congestion start to increase compared to 2021. Thus, the reconfiguration algorithm is used and a new topology is obtained, as is displayed in Figure 6.3. Three of the originally open lines have been closed and three alternative lines have been opened instead. Using this topology, the power flow calculation is repeated and the network loading changes to the one displayed in Figure 6.4.

At first glance it may seem like not much has changed compared to the scenario for 2030 in the base topology, as presented in Figure 5.4b. The main difference is that there is one additional line experiencing congestion now. Similar to the error heat map used in previous chapters, Figure 6.5 represents the current overloading size for every line for every time step in the base topology as well as for the optimised topology. In the figure, it is possible to identify that different lines are now experiencing congestion than in the base topology. Moreover, there are less occurrences of congestion in the optimised topology than in the base topology. Also note

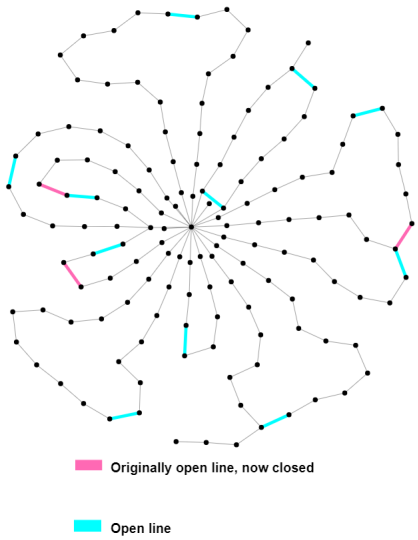

Figure 6.3: The new network topology obtained from using the reconfiguration algorithm for the third week of scenario 2030.

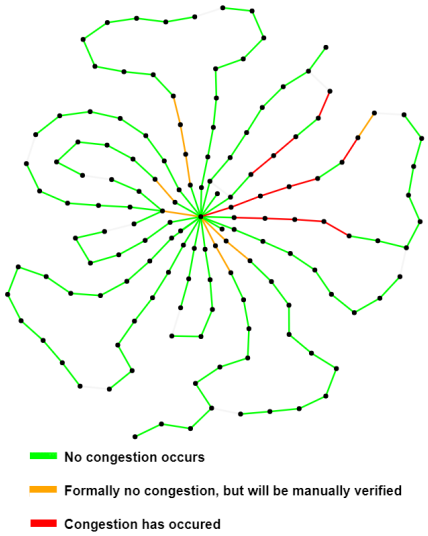

Figure 6.4: The occurrences of congestion within the new network topology for the third week of scenario 2030.

that the peaks of congestion align with the peaks in electricity demand, which is as expected.

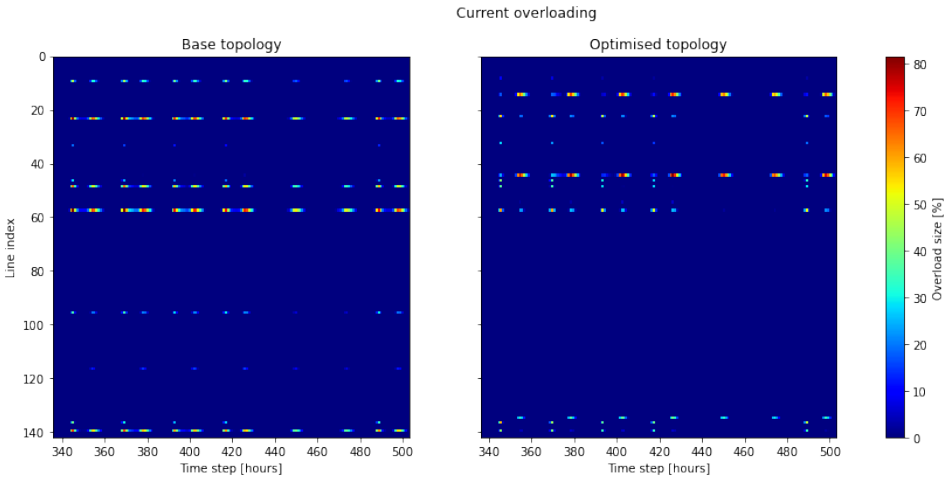

Figure 6.5: Heat map of the occurrences of line current overloading for the considered time frame in the 2030 scenario.

When looking at the data more in-depth, further differences can be identified. In Table 6.2, the parameters of interest for both the scenario in the base topology, as well as the new optimised topology are presented. First, there are the active power losses, which drop from 19.36 MW to 17.99 MW, a reduction of 7.08%. The relative improvement offered here is larger than the relative reduction of active power losses for the base topology as presented in Chapter 4. More importantly however, is the reduction in the occurrence of congestion within the network, which drops from 507 to 303, a reduction of 40.24%. Additionally, the average size of the occurrences of congestion drop from 25.48% overloading to 16.88%. Also, the maximum overloading drops from 81.58% to 55.91%. Finally, the instances of overloading which surpass the limit of line loading for situations of maintenance or disturbances is reduced from 192 to 61, a reduction of 68.23%. This last parameter should ideally not occur at all during the normal operation as analysed here, however it is encouraging to know that its occurrence is at least reduced.

An overview of the distribution of instances of congestion can be found in Figure 6.6, for both the base topology and the optimised version. It is important to note that both plots utilise the same scale for the y-axis, meaning that the data can be compared quantitatively, despite the total amount of occurrences of congestion for the optimised topology being lower. It becomes clear from the figure as well that the congestion has

Table 6.2: Summary of results for scenario 2030.

	Base topology	Optimised topology
Active power losses [MW]	19.36	17.99
Number of lines experiencing congestion	11	12
Instances of congestion	507	303
Average overloading size [%]	25.48	16.88
Maximum overloading size [%]	81.58	55.91
Instances of congestion above maintenance/disturbance limit	192	61

been greatly reduced when considering the entire time frame, as the plot of the optimised topology is basically a shrunken version of the base topology. An important difference which can be observed between the two plots is that the overloading size for the optimised topology tends to be closer to just over 0% (as congestion is only counted if overloading > 0%), whereas the base topology reaches a peak occurrence around 10%.

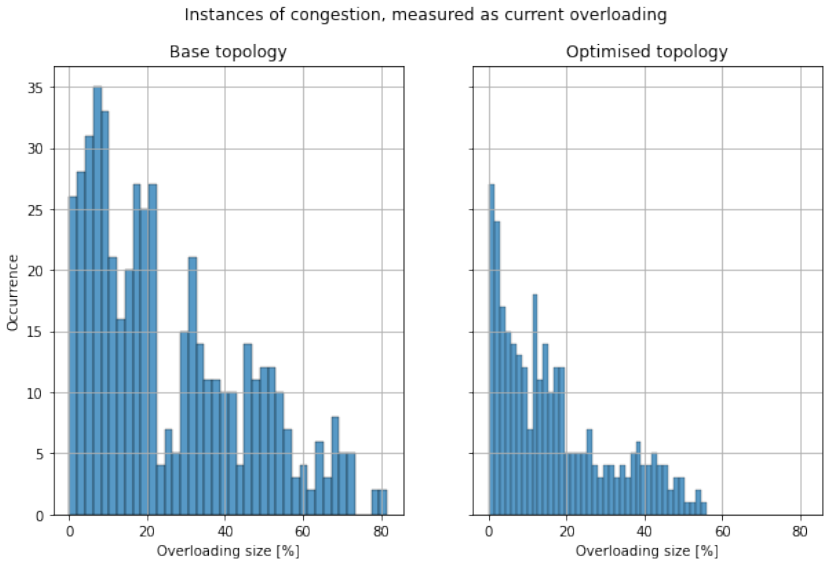

Figure 6.6: Sizes of the current overloading (in percentages) for each occurrence of congestion for the 2030 scenario.

Overall, the reconfiguration algorithm has been able to provide improvements for all the analysed parameters for the 2030 scenario, bar the number of lines experiencing congestion. This includes the total amount of occurrences of congestion, the average size of overloading and the maximum size of overloading. Unfortunately, congestion does still occur, but its severity has been reduced. Two important conclusions can be drawn from this observation. First, the reconfiguration algorithm alone is not enough to remove severe cases of congestion within the MV grid. Second, the reconfiguration algorithm is able to reduce the encountered congestion within the network to a significant degree (more than 40%), meaning that the dependency on other flexibility resources is reduced.

6.3. Scenario 2040

Next is the 2040 scenario, where congestion is appearing in a significant number of lines within the network. The reconfiguration algorithm is used, which results in the new topology as highlighted in Figure 6.7. Note that the voltage and current constraints have been relaxed compared to the previous two scenarios to ensure feasibility. A total of three new lines are opened; the same ones as for the 2030 scenario. With the new topology, a power flow calculation is performed to obtain the line loading, resulting in Figure 6.8.

An overview of the spatial and temporal relation of the occurrences of congestion can be found in Figure 6.9. Note how the maximum value of the colouring has increased compared to the 2030 scenario, with peaks over

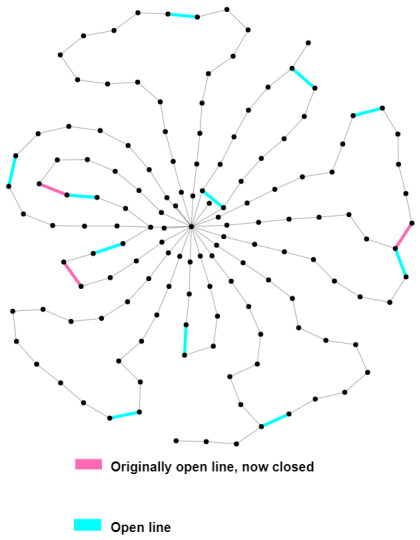

Figure 6.7: The new network topology obtained from using the reconfiguration algorithm for the third week of scenario 2040.

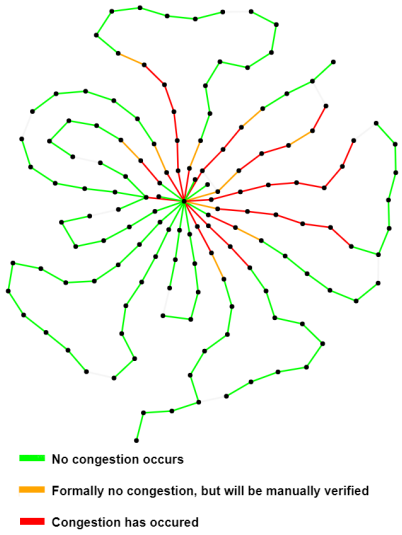

Figure 6.8: The occurrences of congestion within the new network topology for the third week of scenario 2040.

200%. Apart from that, it can be observed that the congestion in certain lines has changed in the optimised topology, which is especially accentuated between lines 40 and 60. Here, the periods during which the lines experience congestion are shortened, or at least interrupted. Also, the peaks in congestion are reduced and once again align with the peaks in electricity demand.

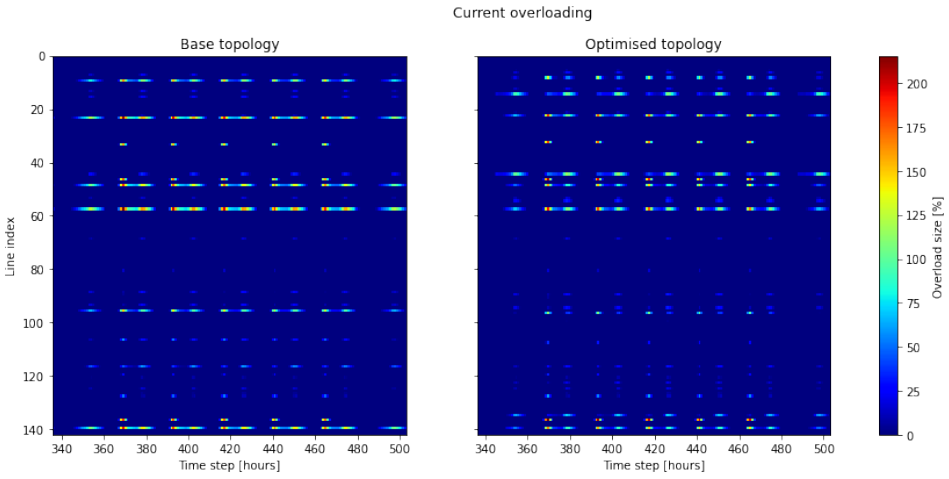

Figure 6.9: Heat map of the occurrences of line current overloading for the considered time frame in the 2040 scenario.

A summary of the most relevant parameters is given in Table 6.3. The active power losses have once again decreased, this time from 35.82 MW to 32.60 MW, a reduction of 8.99%. This is a larger improvement compared to the 2030 scenario. However, the other parameters are worth discussing further. First of all, the total number of lines experiencing congestion has increased from 30 to 33, as has the total amount of occurrences of congestion, rising from 1248 to 1308 (an increase of 4.81%). Thus, in regards to the occurrence of congestion, the reconfiguration algorithm has actually worsened the situation. However, when analysing the size of the congestion, it can be observed that the algorithm does bring about other improvements. In particular, both the average overloading size and the maximum overloading size have decreased, from 53.38% to 33.63% and from 215.64% to 186.46%, respectively. Additionally, the total number of violations above the maintenance/disturbance limit has also decreased from 714 to 489, a reduction of 31.51%.

An overview of the size for each occurrence of congestion for both the base topology and the optimised topol-

Table 6.3: Summary of results for scenario 2040.

	Base topology	Optimised topology
Active power losses [MW]	35.82	32.60
Number of lines experiencing congestion	30	33
Instances of congestion	1248	1308
Average overloading size [%]	53.38	33.63
Maximum overloading size [%]	215.64	186.46
Instances of congestion above maintenance/disturbance limit	714	489

ogy can be found in Figure 6.10. The most noticeable difference between the two plots is perhaps the larger peaks for the optimised topology between 0% and 50%. These larger peaks are mostly caused by the larger number of occurrences of congestion. The improvements offered by the optimised topology start to show more clearly after 50% overloading, where the peaks tend to be lower compared to the base topology. As reported earlier, the maximum overloading has also reduced, which is a trend that can be observed for all peaks after 100% overloading.

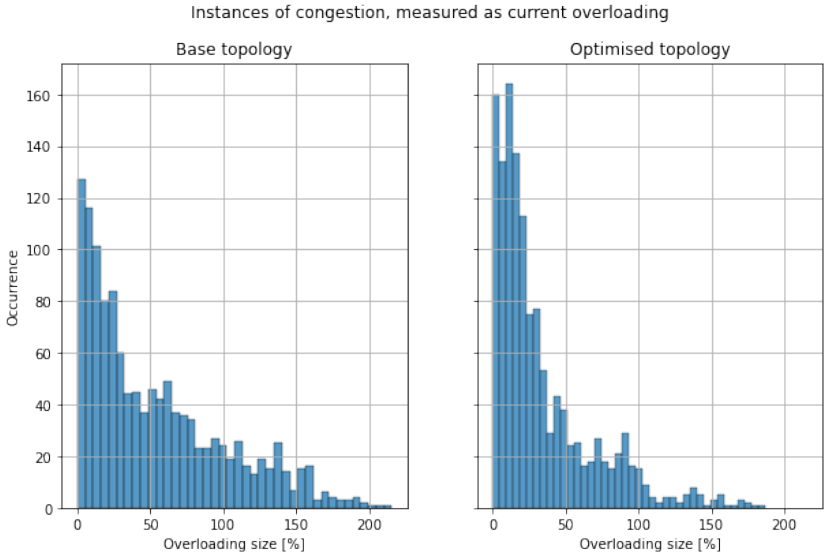

Figure 6.10: Sizes of the current overloading (in percentages) for each occurrence of congestion for the 2040 scenario.

For the 2040 scenario the limitations of the reconfiguration algorithm start to show, as it is not able to improve upon every parameter of interest. However, this does not mean that the reconfiguration algorithm is bringing no improvements. Rather, the algorithm seems to be spreading the overloading within the network: increasing it in places where previously no problems arose to lighten the strain on the parts already experiencing congestion. An advantage of this would be that it allows other forms of flexibility to be used within a wider area and still contribute to resolving the congestion problems. A clear disadvantage is the more widespread occurrence of congestion throughout the network.

It should also be noted that the overloading of the lines start to reach rather high values, with the maximum in both the base and optimised topology surpassing 150%. This would not be a very realistic number to find within a real-world situation, as by this point the DSO would start to take action to prevent the assets connected to the MV grid from being damaged. Its occurrence within the simulation likely originates from two sources. The first being that within the simulation there is no accounting for possible reinforcement of the grid. This would mean that the analysed grid has gone without any reinforcement for almost 20 years. The second is the limited depth by which the future scenarios are formulated, which are currently rather basic.

Despite the 2040 scenario thus being less realistic, its results still offer useful insight: both in terms of the

continued improvements offered by the reconfiguration algorithm, while also highlighting the limitations of its use. Basically, the initial conclusions drawn from the 2030 scenario are further reinforced: the reconfiguration algorithm is a useful tool to reduce the severity of congestion, but cannot resolve it on its own as the congestion becomes more severe.

6.4. Scenario 2050

Before the results of the 2050 scenario are presented, it is important to note that this scenario will be a more severe case of the situation described in the 2040 scenario. As such, the same statements regarding the accuracy of the scenario will also apply here, meaning that it will not be a realistic situation which may actually occur. Despite this, the results do provide some additional insight regarding the reconfiguration and as such its inclusion does benefit the overall analysis of the reconfiguration algorithm.

Having said that, the congestion observed in the 2040 scenario has spread to even more lines within the network and has become even more severe for the 2050 scenario. Thus, the reconfiguration algorithm is used and a new topology is obtained as in Figure 6.11, which is once again the same as the previous two scenarios. Additionally, the new loading within the system is calculated using a power flow calculation, resulting in Figure 6.12.

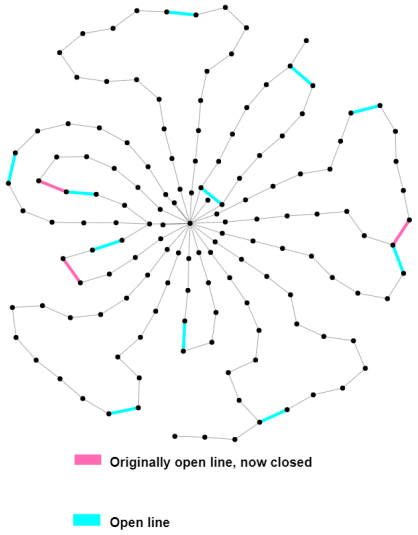

Figure 6.11: The new network topology obtained from using the reconfiguration algorithm for the third week of scenario 2050.

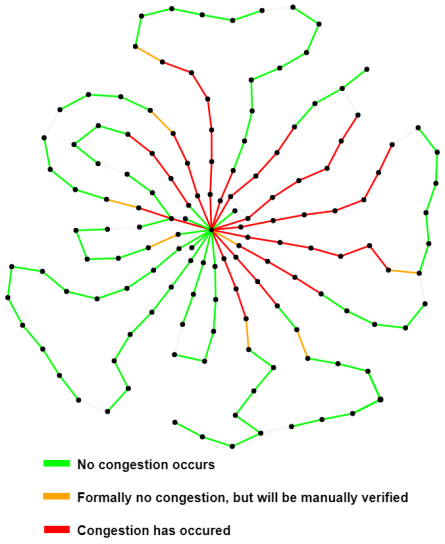

Figure 6.12: The occurrences of congestion within the new network topology for the third week of scenario 2050.

Once again, the spatial and temporal relation of the occurrences of congestion can be found in Figure 6.13. The maximum value of the overloading has once again increased, now reaching over 250%. The difference between the base topology and the optimised topology is still most pronounced between lines 40 and 60. It is interesting to note that the occurrences of lower valued instances of congestion are increasing over the decades. This is reflected in the lighter blue streaks which occur within Figure 6.13. However, it is also important to keep in mind that the scale at which the size of congestion is plotted changes per scenario. That is to say that the trend is only relative to the occurrence of overloading, not to its magnitude.

The active power losses are reduced from 51.14 MW to 46.84 MW, a reduction of 8.41%, which is similar compared to the 2030 and 2040 scenario. The number of congested lines has increased from 43 to 48 and additionally, the total occurrences of congestion have increased from 2025 to 2183. The average overloading has decreased from 54.06% to 39.66%, however the maximum overloading is the same for both topologies at 297.34%. Finally, the occurrences of congestion with an overloading surpassing the maintenance and disturbance limit have decreased by 7.62%, from 1089 to 1006. These results are summarised in Table 6.4.

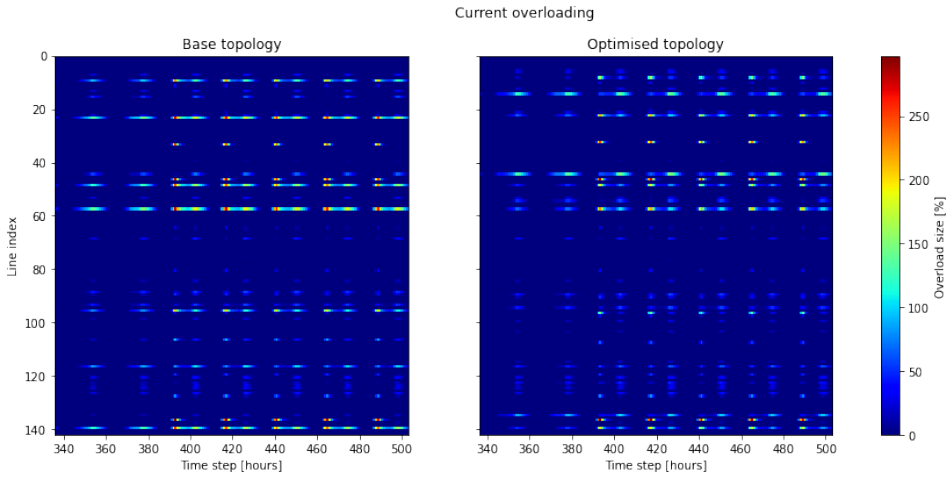

Figure 6.13: Heat map of the occurrences of line current overloading for the considered time frame in the 2050 scenario.

Table 6.4: Summary of results for scenario 2050.

	Base topology	Optimised topology
Active power losses [MW]	51.14	46.84
Number of lines experiencing congestion	43	48
Instances of congestion	2025	2183
Average overloading size [%]	54.06	39.66
Maximum overloading size [%]	297.34	297.34
Instances of congestion above maintenance/disturbance limit	1089	1006

Overall, with the results as presented above, it is safe to conclude that the reconfiguration algorithm does not offer much anymore in terms of reducing the congestion. It becomes apparent that almost none of the considered parameters is actually improving, apart from the average overloading size and some of the higher occurrences of overloading which surpass the maintenance and disturbance limit. The maximum overloading is also becoming even more unrealistically large, reaching almost 300%. Looking at the distribution of all occurrences of congestion in Figure 6.14, one can wonder how much of the reduction in the average overloading size is caused by an overall lower overloading and how much is caused by an increase of lower-sized occurrences of congestion. Although, the peaks do get lower in the optimised topology compared to the base topology after around 60% overloading. Regardless, the benefits of the reconfiguration algorithm are far less pronounced as the congestion has become more severe.

With the previous observation for the 2040 scenario already in place, it may be useful to argue why the 2050 scenario is still included. Despite the 2050 scenario being even less realistic than the 2040 scenario, the situation it describes does go to highlight the moment at which reconfiguration is no longer adding benefits to the considered network. Thus, while the reconfiguration algorithm can provide benefits in case congestion occurs, if this congestion is too large the benefits start to deteriorate until they practically disappear.

This highlights an important consideration for the use of reconfiguration as a means to reduce congestion. Namely, that it is intended as a short-term solution. It was not expected that the reconfiguration algorithm would be able to resolve the congestion by itself. It needs additional sources of flexibility and in the long term also grid reinforcement will still need to be carried out. However, in the current situation of the MV grids in the Netherlands, it does offer a quick and relatively cheap means to reduce the congestion while it is not too severe yet.

Another interesting observation which can be made based on all the scenarios is that the same three originally opened switches are replaced by the same originally closed switches for each scenario, bar the 2021 scenario. This can imply that these three switches can contribute the most towards altering the power flow within the network when considering the future developments as defined in Chapter 5. Additionally, these

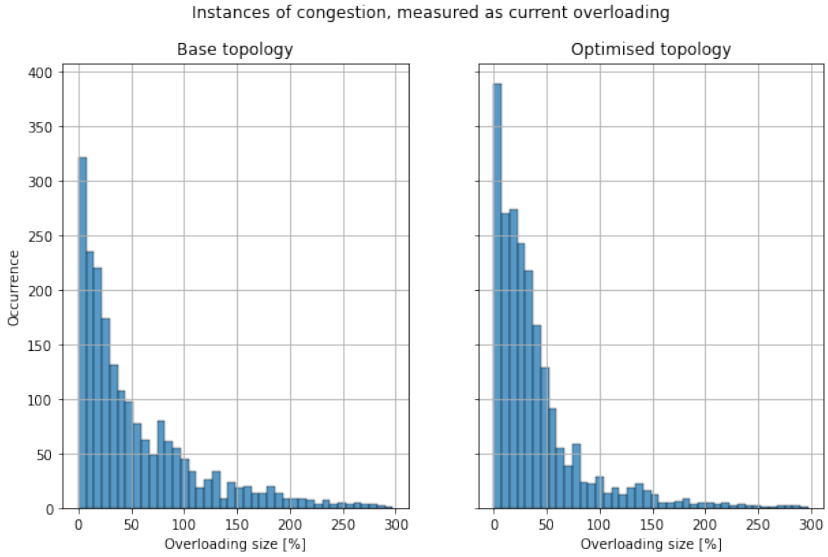

Figure 6.14: Sizes of the current overloading (in percentages) for each occurrence of congestion for the 2050 scenario.

three scenarios all experience rather severe cases of congestion, whereas this is rather limited for the 2021 scenario. Based on this observation, it seems like the reconfiguration algorithm is able to provide more diverse topologies when the effects imposed by congestion are less severe.

6.5. Comparison with PowerFactory

Similar to Section 4.3.5, a comparison can be made between the solution provided by the reconfiguration algorithm and the functionalities offered by PowerFactory. Once again, the comparison will be made to the iterative exploration of the meshes and a genetic algorithm with population settings as in Appendix C. Both algorithms will be compared to the base case of scenario 2030 as it offers a rather large occurrence of congestion while being one of the two more accurate scenarios considered. Meanwhile, interesting similarities and differences to the solution in Section 6.2 are analysed while presenting the results.

6.5.1. Iterative exploration of meshes

Utilising an iterative exploration of the meshes in PowerFactory for the 2030 scenario yields a new network configuration, as presented in Figure 6.15. Similar to the solution of the reconfiguration algorithm, a total of three new switches are opened by the iterative exploration compared to the base case. However, only one of them is the same. Instead of two switches changing on the left-hand side of the network, only one is changed. Meanwhile, two switches are altered on the right-hand side. The top switch is changed to the same position as by the reconfiguration algorithm. However, the bottom switch is also changed and is now moved to the left. Performing a power flow calculation using the new topology results in the lines being loaded as in Figure 6.16.

Once again, the number of lines experiencing congestion has actually increased in the optimised topology, from 11 to 12. However, when looking at the heat map of overloading sizes, shown in Figure 6.17, it becomes clear that a lot less congestion is actually occurring in the optimised topology. This is most apparent from the lower occurrence of peaks between lines 40 and 60 and the lower value of the ones that are there. Also, note how two different lines are now experiencing moments of congestion between lines 120 and 140.

When looking at the other parameters, clear differences can be observed between this solution and the solution provided by the reconfiguration algorithm. The results for all three topologies are summarised in Table 6.5, where 'base' refers to the base topology, 'RA' refers to the optimised topology obtained by the reconfiguration algorithm and 'IEOM' refers to the optimised topology obtained by PowerFactory utilising the iterative exploration of the meshes. The first difference compared to the reconfiguration algorithm is in regards to

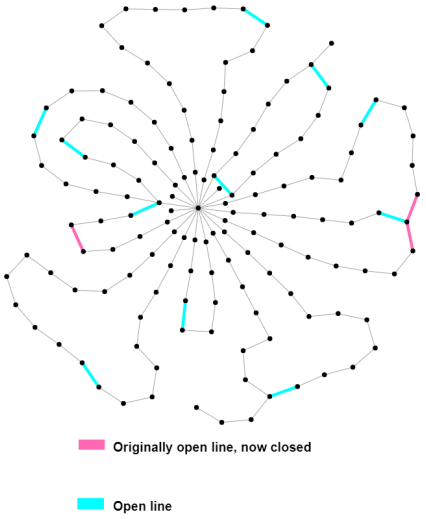

Figure 6.15: The new network topology obtained from using the iterative exploration of the meshes in PowerFactory for the third week of scenario 2030.

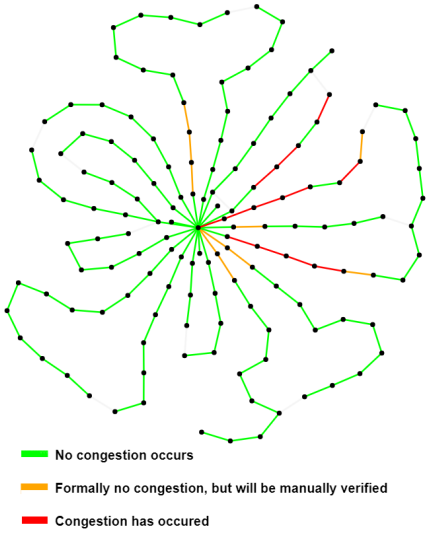

Figure 6.16: The occurrences of congestion within the new network topology obtained from PowerFactory for the third week of scenario 2030.

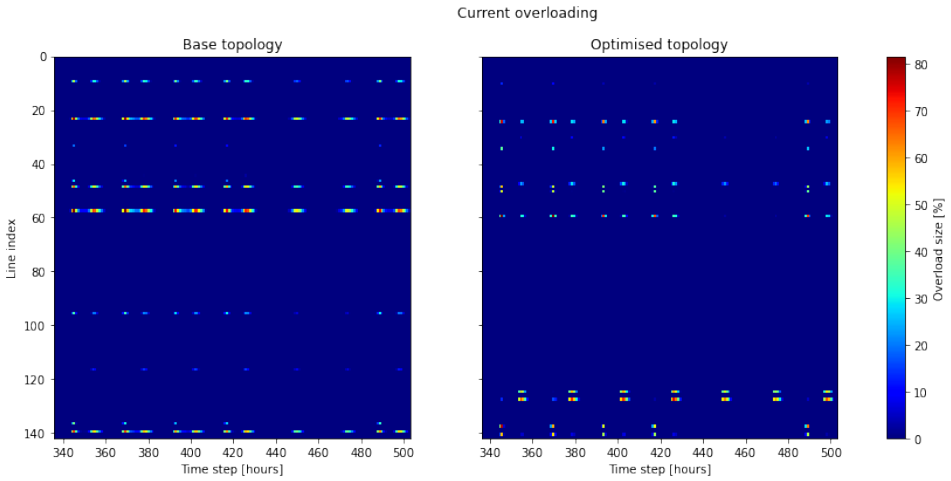

Figure 6.17: Heat map of the occurrences of line current overloading for the considered time frame in the 2030 scenario using the iterative exploration of meshes in PowerFactory.

the value of the objective function, which is equal to 18.52 MW over the entire time frame for the optimised topology by PowerFactory. This constitutes a reduction of 4.34% compared to the base topology, but is almost 3% lower than the 7.08% reduction obtained by the reconfiguration algorithm.

However, with regards to the other parameters, the active power losses is actually the only parameter with less improvement by the iterative exploration of meshes than the reconfiguration algorithm. The occurrence of congestion has dropped by 53.25% compared to the base topology, for a total of 237 occurrences of congestion over the entire time frame. The average overloading has dropped from 25.48% to 13.88% and the maximum is now 41.45% instead of 81.58%. Finally, the occurrence of congestion with an overloading size larger than the limit set for maintenance or a disturbance has dropped from 192 to only 24, a reduction of 87.5%.

The occurrences of congestion have also been plotted with regards to the overloading size in Figure 6.18, comparing the base topology to the optimised topology obtained using the iterative exploring of meshes. By analysing the figure it becomes clear that the optimised topology has far fewer occurrences of congestion compared to the base topology, with far smaller sizes with regards to overloading. Combining all of these

Table 6.5: Summary of the results for scenario 2030. Base refers to the base topology. RA refers to the topology obtained by using the reconfiguration algorithm. IEOM is referring to the topology obtained using the iterative exploring of meshes by PowerFactory.

	Base	RA	IEOM
Active power losses [MW]	19.36	17.99	18.52
Number of lines experiencing congestion	11	12	12
Instances of congestion	507	303	237
Average overloading size [%]	25.48	16.88	13.88
Maximum overloading size [%]	81.58	55.91	41.45
Instances of congestion above maintenance/disturbance limit	192	61	24

results makes it safe to conclude that the iterative exploring of meshes by PowerFactory is better performing than the reconfiguration algorithm in this case. The main advantage offered by PowerFactory is that it can consider all switches at the same time.

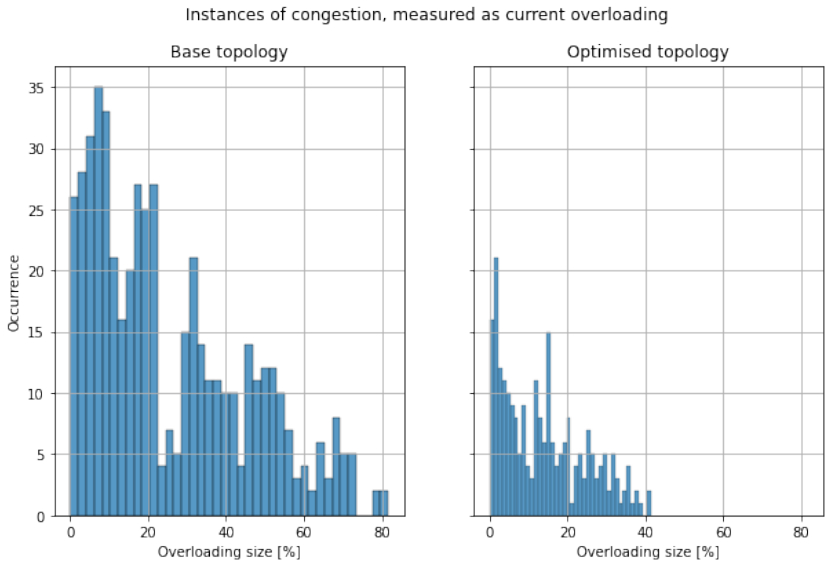

Figure 6.18: Sizes of the current overloading (in percentages) for each occurrence of congestion in the PowerFactory solution using an iterative mesh exploration for the 2030 scenario.

However, this is not to say that the solution obtained by PowerFactory is superior in every situation. Most importantly with regards to flexibility, as the algorithm provided by PowerFactory is limited in terms of the constraints which can be used during the optimisation. Thus, while considering all switches at once can be considered an advantage for the optimisation itself, it is limiting when some switches should not be considered during the optimisation at all. This could prove problematic, for example in case the age of components or their location become important parameters to be taken into account for the optimised topology. Additionally, the objective function is actually lower for the reconfiguration algorithm, being 17.99 MW, compared to the 18.52 MW obtained by using PowerFactory. This motivates the exploration of a different objective function which could improve the solution of the reconfiguration algorithm, however, this is further discussed during the recommendations in Section 7.3. Overall, both algorithms provide a clear improvement for the analysed parameters compared to the base topology, highlighting the effectiveness of network reconfiguration to reduce congestion within said network.

6.5.2. Genetic algorithm

Utilising the genetic algorithm for the tie open point optimisation in PowerFactory for the 2030 scenario yields a new network configuration, as presented in Figure 6.19. The solution offered by the genetic algorithm proposes the change of six different switches to be opened compared to the base topology. This is double the amount of switching operations compared to the reconfiguration algorithm (or the iterative exploration of

meshes for that matter). The most peculiar change is perhaps the change in the bottom left loop, since no congestion actually occurs here. The new configuration results in the network loading as presented in Figure 6.20.

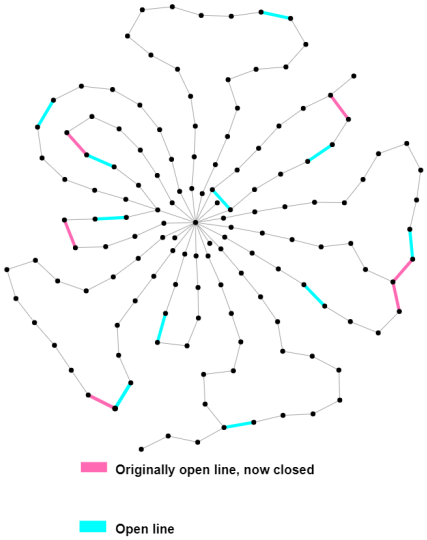

Figure 6.19: The new network topology obtained from using the genetic algorithm in PowerFactory for the third week of scenario 2030.

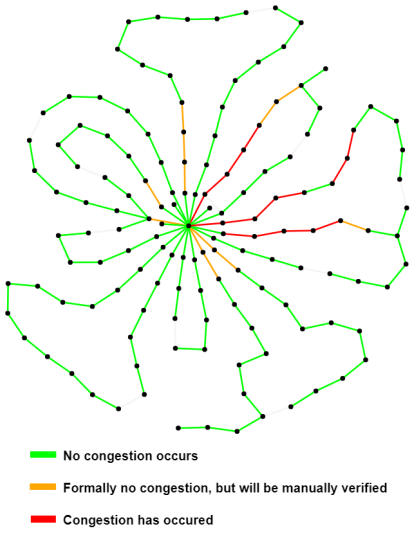

Figure 6.20: The occurrences of congestion within the new network topology obtained from PowerFactory for the third week of scenario 2030.

One thing which can be observed in Figure 6.20, is that the total number of lines experiencing congestion has increased from 11 to 14. This increase also becomes apparent when observing the heat map of the overloading in Figure 6.21. Here, the additional lines experiencing congestion can also be observed, especially between lines 0 and 20. It is also noticeable that there are a lot more peaks in the optimised topology of the genetic algorithm compared to the reconfiguration algorithm and the iterative exploration of meshes.

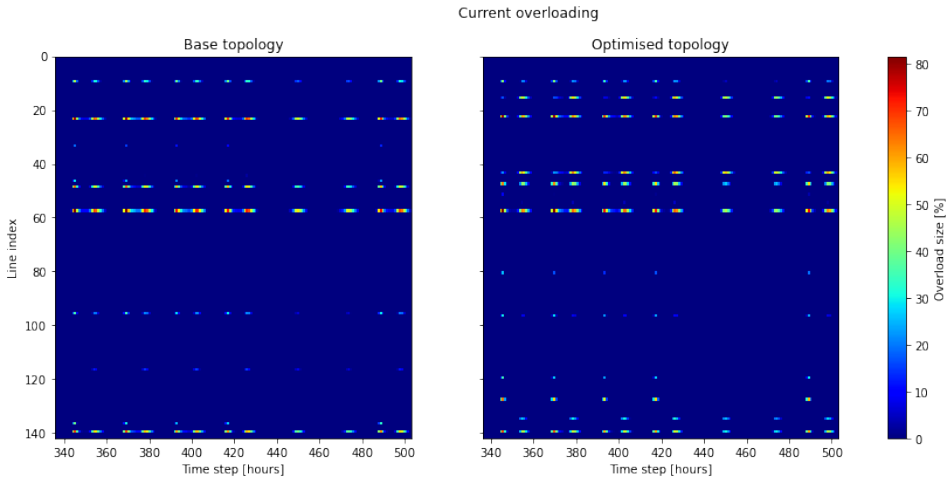

Figure 6.21: Heat map of the occurrences of line current overloading for the considered time frame in the 2030 scenario using the genetic algorithm in PowerFactory.

Contrary to the previous results, the solution offered by the genetic algorithm also increases the total amount of occurrences of congestion; rising from 507 in the base topology to 562 in the optimised topology. The value of the objective function did decrease, to 19.09 MW active power losses over the considered time frame. However, this only constitutes a reduction of 1.39%, which is significantly lower than the reconfiguration algorithm. The average and maximum overloading size did reduce, from 25.48% to 22.14% and from 81.58%

to 72.22%, respectively. Subsequently, the number of occurrences of congestion surpassing the maintenance and disturbance limit has also decreased, from 192 to 180, a reduction of 6.25%. These results are summarised in Table 6.6. When analysing Table 6.6, it becomes clear that only some of the parameters are improved upon by the genetic algorithm compared to the base topology. Simultaneously, the improvements which are offered are less significant than those of the reconfiguration algorithm.

Table 6.6: Summary of the results for scenario 2030. Base refers to the base topology. RA refers to the topology obtained by using the reconfiguration algorithm. GA is referring to the topology obtained using a genetic algorithm by PowerFactory.

	Base	RA	GA
Active power losses [MW]	19.36	17.99	19.09
Number of lines experiencing congestion	11	12	14
Instances of congestion	507	303	562
Average overloading size [%]	25.48	16.88	22.14
Maximum overloading size [%]	81.58	55.91	72.22
Instances of congestion above maintenance/disturbance limit	192	61	180

The occurrences of congestion relative to the overloading is presented in Figure 6.22. The most noticeable difference between the base topology and the optimised topology is the reduction of the occurrences of congestion with an overloading larger than 45%. Meanwhile, the increase in the total amount of occurrences of congestion is most prevalent for lower overloading sizes, between 0% and 15%. The occurrences of congestion larger than 60% has also been reduced significantly in the optimised topology, which contributes to the lower maximum overloading as well.

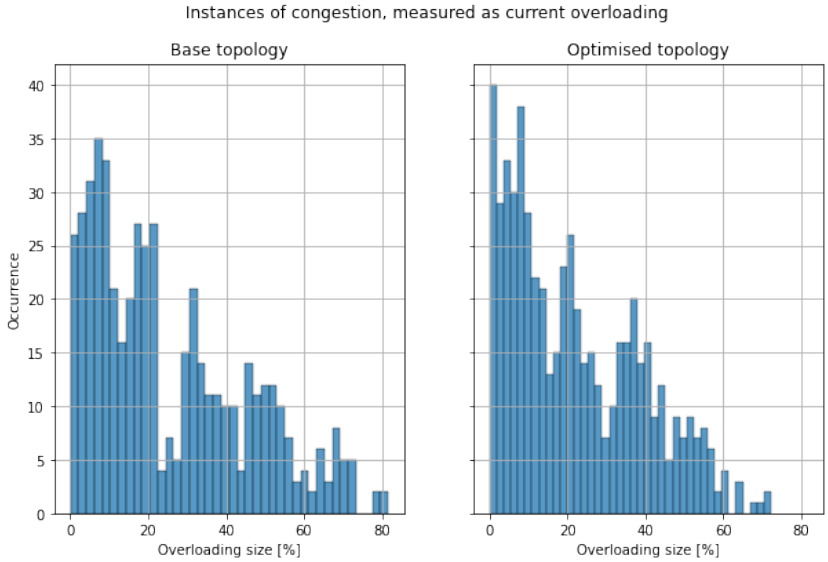

Figure 6.22: Sizes of the current overloading (in percentages) for each occurrence of congestion in the PowerFactory solution using a genetic algorithm for the 2030 scenario.

Overall, it is safe to conclude that the genetic algorithm does not offer a superior solution compared to the reconfiguration algorithm. Not all parameters are improved upon, some are even made worse. Meanwhile, the ones that are improved, are improved to a lesser extent than the solution offered by the reconfiguration algorithm. The same reasons as mentioned throughout this thesis probably apply here, mainly that the genetic algorithm is a meta-heuristic approach which cannot guarantee a global optimum.

6.5.3. Voltage analysis

It is interesting to note that the same trend in regards to the objective function as presented in Chapter 4 can also be observed here. The reconfiguration algorithm offers the best objective function value, followed by the

iterative exploration of meshes and finally the genetic algorithm. Because of this trend, it can be insightful to also compare the voltage levels of the different optimisations, as voltage is closely related to losses. An overview of the voltage amplitude for each topology is given in Figure 6.23. In the figure 'Base' refers to the base topology, 'RA' refers to the topology obtained by the reconfiguration algorithm, 'IEOM' refers to the iterative exploration of meshes and GA refers to the solution of the genetic algorithm.

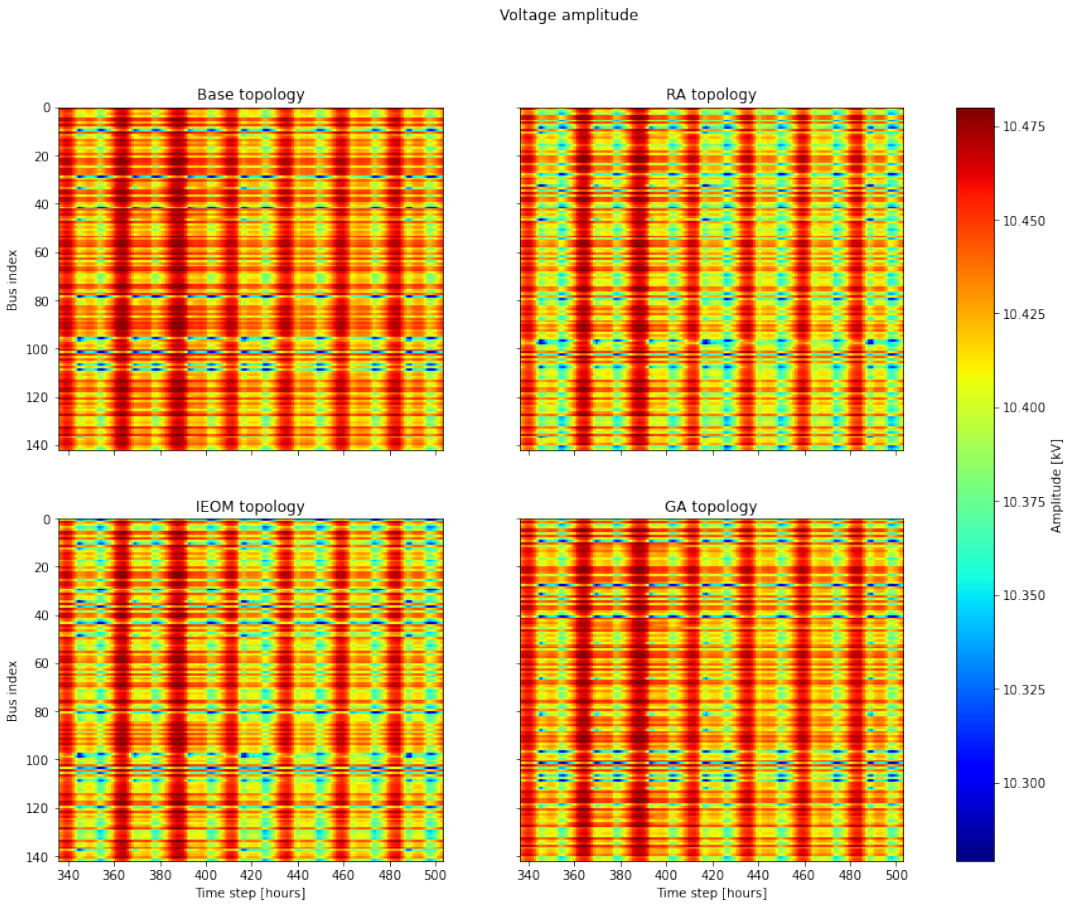

Figure 6.23: Overview of the voltage amplitude encountered throughout the network for the considered time frame in the 2030 scenario for each of the considered algorithms. Base refers to the base topology, RA is the solution offered by the reconfiguration algorithm, IEOM is the solution offered by the iterative exploration meshes and GA refers to the genetic algorithm.

From Figure 6.23, it becomes clear that for each of the topologies it holds that the voltage amplitude is well within the limits of +/- 5% of the 10.5 kV rated value. The most noticeable difference is perhaps between the base topology and the genetic algorithm compared to the reconfiguration algorithm and the iterative exploration of meshes. For the former pair, the voltage tends to be higher throughout the network during more moments of the considered time frame, indicated by the deep red colour. Contrary to this, the latter pair has a higher occurrence of lower valued voltage amplitude, indicated by the more frequent presence of yellow and green colours. It should be noted that the genetic algorithm does offer some improvements with regards to the base topology, as the red colour is not quite as frequent and instead more of the plot is coloured yellow. However, this is far less substantial than the improvements of the reconfiguration algorithm and the iterative exploration of meshes.

Interestingly enough, the maximum value is actually the same for each topology, at 10.48 kV. Thus, the difference in losses is mostly caused by the higher occurrence of larger voltage amplitudes, rather than just the maximum value. This is also evident when comparing the voltage distribution of, for example, the reconfiguration algorithm and the iterative exploration of meshes, displayed in Figure 6.24 (the distribution of each topology is provided in Appendix D). From the figure, it can be observed that the distributions are very similar for both topologies, only the iterative exploration of meshes has higher peaks in general. These higher

peaks signify a higher occurrence of larger amplitude values. This difference between the distributions likely represents the difference in objective function value between the two topologies as well.

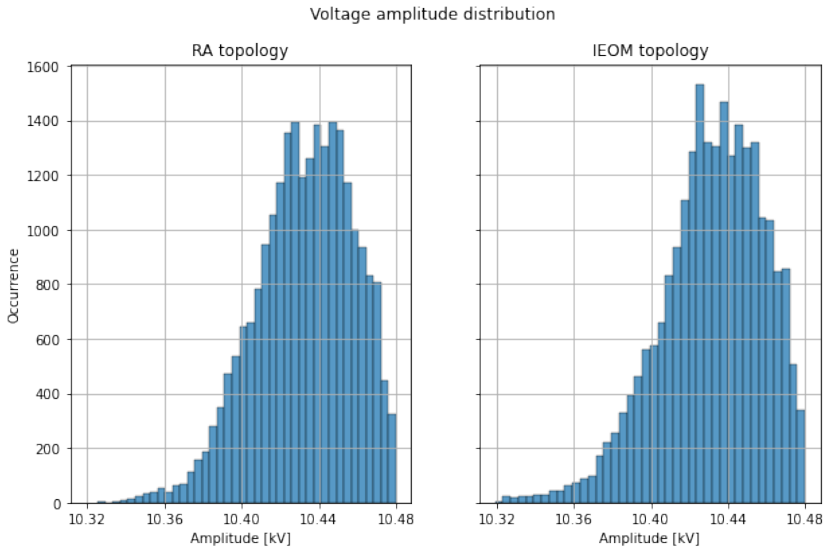

Figure 6.24: Voltage amplitude occurrences for each of the considered topologies. RA refers to the reconfiguration algorithm and IEOM refers to the iterative exploration of meshes.

Overall, each algorithm does offer some improvements in regards to the severity of the encountered congestion, but the reconfiguration algorithm and the iterative exploration of meshes far surpass the improvements offered by the genetic algorithm. Between the reconfiguration algorithm and the iterative exploration of meshes, the main trade-off is between the flexibility offered by the former, while the latter offers a more extensive decision space due to its ability to consider all switches at once.

6.6. Stochastic scenario

For the stochastic scenario, the alterations as covered in Chapter 5 are in place, meaning that the optimisation will now be taking into account ten different demand profiles at the same time, each with a likelihood of occurring of 1/10. However, this also means that the amount of variables has increased by a factor 10. This increased model size unfortunately means that the available hardware is unable to compute a solution for the considered time frame. So, instead the optimisation will be carried out for the period of peak demand, between 17:00 and 20:00. This means that the obtained optimised topology may not be the global optimum, but it should still highlight the considerations for a stochastic optimisation.

As such, the stochastic reconfiguration algorithm is used and the resulting optimised configuration can be found in Figure 6.25. Comparing the configuration with the one obtained from the deterministic 2030 scenario, only one difference can be observed. Namely, the switch in the bottom loop has been moved by one substation, leading to a total of four different switches being altered compared to the base case. However, this loop was not experiencing congestion during the deterministic scenarios, not even in the 2050 scenario where the base load was increased by 50.9%. For comparison, the maximum load increase for the stochastic variations is 6.6%. As a result, the maximum line loading occurring in the network remains unchanged when comparing the deterministic configuration and the stochastic configuration, as can be observed in Figure 6.26 for the deterministic demand profile.

Subsequently, the number of lines experiencing congestion, the total instances of congestion, their average and maximum size and the instances of congestion surpassing the limit during maintenance or a disturbance all remain unchanged compared to the results in Table 6.2 when utilising the optimised configuration for the deterministic 2030 scenario. This also holds when performing the power flow calculation for any of the stochastic variations. The only parameter which does differ is the active power losses, but this is not more

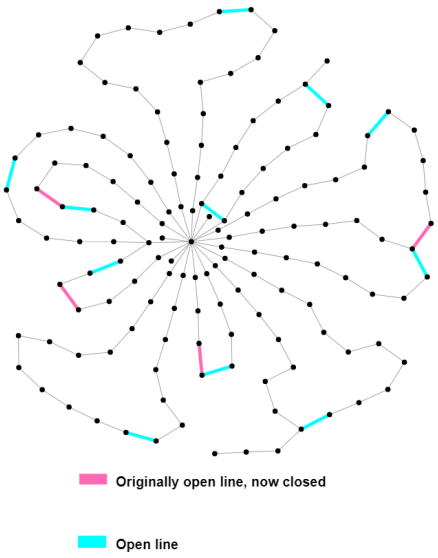

Figure 6.25: The new network topology obtained from using the reconfiguration algorithm for the third week of the stochastic 2030 scenario.

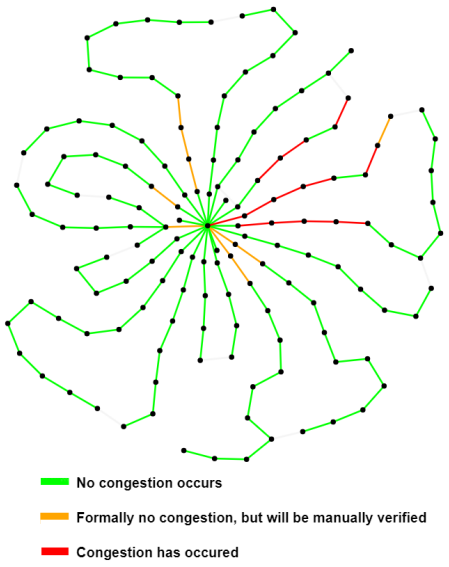

Figure 6.26: The occurrences of congestion within the new network topology obtained from using the reconfiguration algorithm for the third week of the stochastic 2030 scenario.

than 0.01 MW for the entire network over the entire time frame.

Thus, the stochastic scenario provides an almost identical solution to the deterministic version, although it is sub-optimal due to the additional switching action. Taking these results into account, it is safe to conclude that the reconfiguration algorithm provides a robust solution which lessens the severity of the congestion even if the scenarios turn out with larger or smaller increases in the base load.

7

Summary, conclusions and recommendations

7.1. Thesis summary

This work presents a master thesis into modelling and topology optimisation of representative MV networks for the Netherlands. The first chapter introduces the general motivation for carrying out the research, which is centred around the increasing occurrence of congestion within MV grids as a result of the increase of DERs. Additionally, the research questions are introduced, which are focused on the possibility of designing a seasonal reconfiguration algorithm for the MV network topology to reduce congestion in the short term. Chapter 2 goes over an extensive literature study for most of the topics relevant to the thesis as a whole, such as distribution grids, power flow calculations and network reconfiguration.

Next, in Chapter 3, the case study network is introduced, which consists of a large city within the Netherlands for which real data has been made available by one of the Dutch DSOs. The real data primarily consist of a PowerFactory model, which has been used as a benchmark for the developed model. The chapter goes into further detail regarding the encountered grid assets, as well as the network topology and the configuration in the base case.

The methodology is presented in Chapter 4 and consists of three parts. First, a nonlinear power flow algorithm is introduced, which is used for modelling the current system state. This model is subsequently verified against the provided PowerFactory model to ensure its accuracy. Each of the considered parameters are accurately modelled by the power flow algorithm, each having an average error below 1%. Second, the power flow algorithm is linearised to enable the formulation of a MILP reconfiguration algorithm in the last section of the methodology. Both the nonlinear and linear power flow algorithms, as well as the reconfiguration algorithm, are implemented in the high-level programming language Python. And to be more specific, in the Python-based optimisation modelling language called Pyomo.

Next, with the methodology in place, it is time to test the functionality of the reconfiguration algorithm. To this end, several future scenarios are formulated in Chapter 5. The scenarios are meant to illustrate the capabilities of the reconfiguration algorithm to reduce congestion within the MV grid. As such, each subsequent scenario has more severe cases of congestion. At the same time, measures such as grid reinforcement or forms of flexibility by the producers and consumers are excluded from the considerations made. That means that the considered situation is a worst-case scenario. Additionally, a stochastic scenario is introduced, which provides a measure of sensitivity analysis for the presented algorithm and its solution.

Finally, the results for each of the scenarios are presented in Chapter 6. A clear trend can be observed in regard to the functionality of the reconfiguration algorithm as the scenarios increase in time and the congestion within the network becomes more and more severe. For the initial scenario of 2021, the reconfiguration algorithm is able to completely remove the congestion for the considered time frame. For the 2030 scenario, the reconfiguration algorithm still performs adequately, being able to reduce the occurrence of congestion by

more than 40%.

However, the limitations of the reconfiguration algorithm also start to show in the subsequent scenarios. For the 2040 scenario, the reconfiguration algorithm is no longer able to reduce the occurrences of congestion within the network. Instead, it lowers the average and maximum size of line overloading by slightly increasing the overall occurrence of congestion. Thus, the occurrence of congestion is not reduced, but its severity is. The added benefits from the reconfiguration algorithm finally start to almost disappear as the 2050 scenario is analysed, where only small improvements can be observed.

The reconfiguration algorithm is also compared to an iterative exploration of meshes and a genetic algorithm, both available from PowerFactory. When comparing the reconfiguration algorithm to other approaches of optimising the network topology offered by PowerFactory, some important observations can be made. First of all, the reconfiguration algorithm offers a significantly better solution than the genetic algorithm. Meanwhile, the solution offered by the reconfiguration algorithm with regard to the occurrence of congestion offers less improvement than the iterative exploration of meshes in PowerFactory. However, the value of the objective function is better for the reconfiguration algorithm than for the iterative exploration of meshes. Additionally, the PowerFactory algorithms can only consider all switches at once. This can be considered an advantage for the optimisation itself, but it is a limiting factor when some switches should not be considered during the optimisation at all. Most importantly however, is that both solutions highlight the ability of network reconfiguration to reduce congestion within said network.

7.2. Conclusions

With the results for each of the scenarios in place, there are a couple of conclusions which can be drawn. Arguably the most important conclusion is that the developed algorithm is shown to be able to provide significant improvements with regards to the occurrence of congestion within the network in the short term, either completely removing it, or reducing the occurrence of congestion by more than 40%. Switching operations are relatively cheap compared to grid reinforcement, while still being within the direct control of the DSO. Additionally, the practical application of the reconfiguration algorithm can be used in the short term, as the operation itself is already carried out by the DSO during maintenance for example. A transition from the current 4-year reconfiguration is thus primarily limited by convention. To the best of the author's knowledge, this thesis is the first to highlight the added benefit of seasonal network reconfiguration in the modern electricity grid in the Netherlands, considering the developments of the last two decades.

It is also important to once again highlight the limitations of the reconfiguration algorithm. Because despite its added benefits, these same benefits start to be lessened as the congestion within the network becomes more severe. In such cases the algorithm is spreading the overloading within the network: increasing it in places where previously no problems arose to lighten the strain on the parts already experiencing congestion. Thus, it is important to conclude that the reconfiguration algorithm by itself is not enough to remedy the problems encountered within the MV grid in the long term. Instead, the reconfiguration algorithm would need to be supplemented by other flexibility sources, such as EV's, and traditional grid reinforcement. However, the direct need and size of these other measures can be reduced by the application of seasonal reconfiguration. In short, network reconfiguration is part of the solution, but it is not the solution itself.

With those conclusions out of the way, it may be useful to reevaluate the posed research questions. First of: *What assumptions and network parameters need to be considered in order to design a representative network simulation for a large city in the Netherlands?* In terms of assumptions there are quite a few mentioned throughout this thesis, primarily in Chapters 3 and 4. Some of these assumptions are based on the typical operations carried out by the DSO, while others are imposed by the network modelling. Examples include that only load-switch-disconnectors can be used for the reconfiguration and that no parallel lines exist within the network. Depending on the application, these assumptions will need to be expanded, altered or removed, but it can be safely said that there are quite a few necessary to keep the simulation manageable for one person. With regards to the network parameters, since congestion was the primary problem being resolved within this work, the line current was the most important parameter for the final analysis. However, other parameters, such as the bus voltage and the active power losses all contribute to the final considerations made.

The next question posed was: *How to formulate the mixed-integer linear program meant to implement the network reconfiguration algorithm?* This question has been answered in full by the methodology in Chapter 4, culminating in the final formulation described by Equations 4.23 to 4.45.

The third question posed: *What is the impact of different load profile scenarios on the MV grid?*, can be answered with the use of the scenarios presented in Chapter 5. Although the scenario formulations are somewhat simplistic compared to the possibilities, they do still highlight the expected growth in electricity demand over the next few decades, as well as the increasing penetration and dependence on DERs. The impact of these increases will likely result in an increase in the occurrence of congestion within the distribution grid. Congestion is already a real problem within the Netherlands, as illustrated by Figure 1.1. Unless actions are taken to remedy it, it will only grow in severity and frequency.

Finally, the last sub-research question was: *Is it possible to optimise the topology of the MV grid (in a consistent manner) to cover a wide range of different load profile scenarios by adjusting the normally open switches and thus changing the topology?* The short answer to this is yes. The full answer is a bit more nuanced though. When analysing the results presented in Chapter 6, it becomes apparent that the presented reconfiguration algorithm is able to reduce the severity of congestion for every considered scenario. However, these improvements start to reduce as the congestion becomes more severe and almost disappears for the final scenario in 2050. Furthermore, the stochastic scenario provides an optimised topology taking into account ten different variations of the 2030 scenario, resulting in an almost identical solution to the one provided in the deterministic case. This goes to highlight the robustness of the provided solution by the reconfiguration algorithm to cover a wide range of different load profile scenarios.

All of this culminates in answering the research question posed at the start of this thesis:

How seasonal optimisation of the medium voltage grid topology by the use of a grid reconfiguration algorithm can help to overcome structural congestion?

In short, by utilising the reconfiguration algorithm presented in this work, it is possible to reduce congestion within a MV grid. This, by closing some of the normally open switches and opening others within the network. The result is a new topology for the MV grid, which alters the flow of power therein. This allows for a consistent reduction of the experienced congestion and, depending on the severity, is sometimes even able to completely remove it. The benefit of this operation is that it is a short-term and low-cost solution which can be implemented by the DSO without relying on other external parties. Additionally, due to the considerations made within this work, this solution does not rely on remotely operable switches and can instead be applied within the Dutch grid where manually operated switches are present.

7.3. Recommendations

The final part of this thesis will consist of possible improvements and additions which can be made, based on the knowledge and experience gained during the project.

Perhaps the most important aspect which could be improved upon is the modelling considerations affecting the reactive power within the power flow algorithm (and subsequently the reconfiguration algorithm). Taking these consideration into account proved too much for the provided time for the master thesis, but would greatly benefit its accuracy and completeness.

Similarly, future work can focus on analysing different objective functions to further improve the reduction of congestion within the network. Currently, the objective function offered by the reconfiguration algorithm is the best out of the considered approaches. However, its reduction of the encountered congestion is not. This signifies that the objective function can be altered to better reflect the intended outcome of network congestion reduction and subsequently improve the offered solution.

As was already mentioned, the scenario formulation can be made much more in-depth to further test the functionality of the reconfiguration algorithm. Such work could likely fill a master thesis on its own, but would nevertheless greatly improve the considerations made within this work with regards to the added benefits of the reconfiguration algorithm.

One way to expand the scenarios is to introduce the increasing penetration of heat pumps and wind farms therein. They would be a welcome complement to the PV installations and EV's currently considered and together form a more complete prediction of the developments within the distribution grid.

Other aspects of improvement primarily involve the size of the model and the relation to the computation time of the simulations. For example, it would be possible to expand the decision space for the reconfiguration algorithm to more than one week in case more powerful computational hardware is used. However, such resources were not provided for this thesis and as such the decision space had to be limited to keep computation times reasonable.

Subsequently, more research could be done with regards to the scalability of the solutions presented here. With increasing model sizes and complexity, the ability to compute solutions of larger-scale problems within a reasonable time becomes more and more valuable. It should also be noted that since the algorithm presented here implements seasonal reconfiguration, the computation time could in theory be several months long. While the practicality of this could rightfully be put into question, it does highlight the low priority of the computation time for the algorithm in case of practical application. The main motivation to keep the computation time short is the need to develop the algorithm to begin with.

Alternatively, it could be considered to implement the algorithm in a different high-level programming language, as Python is not the most optimal choice with regards to memory usage or speed.

In Chapter 6, it was also mentioned that the reconfiguration algorithm seems to propose more diverse network configurations when the effects of congestion are less severe. A consequence of this could be that, should congestion prove to be less of a problem in the future, the reconfiguration algorithm could be used to suggest alternative switching operations which could limit the amount of stress experienced by the switching gear used at any given time within the network. This could be a possibility explored in future work.

Other future work could include broadening the considerations made within this work in regards to the MV grid, to the LV and HV grid. Both would require different considerations, but could add to the overall applicability of the network reconfiguration. This especially holds as the TSO is starting to benefit more from utilising flexibility options within the distribution networks and the MV grid becomes less static due to the introduction of flexibility options in the LV grid.

A recommendation with regards to the applicability of network reconfiguration to the Dutch grid would be to further introduce remotely operable switches, as it would allow for switching actions closer to day-ahead or real-time. However, aspects such as the number of switching actions should be reconsidered if this came to pass.

Bibliography

[1] William J. Nacmanson, Jing Zhu and Luis (Nando) Ochoa, "Ev integration project-milestone 6: Network modelling and ev impact assessment," 2021.

[2] S. Huang, Q. Wu, L. Cheng, and Z. Liu, "Optimal reconfiguration-based dynamic tariff for congestion management and line loss reduction in distribution networks," *IEEE Transactions on Smart Grid*, vol. 7, no. 3, pp. 1295–1303, 2016.

[3] Stedin. Netcapaciteit en Transportprognoses. (2022, March 15). [Online]. Available: https://www.stedin.net/zakelijk/congestiemanagement-en-transportprognoses

[4] S. Huang, Q. Wu, Z. Liu, and A. H. Nielsen, "Review of congestion management methods for distribution networks with high penetration of distributed energy resources," in *IEEE PES Innovative Smart Grid Technologies, Europe*, 2014, pp. 1–6.

[5] M. Rossi, G. Viganò, and D. Moneta, "Hosting capacity of distribution networks: Evaluation of the network congestion risk due to distributed generation," in *2015 International Conference on Clean Electrical Power (ICCEP)*, 2015, pp. 716–722.

[6] F. Shen, S. Huang, Q. Wu, S. Repo, Y. Xu, and J. Østergaard, "Comprehensive congestion management for distribution networks based on dynamic tariff, reconfiguration, and re-profiling product," *IEEE Transactions on Smart Grid*, vol. 10, no. 5, pp. 4795–4805, 2019.

[7] 50hertz. Redispatch. (2022, March 14). [Online]. Available: https://www.50hertz.com/en/Grid/Systemcontrol/Redispatch

[8] Stedin, "Stedin investeringsplan 2022," 2022. [Online]. Available: https://www.stedin.net/-/media/project/online/files/jaarverslagen-en-publicaties/investeringsplan-2022.pdf

[9] Netbeheer Nederland. Capaciteitskaart elektriciteitsnet. (2022, May 13). [Online]. Available: https://capaciteitskaart.netbeheernederland.nl/

[10] Delft University of Technology. ROBUST. (2022, March 15). [Online]. Available: https://www.tudelft.nl/en/ewi/over-de-faculteit/afdelingen/electrical-sustainable-energy/intelligent-electrical-power-grids-iepg-group/projects/current-projects/robust

[11] P. Gabrielli, A. Poluzzi, G. J. Kramer, C. Spiers, M. Mazzotti, and M. Gazzani, "Seasonal energy storage for zero-emissions multi-energy systems via underground hydrogen storage," *Renewable and Sustainable Energy Reviews*, vol. 121, p. 109629, 2020. [Online]. Available: https://www.sciencedirect.com/science/article/pii/S1364032119308366

[12] R. Sarfi, M. Salama, and A. Chikhani, "A survey of the state of the art in distribution system reconfiguration for system loss reduction," *Electric Power Systems Research*, vol. 31, no. 1, pp. 61–70, 1994. [Online]. Available: https://www.sciencedirect.com/science/article/pii/0378779694900299

[13] P. Schavemaker and L. van der Sluis, *Electrical Power System Essentials*. Wiley, 2017. [Online]. Available: https://www.wiley.com/en-au/Electrical+Power+System+Essentials%2C+2nd+Edition-p-9781118803479

[14] Ministry of Economic Affairs and Climate Policy, Netherlands. Netcode elektriciteit. (2022, March 17). [Online]. Available: https://wetten.overheid.nl/BWBR0037940/2022-02-09

[15] M. Lavorato, J. F. Franco, M. J. Rider, and R. Romero, "Imposing radiality constraints in distribution system optimization problems," *IEEE Transactions on Power Systems*, vol. 27, no. 1, pp. 172–180, 2012.

[16] European Union, "Directive (eu) 2019/944 of the european parliament and of the council of 5 june 2019 on common rules for the internal market for electricity and amending directive 2012/27/eu (text with eea relevance.)," *Official Journal of the European Union*, 2019.

[17] Energiewijzer. Wet onafhankelijk netbeheer. (2022, March 17). [Online]. Available: https://energiewijzer.nl/energiebegrippen/wet-onafhankelijk-netbeheer/

[18] A. Keane, L. F. Ochoa, C. L. T. Borges, G. W. Ault, A. D. Alarcon-Rodriguez, R. A. F. Currie, F. Pilo, C. Dent, and G. P. Harrison, "State-of-the-art techniques and challenges ahead for distributed generation planning and optimization," *IEEE Transactions on Power Systems*, vol. 28, no. 2, pp. 1493–1502, 2013.

[19] Ministry of Economic Affairs and Climate Policy, Netherlands. Elektriciteitswet 1998. (2022, March 17). [Online]. Available: https://wetten.overheid.nl/BWBR0009755/2021-07-01

[20] D-Cision, "Onderzoek naar de toepassing van congestiemanagement in het station middelharnis 50/13 kv," 2021. [Online]. Available: https://www.stedin.net/-/media/project/online/files/zakelijk/congestiemanagement/stedin-onderzoek-toepassing-congestiemanagement-middelharnis-5013-kv-versie-10.pdf

[21] ——, "Onderzoek naar de toepassing van congestiemanagement in de 50 kv noordring (schouwen-duiveland en tholen)," 2020. [Online]. Available: https://energeia-binary-external-prod.imgix.net/LZ_R6lesaXBg5BCItUmjRTRXdXw.pdf?dl=Onderzoek+congestiemanagement+Schouwen-Duiveland+en+Tholen.pdf

[22] ——, "Onderzoek naar de toepassing van congestiemanagement voor dordtse kil iii en iv," 2021. [Online]. Available: https://www.stedin.net/-/media/project/online/files/zakelijk/congestiemanagement/15-onderzoek-toepassing-congestiemanagement-dordtse-kil-iii-en-iv_2-september-2021.pdf

[23] Enexis, "Onderzoek naar de toepassing van congestiemanagement op hs/ms station boxtel," 2021. [Online]. Available: https://www.enexis.nl/-/media/files/zakelijk/aansluitingen/congestie-onderzoeken/noord-brabant/rapport-congestiemanagement-boxtel.pdf

[24] GOPACS. How does GOPACS work? (2022, August 8). [Online]. Available: https://en.gopacs.eu/about-gopacs-copy/

[25] A. T. Procopiou, L. . Nando, and . Ochoa, "Deliverable 1 "hv-lv modelling of selected hv feeders" active management of lv networks view project active management of low voltage networks view project," 2019. [Online]. Available: https://www.researchgate.net/publication/334458042

[26] Y. Rebours, "A comprehensive assessment of markets for frequency and voltage control ancillary services," Ph.D. dissertation, School of Electrical and Electronic Engineering, University of Manchester, Manchester, 2008. [Online]. Available: https://www.proquest.com/openview/4ebd42d210bef87e75fbb181857a2b55/1?pq-origsite=gscholar&cbl=2026366&diss=y

[27] L. Haarla, O. Mäkelä, G. Brønmo, K. Johansen, P.-F. Bach, and G. Kjølle, "Generally accepted reliability principle with uncertainty modelling and through probabilistic risk assessment collaborative project d1.2 current practices, drivers and barriers for new reliability standards," 6 2014. [Online]. Available: https://www.sintef.no/globalassets/project/garpur/deliverables/garpur-d1.2-current-practices-drivers-and-barriers-for-new-reliability-standards.pdf

[28] A. Kulmala, M. Alonso, S. Repo, H. Amaris, A. Moreno, J. Mehmedalic, and Z. Al-Jassim, "Hierarchical and distributed control concept for distribution network congestion management," *IET Generation, Transmission & Distribution*, vol. 11, no. 3, pp. 665–675, 2017.

[29] G. Granelli, M. Montagna, F. Zanellini, P. Bresesti, R. Vailati, and M. Innorta, "Optimal network reconfiguration for congestion management by deterministic and genetic algorithms," *Electric Power Systems Research*, vol. 76, no. 6, pp. 549–556, 2006. [Online]. Available: https://www.sciencedirect.com/science/article/pii/S0378779605002257

[30] D. Menniti, M. Merlo, N. Scordino, N. Sorrentino, and F. Zanellini, "A dso-oriented mathematical model for dispersed generation management on mv networks," in *2012 IEEE Power and Energy Society General Meeting*, 2012, pp. 1–8.

[31] X. Li and Q. Xia, "Stochastic optimal power flow with network reconfiguration: Congestion management and facilitating grid integration of renewables," in *2020 IEEE/PES Transmission and Distribution Conference and Exposition (T D)*, 2020, pp. 1–5.

[32] A. V. Ramesh and X. Li, "Network reconfiguration impact on renewable energy system and energy storage system in day-ahead scheduling," *CoRR*, vol. abs/2103.13321, 2021. [Online]. Available: https://arxiv.org/abs/2103.13321

[33] H. Mahboubi and J. Lavaei, "Analysis of semidefinite programming relaxation of optimal power flow for cyclic networks," in *2018 IEEE Conference on Decision and Control (CDC)*, 2018, pp. 3203–3210.

[34] J. K. Skolfield and A. R. Escobedo, "Operations research in optimal power flow: A guide to recent and emerging methodologies and applications," *European Journal of Operational Research*, vol. 300, no. 2, pp. 387–404, 2022. [Online]. Available: https://www.sciencedirect.com/science/article/pii/S0377221721008481

[35] F. Capitanescu, "Critical review of recent advances and further developments needed in ac optimal power flow," *Electric Power Systems Research*, vol. 136, pp. 57–68, 2016. [Online]. Available: https://www.sciencedirect.com/science/article/pii/S0378779616300141

[36] H. Abdi, S. D. Beigvand, and M. L. Scala, "A review of optimal power flow studies applied to smart grids and microgrids," *Renewable and Sustainable Energy Reviews*, vol. 71, pp. 742–766, 2017. [Online]. Available: https://www.sciencedirect.com/science/article/pii/S1364032116311583

[37] DIgSILENT. Load Flow Analysis. (2022, August 4). [Online]. Available: https://www.digsilent.de/en/load-flow-analysis.html

[38] L. Zhang and B. Zhang, "An iterative approach to improving solution quality for ac optimal power flow problems," in *Proceedings of the Thirteenth ACM International Conference on Future Energy Systems*, ser. e-Energy '22. New York, NY, USA: Association for Computing Machinery, 2022, p. 289–301. [Online]. Available: https://doi.org/10.1145/3538637.3538858

[39] E. B. Fisher, R. P. O'Neill, and M. C. Ferris, "Optimal transmission switching," *IEEE Transactions on Power Systems*, vol. 23, no. 3, pp. 1346–1355, 2008.

[40] H. Zhao, M. Tanneau, and P. Van Hentenryck, "A linear outer approximation of line losses for dc-based optimal power flow problems," *Electric Power Systems Research*, vol. 212, p. 108272, 2022. [Online]. Available: https://www.sciencedirect.com/science/article/pii/S0378779622004680

[41] X. Bai, H. Wei, K. Fujisawa, and Y. Wang, "Semidefinite programming for optimal power flow problems," *International Journal of Electrical Power & Energy Systems*, vol. 30, no. 6, pp. 383–392, 2008. [Online]. Available: https://www.sciencedirect.com/science/article/pii/S0142061507001378

[42] B. Kocuk, S. S. Dey, and X. A. Sun, "Inexactness of sdp relaxation and valid inequalities for optimal power flow," *IEEE Transactions on Power Systems*, vol. 31, no. 1, pp. 642–651, 2016.

[43] E. Davoodi, E. Babaei, B. Mohammadi-Ivatloo, M. Shafie-Khah, and J. P. S. Catalão, "Multiobjective optimal power flow using a semidefinite programming-based model," *IEEE Systems Journal*, vol. 15, no. 1, pp. 158–169, 2021.

[44] S.-C. Kim and S. R. Salkuti, "Optimal power flow based congestion management using enhanced genetic algorithms," *International Journal of Electrical and Computer Engineering (IJECE)*, vol. 9, p. 875, 4 2019.

[45] X. Li, P. Balasubramanian, M. Sahraei-Ardakani, M. Abdi-Khorsand, K. W. Hedman, and R. Podmore, "Real-time contingency analysis with corrective transmission switching," *IEEE Transactions on Power Systems*, vol. 32, no. 4, pp. 2604–2617, 2017.

[46] B. Enacheanu, B. Raison, R. Caire, O. Devaux, W. Bienia, and N. HadjSaid, "Radial network reconfiguration using genetic algorithm based on the matroid theory," *IEEE Transactions on Power Systems*, vol. 23, no. 1, pp. 186–195, 2008.

[47] A. Merlin and H. Back, "Search for a minimal-loss operating spanning tree configuration in an urban power distribution system," 1975, pp. 1–18.

[48] J. Rolim and L. Machado, "A study of the use of corrective switching in transmission systems," *IEEE Transactions on Power Systems*, vol. 14, no. 1, pp. 336–341, 1999.

[49] J. Mendoza, R. Lopez, D. Morales, E. Lopez, P. Dessante, and R. Moraga, "Minimal loss reconfiguration using genetic algorithms with restricted population and addressed operators: real application," *IEEE Transactions on Power Systems*, vol. 21, no. 2, pp. 948–954, 2006.

[50] T. Potluri and K. W. Hedman, "Impacts of topology control on the acopf," in *2012 IEEE Power and Energy Society General Meeting*, 2012, pp. 1–7.

[51] M. Mahdavi, H. H. Alhelou, N. D. Hatziargyriou, and A. Al-Hinai, "An efficient mathematical model for distribution system reconfiguration using ampl," *IEEE Access*, vol. 9, pp. 79 961–79 993, 2021.

[52] A. Akrami, M. Doostizadeh, and F. Aminifar, "Optimal reconfiguration of distribution network using μpmu measurements: a data-driven stochastic robust optimization," *IEEE Transactions on Smart Grid*, vol. 11, pp. 420–428, 06 2019.

[53] Artelys Knitro User's Manual. Mixed-integer nonlinear programming. (2022, August 12). [Online]. Available: https://www.artelys.com/docs/knitro/2_userGuide/minlp.html

[54] J. F. Franco, M. J. Rider, M. Lavorato, and R. Romero, "A mixed-integer lp model for the reconfiguration of radial electric distribution systems considering distributed generation," *Electric Power Systems Research*, vol. 97, pp. 51–60, 2013. [Online]. Available: https://www.sciencedirect.com/science/article/pii/S0378779612003574

[55] A. Kulmala, S. Repo, and P. Järventausta, "Coordinated voltage control in distribution networks including several distributed energy resources," *IEEE Transactions on Smart Grid*, vol. 5, no. 4, pp. 2010–2020, 2014.

[56] J. Zhu, "Optimal reconfiguration of electrical distribution network using the refined genetic algorithm," *Electric Power Systems Research*, vol. 62, no. 1, pp. 37–42, 2002. [Online]. Available: https://www.sciencedirect.com/science/article/pii/S037877960200041X

[57] A. Uniyal and S. Sarangi, "Optimal network reconfiguration and dg allocation using adaptive modified whale optimization algorithm considering probabilistic load flow," *Electric Power Systems Research*, vol. 192, p. 106909, 2021. [Online]. Available: https://www.sciencedirect.com/science/article/pii/S0378779620307070

[58] H. S. Ramadan and A. Helmi, "Optimal reconfiguration for vulnerable radial smart grids under uncertain operating conditions," *Computers & Electrical Engineering*, vol. 93, p. 107310, 2021. [Online]. Available: https://www.sciencedirect.com/science/article/pii/S0045790621002871

[59] M. U. Usman and M. O. Faruqe, "Applications of synchrophasor technologies in power systems," *Journal of Modern Power Systems and Clean Energy*, vol. 7, no. 2, pp. 211–226, 2018.

[60] H. Mohsenian-Rad, E. Stewart, and E. Cortez, "Distribution synchrophasors: Pairing big data with analytics to create actionable information," *IEEE Power and Energy Magazine*, vol. 16, no. 3, pp. 26–34, 2018.

[61] T. Zhong, H.-T. Zhang, Y. Li, L. Liu, and R. Lu, "Bayesian learning-based multi-objective distribution power network reconfiguration," *IEEE Transactions on Smart Grid*, vol. 12, no. 2, pp. 1174–1184, 2021.

[62] W. Huang, W. Zheng, and D. J. Hill, "Distribution network reconfiguration for short-term voltage stability enhancement: An efficient deep learning approach," *IEEE Transactions on Smart Grid*, vol. 12, no. 6, pp. 5385–5395, 2021.

[63] M. Subramanian, J. Viebahn, S. H. Tindemans, B. Donnot, and A. Marot, "Exploring grid topology reconfiguration using a simple deep reinforcement learning approach," in *2021 IEEE Madrid PowerTech*, 2021, pp. 1–6.

[64] S. Lei, C. Chen, Y. Song, and Y. Hou, "Radiality constraints for resilient reconfiguration of distribution systems: Formulation and application to microgrid formation," *IEEE Transactions on Smart Grid*, vol. 11, no. 5, pp. 3944–3956, sep 2020. [Online]. Available: https://doi.org/10.1109%2Ftsg.2020.2985087

[65] M. Grant, S. Boyd, and Y. Ye, *Disciplined Convex Programming*. Boston, MA: Springer US, 2006, pp. 155–210. [Online]. Available: https://doi.org/10.1007/0-387-30528-9_7

[66] A. M. Helmi, R. Carli, M. Dotoli, and H. S. Ramadan, "Efficient and sustainable reconfiguration of distribution networks via metaheuristic optimization," *IEEE Transactions on Automation Science and Engineering*, vol. 19, no. 1, pp. 82–98, 2022.

[67] A. A. Heidari, S. Mirjalili, H. Faris, I. Aljarah, M. Mafarja, and H. Chen, "Harris hawks optimization: Algorithm and applications," *Future Generation Computer Systems*, vol. 97, pp. 849–872, 2019. [Online]. Available: https://www.sciencedirect.com/science/article/pii/S0167739X18313530

[68] F. F. C. Silva, P. M. S. Carvalho, and L. A. F. M. Ferreira, "Improving pv resilience by dynamic reconfiguration in distribution grids: Problem complexity and computation requirements," *Energies*, vol. 14, no. 4, 2021. [Online]. Available: https://www.mdpi.com/1996-1073/14/4/830

[69] Z. Guo, Z. Zhou, and Y. Zhou, "Impacts of integrating topology reconfiguration and vehicle-to-grid technologies on distribution system operation," *IEEE Transactions on Sustainable Energy*, vol. 11, no. 2, pp. 1023–1032, 2020.

[70] A. Nikoobakht, J. Aghaei, T. Niknam, H. Farahmand, and M. Korpås, "Electric vehicle mobility and optimal grid reconfiguration as flexibility tools in wind integrated power systems," *International Journal of Electrical Power & Energy Systems*, vol. 110, pp. 83–94, 2019. [Online]. Available: https://www.sciencedirect.com/science/article/pii/S0142061518300796

[71] M. Shahidehopour and Y. Fu, "Benders decomposition: applying benders decomposition to power systems," *IEEE Power and Energy Magazine*, vol. 3, no. 2, pp. 20–21, 2005.

[72] DIgSILENT. PowerFactory Apllications. (2022, July 4). [Online]. Available: https://www.digsilent.de/en/powerfactory.html

[73] ——. How do I model correctly the load behaviour for dynamic simulations? (2022, August 18). [Online]. Available: https://www.digsilent.de/en/faq-reader-powerfactory/how-do-i-model-correctly-the-load-behaviour-for-dynamic-simulations.html

[74] ——, "Digsilent powerfactory, technical reference documentation general load, elm-lod," 2014. [Online]. Available: https://www.researchgate.net/profile/Cleberton-Reiz/post/Why-does-the-RMS-current-obtained-with-the-EMT-DigSILENT-samples-not-have-the-same-value-as-\the-simulated-RMS-current-in-steady-state/attachment/5ef9f15e3909f70001d960f7/AS%3A907761260953600%401593438558096/download/TechRef_GeneralLoad.pdf

[75] ——, "Powerfactory 2022, user manual," 2022.

[76] Phase to Phase, "Netten voor distributie van elektriciteit," 2019. [Online]. Available: https://phasetophase.nl/boek/index.html

[77] P. P. Vergara, J. C. López, M. J. Rider, and L. C. P. da Silva, "Optimal operation of unbalanced three-phase islanded droop-based microgrids," *IEEE Transactions on Smart Grid*, vol. 10, no. 1, pp. 928–940, 2019.

[78] Pyomo. What Is Pyomo? (2022, August 3). [Online]. Available: http://www.pyomo.org/

[79] E. O. Schweitzer III and S. E. Zocholl, "Introduction to symmetrical components," *Schweitzer Engineering Laboratories, Inc.*, 2011.

[80] Y. Kawajir. Ipopt Documentation . (2022, November 4). [Online]. Available: https://coin-or.github.io/Ipopt/

[81] K. Girigoudar and L. A. Roald, "Linearized three-phase optimal power flow models for distribution grids with voltage unbalance," in *2021 60th IEEE Conference on Decision and Control (CDC)*, 2021, pp. 4214–4221.

[82] A. Bernstein, C. Wang, E. Dall'Anese, J.-Y. Le Boudec, and C. Zhao, "Load flow in multiphase distribution networks: Existence, uniqueness, non-singularity and linear models," *IEEE Transactions on Power Systems*, vol. 33, no. 6, pp. 5832–5843, 2018.

[83] J. Stewart, *Calculus : early transcendentals*. Belmont, Cal.: Brooks/Cole, Cengage Learning, 2012.

[84] Gurobi. Gurobi Optimizer. (2022, November 4). [Online]. Available: https://www.gurobi.com/products/gurobi-optimizer/

[85] IEA, "Electricity market report," July 2022. [Online]. Available: https://www.iea.org/reports/electricity-market-report-july-2022

[86] EIA, "International energy outlook 2021," October 2021. [Online]. Available: https://www.eia.gov/outlooks/ieo/

[87] S. Hijgenaar, Z. Erkin, T. Keviczky, J. Siemons, R. Bisschops, and A. Verbraeck, "A decentralised energy trading architecture for future smart grid load balancing," in *Proceedings 2017 IEEE International Conference on Smart Grid Communications (SmartGridComm 2017)*. United States: IEEE, 2017, pp. 77–82. [Online]. Available: http://sgc2017.ieee-smartgridcomm.org/

[88] F. Dekking, C. Kraaikamp, H. Lopuhaä, and L. Meester, *A modern introduction to probability and statistics. Understanding why and how*, 01 2005.

A

Phase impedance to sequence components

A full derivation for transforming the phase impedance values to sequence components is presented in [79]. The relevant parts of which have been adapted for this work as found below.

First, for a balanced system, the self and mutual phase impedances can be written according to:

$$Z_s = Z_{aa} = Z_{bb} = Z_{cc} \tag{A.1}$$

$$Z_m = Z_{ab} = Z_{bc} = Z_{ca} = Z_{ba} = Z_{cb} = Z_{ac} \tag{A.2}$$

Where Z_s is the self impedance and Z_m is the mutual impedance. Next, the positive and zero sequence components are expressed in terms of the self and mutual impedance values according to:

$$Z_0 = Z_s + 2Z_m \tag{A.3}$$

$$Z_1 = Z_s - Z_m \tag{A.4}$$

Where Z_0 is the zero sequence component and Z_1 is the positive sequence component. Rewriting gives:

$$Z_s = \frac{1}{3}(2Z_1 + Z_0) \tag{A.5}$$

$$Z_m = \frac{1}{3}(Z_0 - Z_1) \tag{A.6}$$

Finally, writing the impedance in terms of the resistance and reactance components gives:

$$R_s = \frac{1}{3}(2R_1 + R_0) = R_{aa} = R_{bb} = R_{cc} \tag{A.7}$$

$$X_s = \frac{1}{3}(2X_1 + X_0) = X_{aa} = X_{bb} = X_{cc} \tag{A.8}$$

$$R_m = \frac{1}{3}(R_0 - R_1) = R_{ab} = R_{bc} = R_{ca} = R_{ba} = R_{cb} = R_{ac} \tag{A.9}$$

$$X_m = \frac{1}{3}(X_0 - X_1) = X_{ab} = X_{bc} = X_{ca} = X_{ba} = X_{cb} = X_{ac} \tag{A.10}$$

B

Summer period analysis

This chapter will go over an abbreviated version of the steps taken in Chapters 5 and 6, introducing the scenarios and results for the reconfiguration algorithm, but instead of a winter period, it will focus on a summer period. The period in question is the 26th week of the considered year, ranging from hour 4200 to 4368. The same additions to the provided base data as mentioned in Chapter 5 apply here, meaning an increase in the base load and the additions of distributed generation and demand caused by PV systems and EV usage, respectively. The application of these scenarios within the base topology is highlighted in Figure B.1, where the peak line loading is shown for the entire network. Within the figure, a green colour indicates that the line does not experience congestion during the considered time frame. An orange colour indicates that the line is formally not experiencing congestion yet, but its status will be manually checked by the DSO. Finally, a red colour indicates that a line has experienced one or more moments of congestion during the considered time frame.

The most noticeable difference with the considered winter period is perhaps the severity of the encountered congestion in terms of its occurrence. The first scenario set in 2021 does not encounter any congestion to begin with. The 2030 scenario only has two lines which are congested, which already happened in 2021 for the winter period. In 2040 the congestion is spreading to two of the feeders and in 2050 the congestion is more widespread, but not nearly to the degree as encountered during the winter period. The main cause for this difference is probably two-fold. First, demand is a lot lower during the summer season compared to the winter season (as can also be seen in Figures 1.2 and 3.5b). Second, the local generation has greatly increased compared to the base case for each of the scenarios. Since local demand for electricity is assumed to be supplied by local generation if possible, this results in an overall decrease in the demand for transport capacity and subsequently congestion.

Next, each of the scenarios is subjected to the optimisation of the reconfiguration algorithm, altering the grid topology as is depicted in Figure B.2. The alterations differ per year and range between 5 and 3 switches changing position. The optimised topology in 2030 only differs by one switch position from the one in 2021. The topology in 2040 has two different selected switches compared to 2030 and 2050 only differs by one switch from 2040. This goes to highlight that not many switch operations are necessary to optimise the grid topology, especially once the first optimisation has been carried out.

Next, the maximum line loading throughout the network for the optimised topologies are shown in Figure B.3. Here, a few points are interesting to note. First, the congestion has completely disappeared for the scenario in 2030, as depicted in Figure B.3b. Second, the congestion has actually spread to more feeders in the optimised topology than in the base topology for the 2040 scenario. However, it will be shown that despite this, the new configuration brings great improvements with regards to the severity of the encountered congestion. The maximum loading is rather similar for both 2021 and 2050, but also more on this as the data is analysed.

First, the 2021 scenario will be discussed. This analysis is rather short as neither the base topology nor the optimised topology experience any congestion. However, it is interesting to note that the objective function

value has improved in the optimised topology, going from 6.51 to 6.38, as is also shown in Table B.1.

Table B.1: Summary of results for scenario 2021

	Base topology	Optimised topology
Active power losses [MW]	6.51	6.38
Number of lines experiencing congestion	0	0

Next, the results for the 2030 scenario are shown in Table B.2. Here, two lines were experiencing congestion a total of 18 times during the considered time frame in the base topology. However, this congestion has been completely removed in the optimised topology. It should be noted that the congestion was relatively small, with a peak of only 6.68% overloading. Nevertheless, the reconfiguration algorithm provides a satisfactory solution.

Table B.2: Summary of results for scenario 2030

	Base topology	Optimised topology
Active power losses [MW]	9.92	9.44
Number of lines experiencing congestion	2	0
Instances of congestion	18	0
Average overloading size [%]	2.69	0.00
Maximum overloading size [%]	6.68	0.00
Instances of congestion above maintenance/disturbance limit	0	0

Next is the 2040 scenario. Since congestion is a bit more prevalent in this scenario compared to the previous two, it may be insightful to first take a look at the heat map of the encountered congestion in Figure B.4. Despite more lines experiencing congestion compared to the base topology, the ones that are actually visible on the heat map are more or less equal (the other two being barely visible due to their small overloading size).

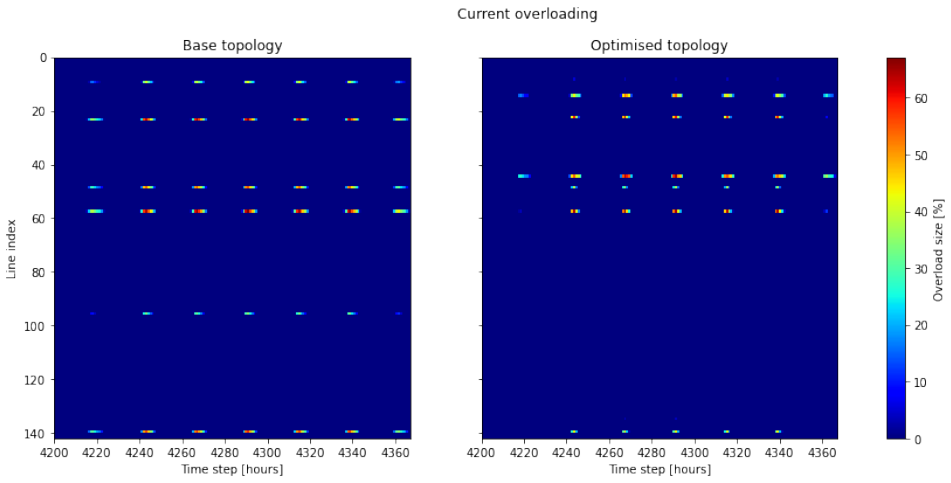

Figure B.4: Heat map of the occurrences of line current overloading for the considered time frame in the 2040 scenario.

The reason for this difference becomes apparent when looking at the data in Table B.3. First, the objective function value has been reduced from 16.25 MW losses over the considered time frame for the entire network, to 15.15 MW, a reduction of 6.77%. As became apparent from Figure B.3c, the amount of lines experiencing congestion has increased from six to eight. However, the occurrences of congestion have been drastically reduced, from 294 to 168, a reduction of 42.86%. Additionally, the average size of line current overloading has been reduced from 28.60% to 12.25% and the maximum has been reduced from 67.15% to only 26.59%. Furthermore, the occurrences of congestion which surpass the limit during maintenance or a disturbance

have been completely removed.

Table B.3: Summary of results for scenario 2040

	Base topology	Optimised topology
Active power losses [MW]	16.25	15.15
Number of lines experiencing congestion	6	8
Instances of congestion	294	168
Average overloading size [%]	28.60	12.25
Maximum overloading size [%]	67.15	26.59
Instances of congestion above maintenance/disturbance limit	129	0

The reduction of the average and maximum size of the encountered line overloading can be further accounted for by looking at Figure B.5. Here, the distribution of the encountered overloading is plotted, with the size relative to its total occurrence. From the figure, it is clear that the encountered congestion has been severely reduced, although the spread is more uniform than encountered for the other scenarios in Chapter 6.

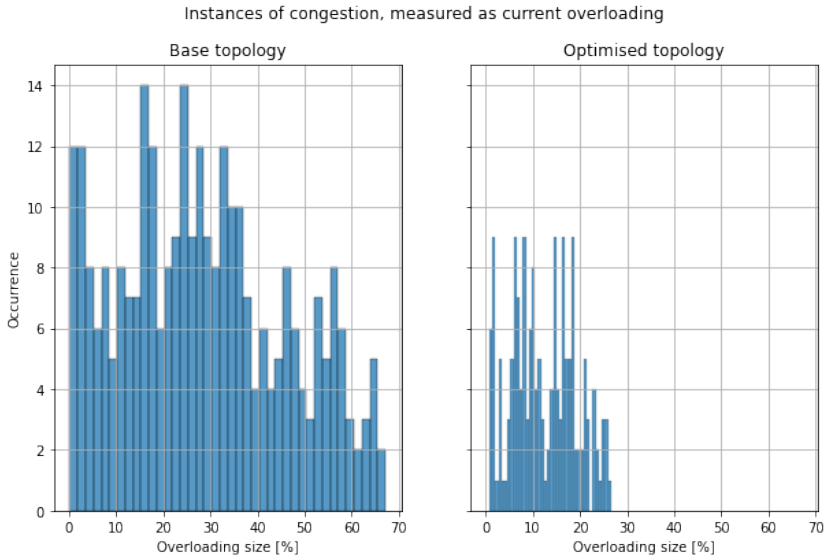

Figure B.5: Sizes of the current overloading (in percentages) for each occurrence of congestion for the 2040 scenario.

Finally, there is the scenario for 2050. Once again, the heat map is covered first, now displayed in Figure B.6. The lines between index 0 and 60 which experience congestion are more or less equally defined for both plots. However, it is interesting to note that the two lines around index 100 and 110 are barely visible in the optimised topology. This already highlights the reduction of the congestion in the optimised topology.

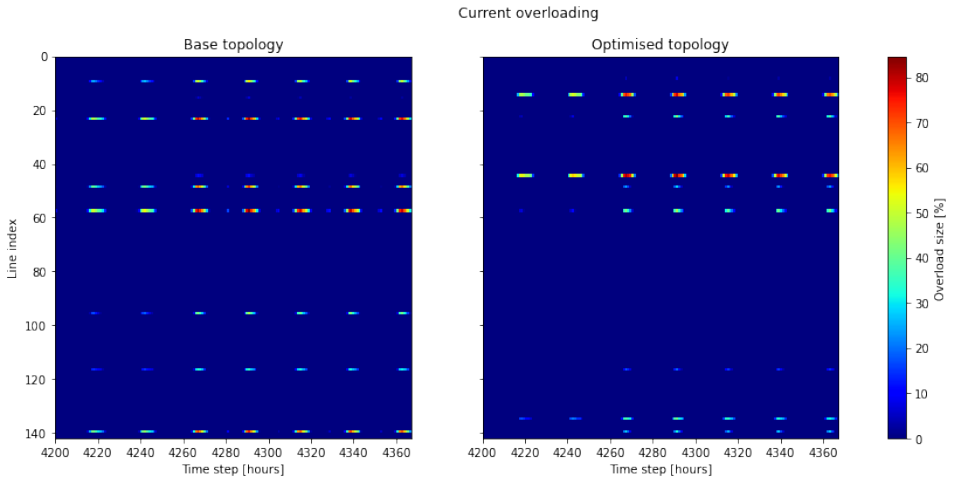

Figure B.6: Heat map of the occurrences of line current overloading for the considered time frame in the 2050 scenario.

This reduction can be further observed when analysing the results in Table B.4. Here, the objective function value has once again been reduced, this time by 6.16%, which is very close to the 6.77% reduction for the 2040 scenario. The amount of lines experiencing congestion is actually the same for both topologies at nine. The biggest improvement can once again be observed for the occurrences of congestion, having dropped from 444 to 280, a reduction of 36.94%. The same observation holds for both this parameter and the remaining ones: less improvement than for the 2040 scenario, but still substantial. The average overloading size has been reduced from 29.74% to 22.29% and the maximum value encountered has dropped from 84.65% to 61.93%. Finally, the occurrences of congestion surpassing the maintenance and/or disturbance limit have decreased from 203 to 81, a reduction of 60.10%.

Table B.4: Summary of results for scenario 2050

	Base topology	Optimised topology
Active power losses [MW]	22.25	20.88
Number of lines experiencing congestion	9	9
Instances of congestion	444	280
Average overloading size [%]	29.76	22.49
Maximum overloading size [%]	84.65	61.93
Instances of congestion above maintenance/disturbance limit	203	81

The distribution of the encountered congestion is shown in Figure B.7. It can be seen that a relatively large amount of the encountered congestion in the base topology actually surpassed 60% overloading, whereas this has been completely removed in the optimised topology. Additionally, it is interesting to note that the optimised topology does not have its peak of congestion occurrences around 0%, as has been observed most often throughout this thesis. Instead, the peak is around 17%.

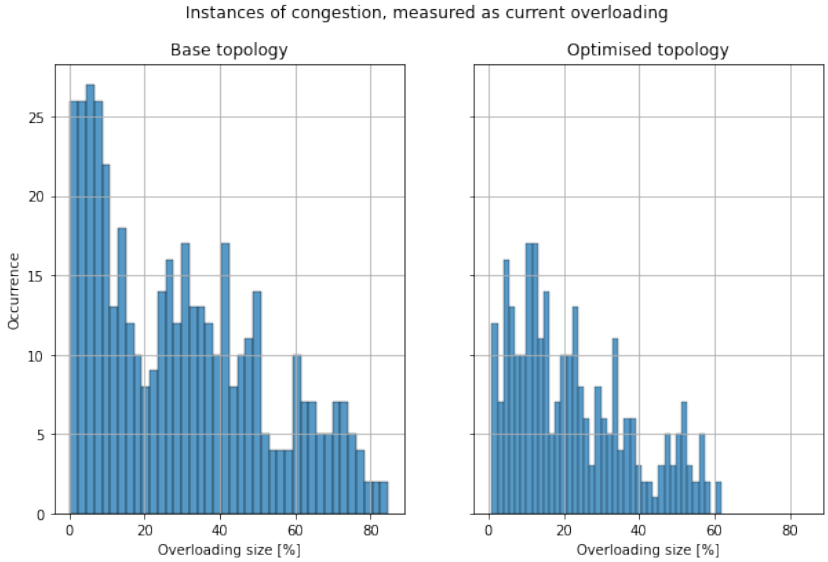

Figure B.7: Sizes of the current overloading (in percentages) for each occurrence of congestion for the 2050 scenario.

Overall, the summer scenario does not offer any insight which was not already gained from the winter period. Instead, the summer period is a much less extreme version with regards to network congestion. However, this does further support the claim that the reconfiguration algorithm is most effective for less extreme cases of congestion. For each of the scenarios covered here, the reconfiguration algorithm has been able to significantly reduce the encountered congestion, even more so than for the winter period. Most importantly, the summer period provides an even better example of the benefits of the reconfiguration algorithm with regards to reducing network congestion within the MV grid.

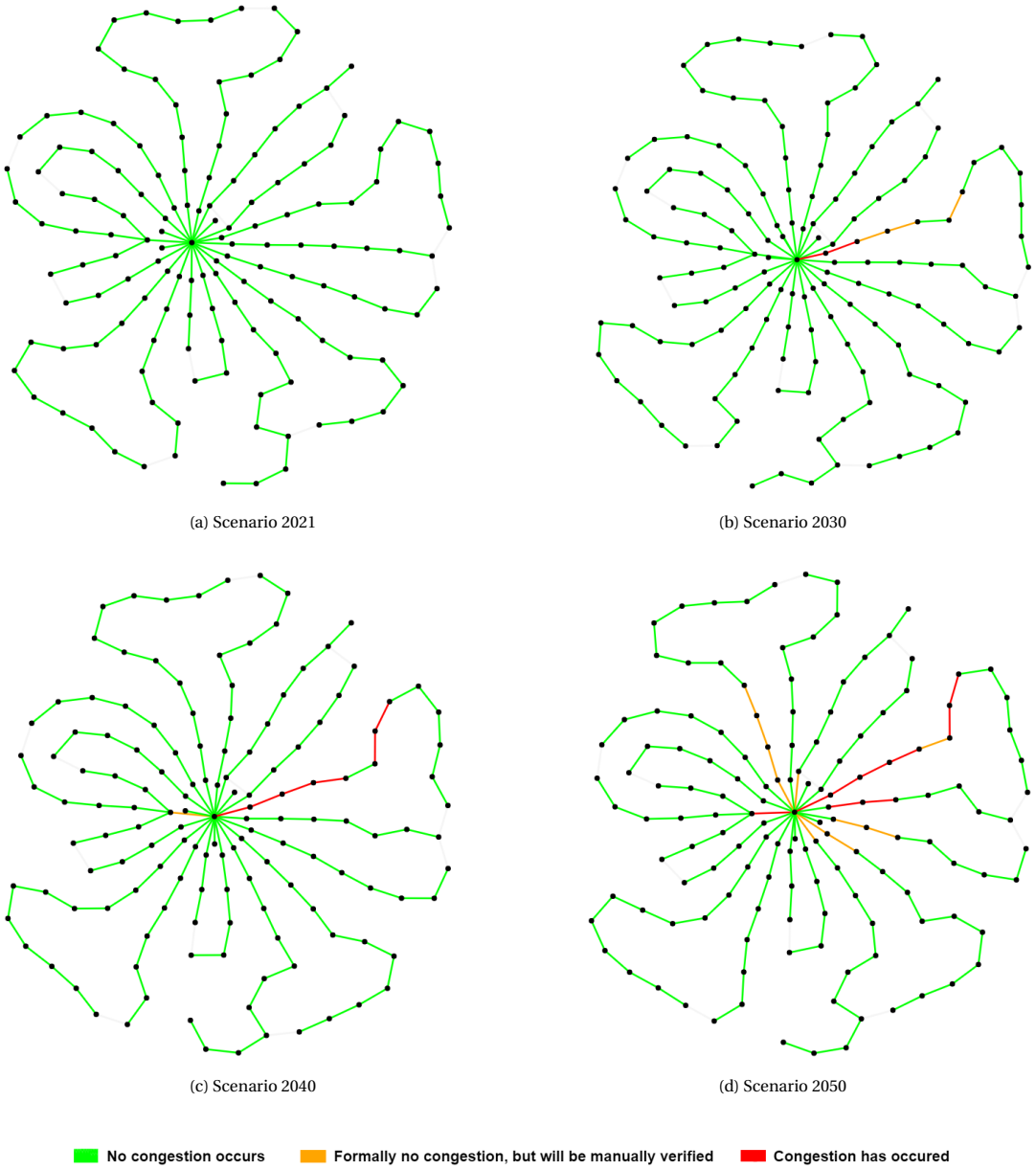

(a) Scenario 2021

(b) Scenario 2030

(c) Scenario 2040

(d) Scenario 2050

Figure B.1: Overview of the effect of the different scenarios with regards to the occurrence of congestion within the base network topology. Within the images a green colour indicates a line without congestion. An orange colour indicates that the line is formally not experiencing congestion yet, but its status will be manually checked. A red colour indicates that a line has experienced one or more moments of congestion during the considered time frame.

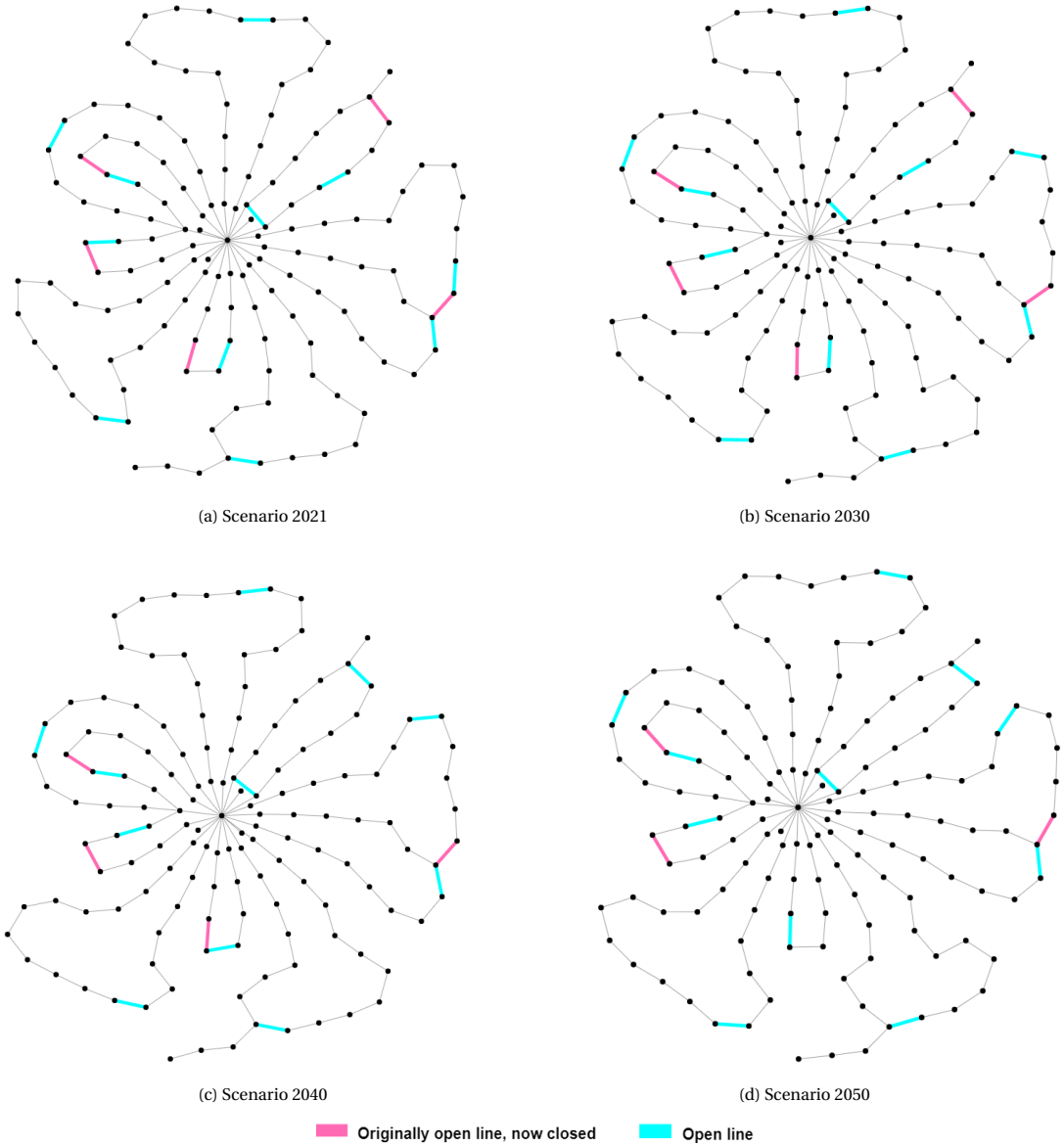

(a) Scenario 2021

(b) Scenario 2030

(c) Scenario 2040

(d) Scenario 2050

Figure B.2: The new network topology obtained from using the reconfiguration algorithm for the 26th week of the year. A pink colour indicates a line that was previously opened in the base topology, but is now closed. A blue line represents an open line in the optimised topology.

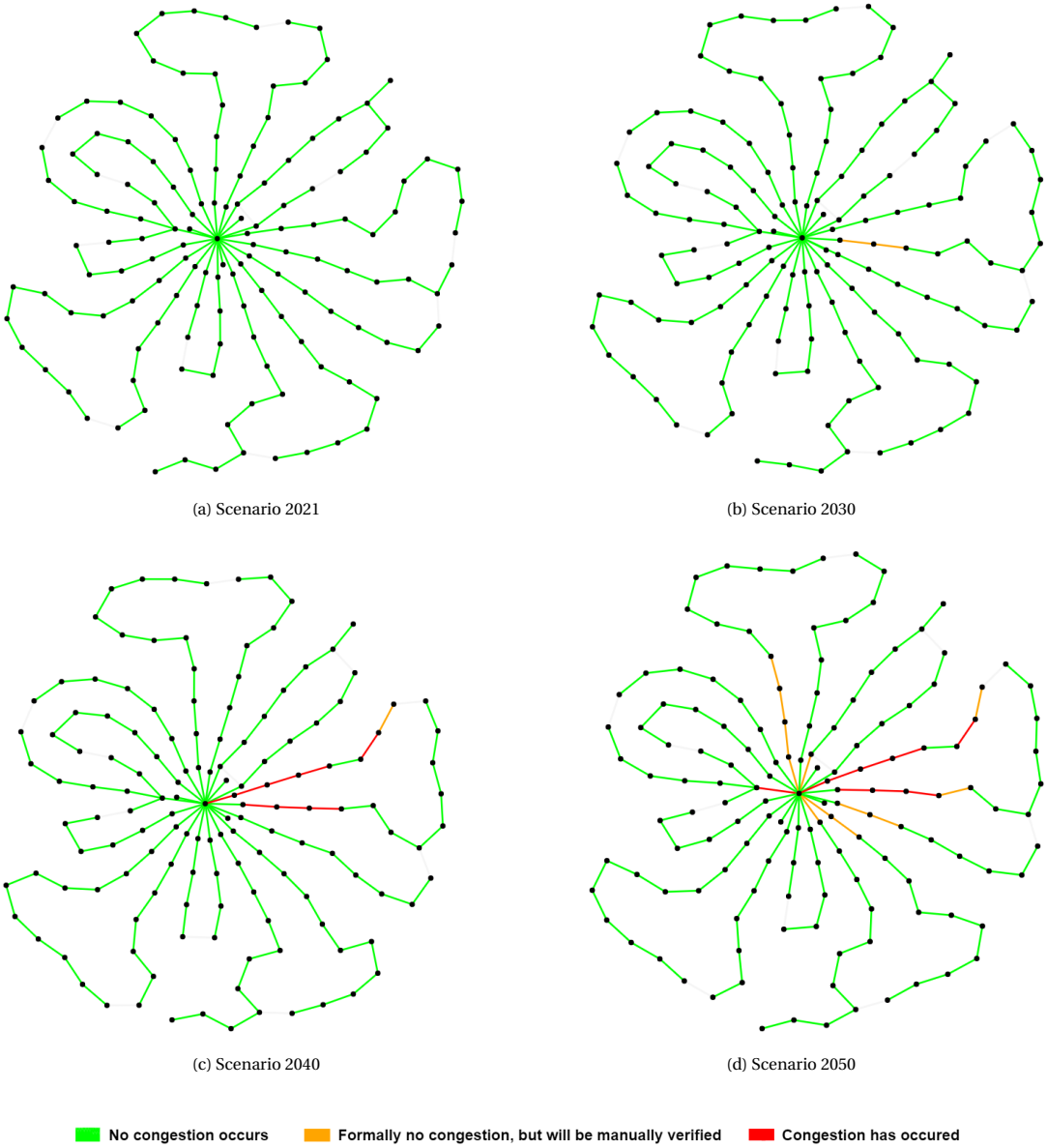

(a) Scenario 2021

(b) Scenario 2030

(c) Scenario 2040

(d) Scenario 2050

Figure B.3: Overview of the effect of the different scenarios with regards to the occurrence of congestion within the optimised network topology. Note that not all topologies are the same for each of the sub-figures. Within the images a green colour indicates a line without congestion. An orange colour indicates that the line is formally not experiencing congestion yet, but its status will be manually checked. A red colour indicates that a line has experienced one or more moments of congestion during the considered time frame.

C

Population parameters genetic algorithm

Below follows an overview of the population parameter values used for the genetic algorithm in PowerFactory. Note that these are the standard values provided by PowerFactory, as optimising them is outside the scope of this thesis. Note that these values do share similarities with other literature sources, such as [29], where the population size and mutation rate are the same. The number of iterations is a factor of 10 higher for the PowerFactory algorithm and the other parameters are not specified. As such, these parameters are deemed satisfactory for the purposes of this thesis.

Table C.1: Population setting for the genetic algorithm in PowerFactory

Size of population	10
Mutation rate	0.1
Number of mutation points	1
Number of crossover points	10
Maximum number of iterations	1000

D

Voltage amplitude data

For the sake of completeness, this appendix provides a complete overview of the voltage data used for the comparison between the different topologies provided by the reconfiguration algorithm, the iterative exploration of meshes and the genetic algorithm for the winter scenario. Figure D.1 highlights the voltage amplitude with respect to the relevant bus and time step. Figure D.2 provides the distributions of the voltage amplitude occurrences. Finally, Table D.1 provides an overview of the maximum, minimum and mean voltage amplitude values of each topology.

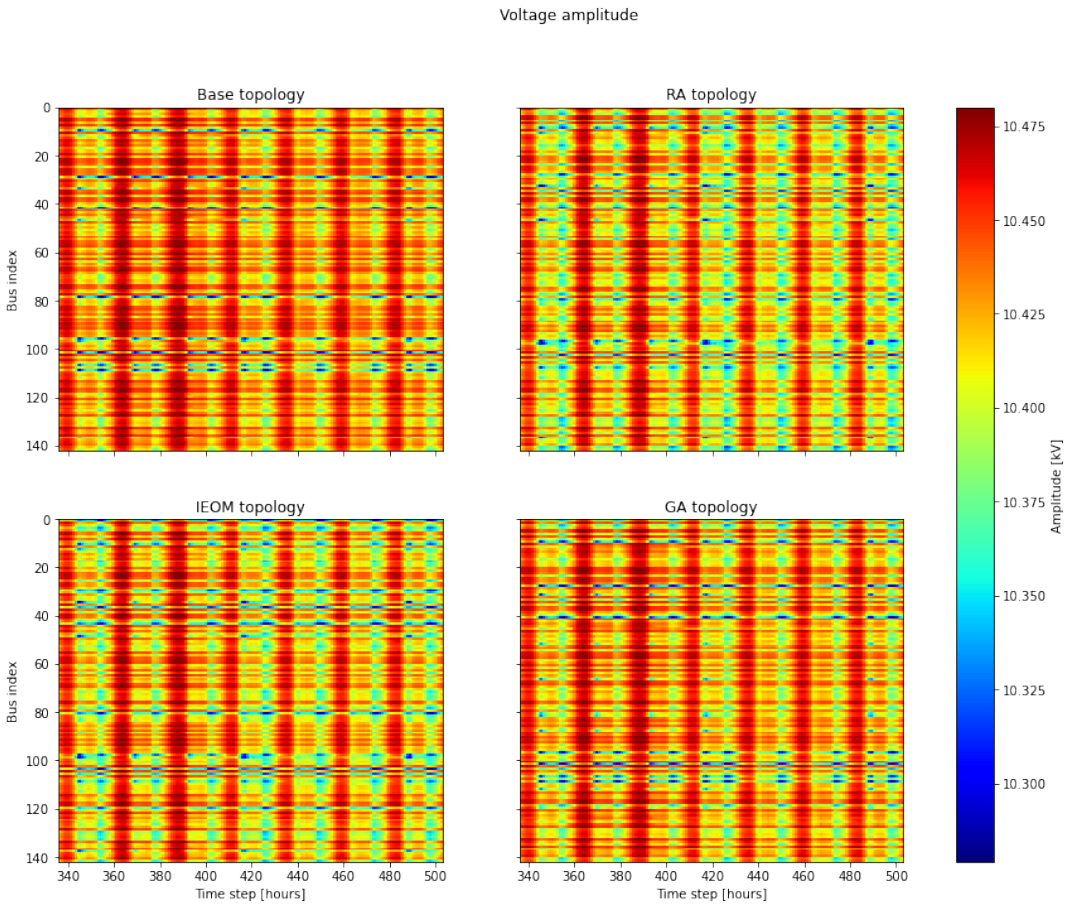

Figure D.1: Overview of the voltage amplitude encountered throughout the network for the considered time frame in the 2030 scenario for each of the considered algorithms. Base refers to the base topology, RA is the solution offered by the reconfiguration algorithm, IEOM is the solution offered by the iterative exploration meshes and GA refers to the genetic algorithm.

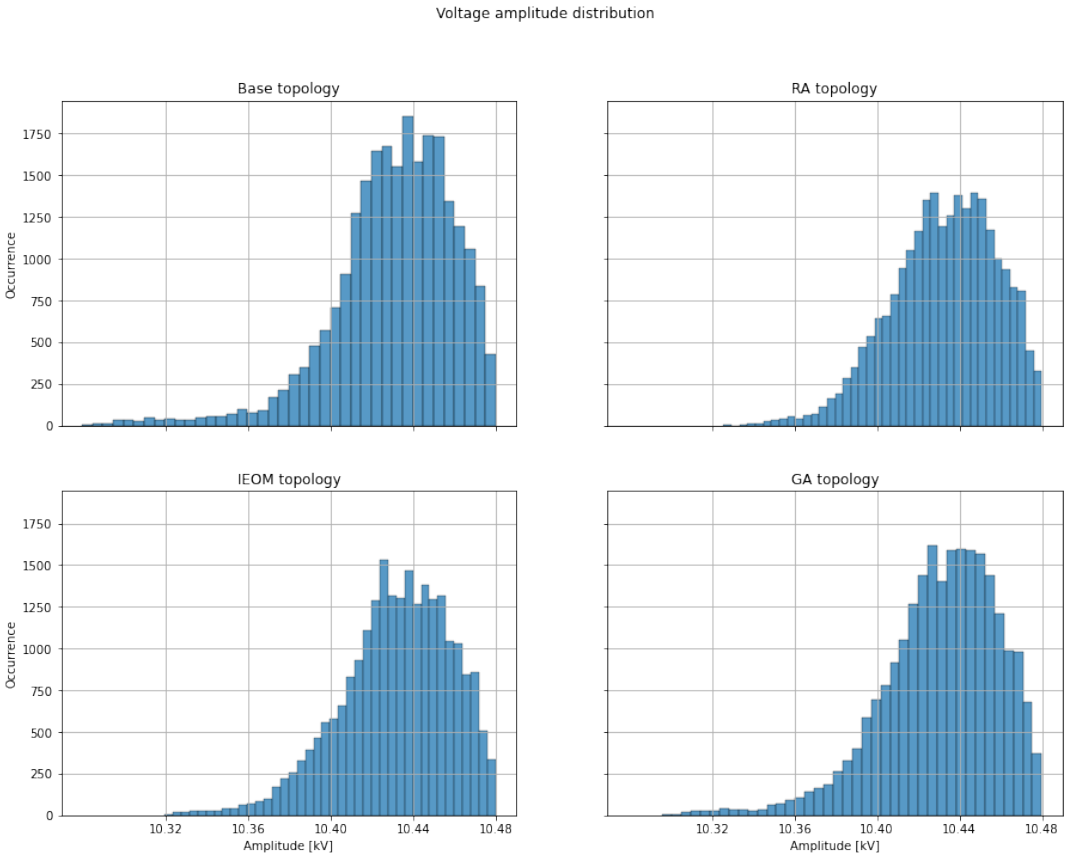

Figure D.2: Voltage amplitude distributions encountered for each topology. Base refers to the base topology, RA is the solution offered by the reconfiguration algorithm, IEOM is the solution offered by the iterative exploration meshes and GA refers to the genetic algorithm.

Table D.1

Topology	Minimum [kV]	Maximum [kV]	Mean [kV]
Base	10.279	10.480	10.431
Reconfiguration algorithm	10.325	10.480	10.433
Iterative exploration of meshes	10.319	10.480	10.432
Genetic algorithm	10.296	10.480	10.431